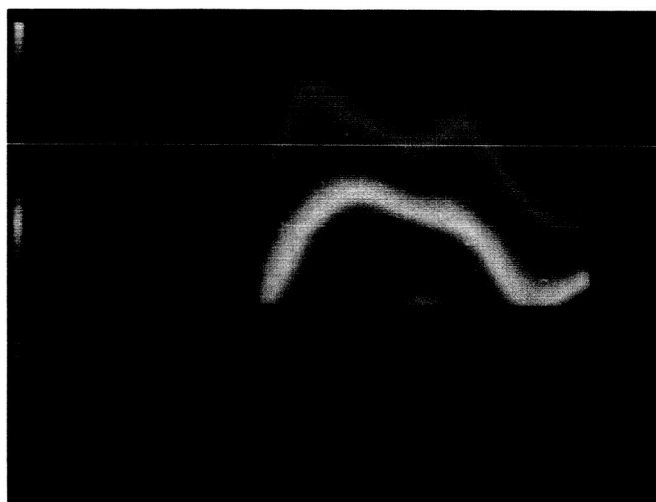


ORIGINAL PAGE  
COLOR PHOTOGRAPH

# HYDROGEN SPECIES



## Panel Members

H.I. Schiff, Chairman

C. Burnett	R. Jones
B. Carli	D. Kley
W.B. DeMore	M. Prather
R. deZafra	J.M. Russell, III
W.F.J. Evans	U. Schmidt
P.D. Guthrie	W.A. Traub
R.F. Hampson	R.T. Watson
W. Heaps	

## CHAPTER 9

### HYDROGEN SPECIES: OBSERVATIONS AND INTERPRETATION

#### TABLE OF CONTENTS

9.0 INTRODUCTION .....	441
9.1 HYDROXYL (OH) MEASUREMENTS .....	441
9.1.1 Balloon-borne Measurements of OH .....	441
9.1.2 Inferred OH Profiles .....	444
9.1.3 Ground Based OH Measurements .....	444
9.2 HYDROPEROXYL (HO <sub>2</sub> ) MEASUREMENTS .....	450
9.2.1 <i>In situ</i> Vertical Profile Measurements of HO <sub>2</sub> .....	450
9.2.2 Ground Based HO <sub>2</sub> Measurements .....	450
9.2.3 Comparisons of Theory and Observations for HO <sub>2</sub> .....	453
9.3 HYDROGEN PEROXIDE (H <sub>2</sub> O <sub>2</sub> ) MEASUREMENTS .....	454
9.4 WATER (H <sub>2</sub> O) MEASUREMENTS .....	456
9.4.1 <i>In situ</i> Vertical Profile Measurements of H <sub>2</sub> O .....	456
9.4.2 LIMS Water Vapor Measurements .....	461
9.4.3 Measurements of H <sub>2</sub> O in the Upper Stratosphere and Mesosphere .....	473
9.5 METHANE (CH <sub>4</sub> ) MEASUREMENTS .....	476
9.5.1 Vertical CH <sub>4</sub> Profiles by <i>In situ</i> Measurements .....	476
9.5.2 Vertical Profiles of CH <sub>4</sub> by Remote Sensing .....	479
9.5.3 Satellite Measurements of CH <sub>4</sub> .....	481
9.5.4 Intercomparison of CH <sub>4</sub> Data .....	488
9.5.5 Total Hydrogen Content of the Stratosphere .....	490
9.6 CONCLUSIONS .....	494
9.7 FUTURE RESEARCH NEEDS .....	495

**PRECEDING PAGE BLANK NOT FILMED**

## 9.0 INTRODUCTION

This chapter discusses measurements of the members of the  $\text{HO}_x$  family - OH,  $\text{HO}_2$  and  $\text{H}_2\text{O}_2$  - and their major source gases,  $\text{H}_2\text{O}$ , and  $\text{CH}_4$ . Emphasis will be placed on measurements which have been made since the 1982 WMO report.

The effects of  $\text{HO}_x$  on ozone destruction are both direct and indirect. Direct control is believed to dominate in the mesosphere and upper stratosphere. At lower altitudes,  $\text{NO}_x$  and  $\text{ClO}_x$  are more important in determining ozone loss but  $\text{HO}_x$  is closely coupled to the other two families and strongly influences their catalytic efficiencies.

The OH radical is mainly responsible for this coupling. In the case of  $\text{NO}_x$  interactions OH deactivates the chain carrier  $\text{NO}_2$  by converting it to the inactive reservoir molecule  $\text{HNO}_3$ . The deactivation is, however, only temporary, since photolysis and reaction of OH with  $\text{HNO}_3$  regenerates the chain carriers. In contrast, the primary interaction of OH with the  $\text{ClO}_x$  family is to convert the inactive HCl molecule to the chain carrier, Cl. The  $\text{ClO}_x$  cycle also interacts with the hydrogen cycle through  $\text{CH}_4$  which provides the main chain termination step by reaction with Cl to form HCl. This mechanism may lead to substantial latitudinal and perhaps seasonal variations in the efficiency of the chlorine catalysis of ozone (Gidel *et al.*, 1983; Solomon and Garcia, 1984b). For these reasons OH is considered to be the most important member of the  $\text{HO}_x$  family and a key species in atmospheric chemistry.

The other chain carrier in the catalytic cycle of ozone destruction,  $\text{HO}_2$ , is coupled to the  $\text{NO}_x$  family largely by its reaction with NO which affects the partitioning of the chain carriers in both families. The  $\text{HO}_x$  and  $\text{NO}_x$  families are also coupled through the  $\text{HO}_2 + \text{NO}_2 + \text{M}$  reaction forming the temporary reservoir species,  $\text{HO}_2\text{NO}_2$ . Although  $\text{H}_2\text{O}_2$  does not directly affect ozone loss it is a major sink molecule for  $\text{HO}_x$  in the lower stratosphere where it can be transported down through the tropopause and removed. Its measurement therefore provides important information to our understanding of the overall  $\text{HO}_x$  budget.

Water vapor provides the primary source of stratospheric hydroxyl radicals through reaction with  $\text{O}(^1\text{D})$ . Intermediate steps in the overall oxidation of  $\text{CH}_4$  to  $\text{CO}_2$  and  $\text{H}_2\text{O}$  generate  $\text{HO}_2$  radicals. Molecular hydrogen represents a small source of  $\text{HO}_x$  in the stratosphere. Concentration measurements of  $\text{H}_2\text{O}$  and  $\text{CH}_4$  provide tests for stratospheric transport and chemistry in multidimensional models. Their concentrations are coupled since the hydrogen content of stratospheric air, primarily  $(\text{H}_2\text{O} + 2 \times \text{CH}_4)$  should remain constant as  $\text{CH}_4$  is converted into  $\text{H}_2\text{O}$ .

Significant advances have been made in the measurement of all these  $\text{HO}_x$  species since the 1982 WMO assessment and the data base for these measurements has been extended appreciably.

The remainder of the chapter describes the measurement techniques, the available data, an assessment of the data reliability, and a comparison of the data with theoretical distributions of stratospheric  $\text{HO}_x$  species predicted from one and two dimensional photochemical models.

### 9.1 HYDROXYL (OH) MEASUREMENTS

#### 9.1.1 Balloon-borne Measurements of OH

The only new measurements reported for the OH vertical profile since the 1982 WMO assessment were obtained using a balloon-borne laser radar system (LIDAR [Heaps and McGee, 1985]). A crude measurement using this technique was made in 1980 and an improved instrument was flown in October 1983.

## HYDROGEN SPECIES

Radiation at 282 nm is transmitted into the atmosphere and is absorbed by the OH radical. Collisions with other atmospheric molecules redistribute the energy into a number of vibrational and rotational levels leading to two bands of fluorescence in the 306 nm - 315 nm region. The strength of the fluorescence is related to the OH concentration [Heaps *et al.*, 1982].

The results from the October, 1983 flight of the lidar system are shown in Figure 9-1a. The closed circles represent all the OH profile measurements made using the *in situ* resonance fluorescence technique up to 1983 and the curves are results from current 2-D models (see Chapter 12). Open circles are from the 1980 LIDAR flight. The crosses are the new lidar data. The vertical bars represent the altitude range through which the gondola ascended while the measurements were being made. The horizontal bars represent one standard deviation of uncertainty arising from counting statistics which ranged from about  $\pm 5\%$  at 38 km to  $\pm 100\%$  at 28 km. The accuracy of all the measurements is  $\pm 50\%$  resulting from the accumulated uncertainty of the calibration. Each measurement corresponds to 1,000 laser shots requiring approximately 4 minutes. The maximum raw signal observed was  $\sim 0.6$  photons/shot. The measurements were obtained at a range of 75-150 meters from the gondola. Although this is close enough to the balloon for outgassing contamination to be a consideration, these measurements are thought to be of good quality because the ascent rate was too rapid for balloon borne contaminants to diffuse into the measurement volume. Later measurements at float (not shown in the figure) show effects that are probably attributable to contamination arising on a time scale of 10-30 minutes. Measurements made at ranges out to 0.5 km agree to within the stated precision with this profile although they have a poorer signal-to-noise ratio.

As can be seen in the figure this profile is generally lower than most previous measurements made by Anderson [1976] using the *in situ* resonance fluorescence technique and is slightly lower than the range predicted by models. The measurements are, however, within the combined uncertainty of the models and the measurements. It is evident that the measurements are insufficient to provide a critical test of HO<sub>x</sub> photochemistry.

It has long been recognized that simultaneous measurements of multiple species are required for meaningful comparisons between theory and measurements. A minimum set for OH would be O<sub>3</sub> and H<sub>2</sub>O. The lidar system makes an O<sub>3</sub> measurement simultaneously with OH measurements by using differential absorption. No satisfactory H<sub>2</sub>O lidar technique has been developed to date. Simultaneous measurements of H<sub>2</sub>O by *in situ* techniques cannot be obtained on the same gondola due to differences in sampling strategy, i.e., the lidar's flight profile involves long duration at float. Consequently a second balloon would be needed for the H<sub>2</sub>O measurements.

Three other balloon-borne instruments have been developed for OH profile measurements. Although all have been flown, results are not yet available for inclusion in this report at this time. Two of these instruments involve remote-sensing far infrared emission in the 60 - 250 cm<sup>-1</sup> region measured by Fourier-transform spectrometers (FTS) in a limb-sounding mode.

The Carli (Istituto di Ricerca Onde Elettromagnetiche) group uses an FTS with a wire grid beamsplitter optimized for longer wavelength, He<sup>4</sup> as well as He<sup>3</sup> cooled bolometers, and an apodized resolution of 0.007 cm<sup>-1</sup> [Carli, *et al.*, 1983, 1984, 1985a]. The Traub group (Smithsonian Astronomical Observatory) uses an FTS with a Mylar beamsplitter optimized for shorter wavelengths, He<sup>4</sup> cooled Ge:Ga photoconductors, and an apodized resolution of 0.064 cm<sup>-1</sup> (Traub *et al.*, 1982).

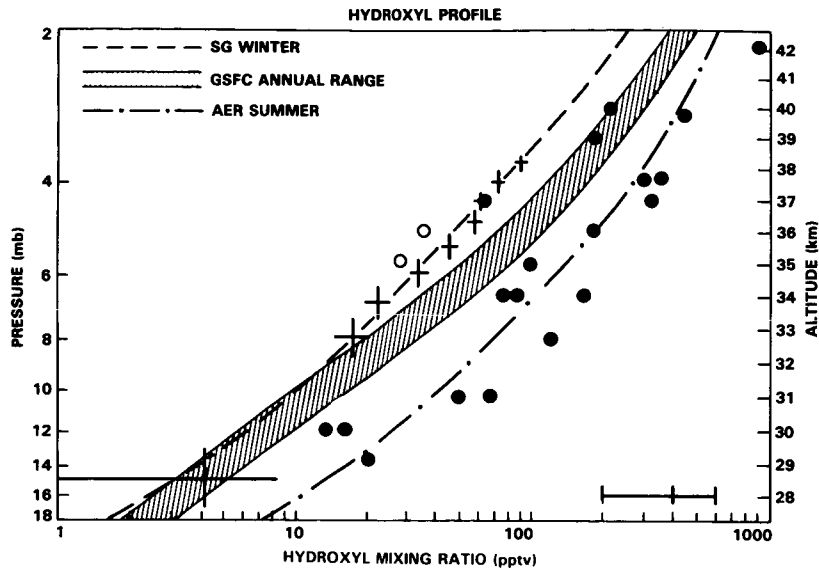


**Figure 9-1a.** OH concentration versus altitude. The circles represent all stratospheric OH measurements prior to 1983: filled circles were obtained by Anderson (1976) using lamps to excite fluorescence and have typical uncertainties of  $\pm 30\%$ ; open circles are from Heaps and McGee, 1983. The crosses are results from the October 1983 flight of Heaps and McGee (1985) taken from Palestine, Texas, 10:30 local time. The height of the crosses represents the altitude range of the measurements; the width of the crosses present the precision ( $1\sigma$ ). The bar at the bottom of the figure represents the accuracy estimates for all the points. Also shown are representative results from several current 2-D models (---, Solomon and Garcia Winter; -.-., AER Summer). The seasonal range shown for the GSFC model is typical for models of this type. Additional details of the models are presented in Chapter 12.

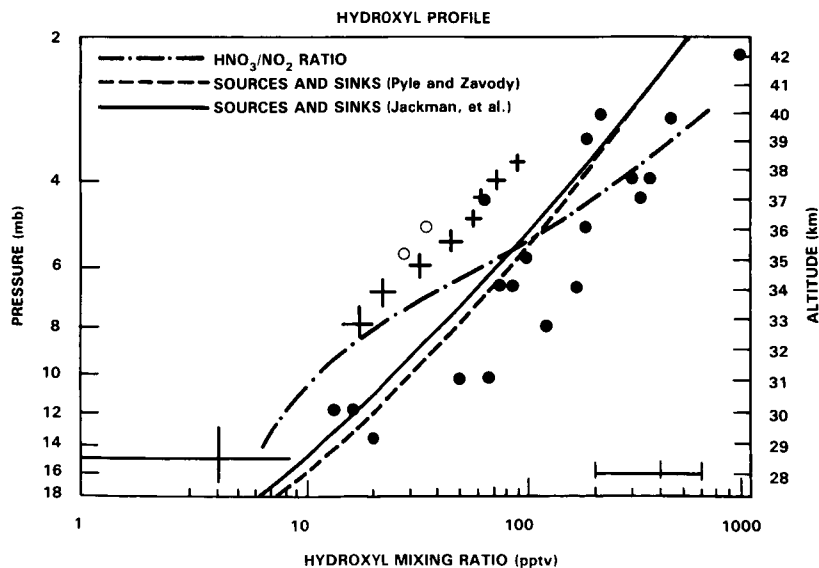


**Figure 9-1b.** Data as in Figure 9.1a. The -.-.; ---; ———; lines represent the OH profiles inferred by Pyle and Zavody from the HNO<sub>3</sub>/NO<sub>2</sub> ratio; by Pyle and Zavody from the sources and sinks; and by Jackman *et al.* from the sources and sinks.

## HYDROGEN SPECIES

Since OH has a strongly increasing mixing ratio with height, the measured signal is generally dominated by emissions from higher altitudes and consequently remote sensing techniques are most sensitive at altitudes below the instrument but above about 30 km. The recovered OH abundances are progressively less accurate below this altitude.

Both the Carli and Traub instruments have OH data from two flights each, which have not yet been fully analyzed. However the following qualitative results are available:

During the BIC-2 campaign on 20 June 1983, both instruments were launched at Palestine, Texas at the same time but on different gondolas. The measurement of OH near  $118\text{ cm}^{-1}$  provides a common point of comparison. On the basis of repeated observations along upward-looking lines of sight, from early afternoon to about midnight, a monotonically decreasing signal is seen, in accord with theoretical expectations. The nighttime signal levels out at a fraction of the daytime signal, indicating that there is still a measurable amount of OH above the balloon. This is also in accord with theoretical models, which, although predicting a strong decrease in stratospheric OH after sunset, also predict a modest increase in mesospheric OH near 80 km, which can account for the detected signal.

Preliminary profile calculations indicate that meaningful concentration measurements can be obtained down to about 25 km from a float altitude of about 38 km.

A final instrument uses an *in situ* fluorescence method similar to that used to make the first OH measurements [Anderson, 1976] except that the resonance lamp is replaced by a laser system. Radiation from a frequency-doubled dye laser, pumped by a Cu vapor laser, is tuned to a number of specific OH absorption features near 282 nm and illuminates a multipath cell through which the atmospheric sample flows. The OH concentration is measured by its induced fluorescence as the balloon descends. The instrument is calibrated in the laboratory by simulating a flow under stratospheric conditions and injecting known quantities of OH into the measurement volume. This instrument can, in principle, provide OH measurements from balloon float altitudes down to the upper troposphere. Although it has been flown once, no results from this instrument are available at the time of writing this report.

### 9.1.2 Inferred OH Profiles

Pyle *et al.* [1983] derived an OH profile based on the ratio of  $\text{HNO}_3$  to  $\text{NO}_2$  using LIMS observations. The photochemical equilibrium between these species breaks down in the lower stratosphere, however, and the LIMS  $\text{HNO}_3$  measurements do not appear to be consistent with other measurements above about 35 km [Gille *et al.*, 1984b, Jackman *et al.*, 1985a].

An alternative approach is to assume equilibrium between total sources and sinks of OH. If the source and sink terms can then be constrained by observations, the equilibrium OH profile can be derived. This approach has been used by Pyle and Zavody [1985a] and by Jackman *et al.* [1985a], using 2-D models with full chemistry, constrained by LIMS and SAMS observations of  $\text{O}_3$ ,  $\text{H}_2\text{O}$ ,  $\text{HNO}_3$ ,  $\text{NO}_2$ ,  $\text{CH}_4$  and temperature. The resulting profiles for  $32^\circ\text{N}$  in winter from these studies and from the  $\text{HNO}_3/\text{NO}_2$  ratio are shown in Figure 9-1b.

### 9.1.3 Ground Based OH Measurements

Column amounts of OH have been obtained, by Burnett and Burnett (1983a), with a Pepsios spectrometer measuring solar absorption of the P1(1) (0.0) line at 308.2 nm. The high resolution and luminosity

of this instrument enables it to clearly distinguish the sharp terrestrial OH absorption feature from the relatively broad solar Fraunhofer lines. Uncertainty, due to statistical noise for a single 3-minute line scan at a solar zenith angle of  $30^\circ$  is about 10%.

The total vertical column abundance,  $N_v(\text{OH})$  ( $\text{cm}^{-2}$ ) is derived from the slant path absorption measurements using an independently determined oscillator strength, the appropriate rotational population distribution for middle atmospheric temperatures, and the geometric correction to the vertical column [Burnett and Burnett, 1981]. Uncertainty in these factors should not total more than a few per cent. Since absorption measurements are inherently relative, the method provides absolute values for the column amounts.

Figure 9-2 shows the hydroxyl radical profile from 16-90 km from the model of Solomon and Garcia for the daytime average at  $37^\circ\text{N}$  in summer. It can be seen that the total column density of OH in the stratosphere (16-48 km) and mesosphere (48-90 km) are approximately equal. The column density of OH in the troposphere is assumed to be approximately 9% of the total.

The OH column abundances observed at Fritz Peak Observatory in Colorado in 1981-82 are shown in Figure 9-3 as a function of the solar zenith angle,  $\chi$ . About 1000 sets of data were taken, representing approximately one third of the days of each season. The bars represent the standard error of the mean and the curve represents the best empirical fit to the data.

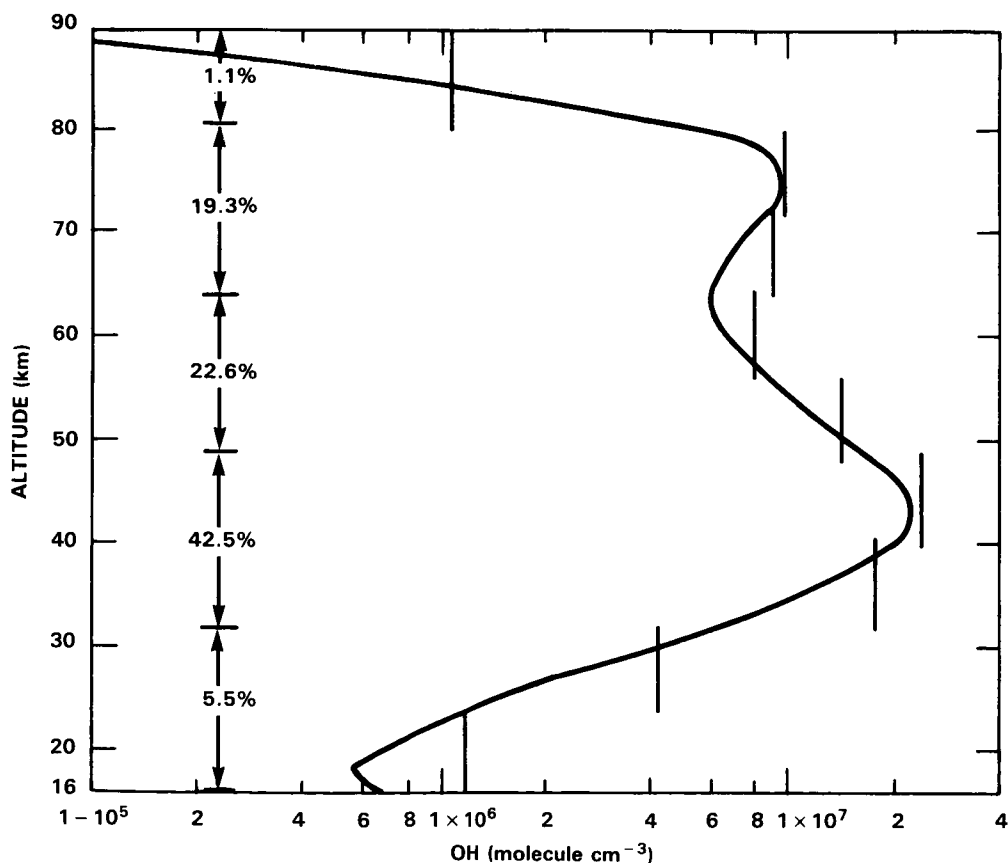


**Figure 9-2.** Hydroxyl profile from 16-90 km from the model of Solomon and Garcia. OH number density ( $\text{molecule cm}^{-3}$ ) for the daytime average at  $37^\circ\text{N}$  in summer. The tropospheric column of OH is assumed to be approximately 9%.

## HYDROGEN SPECIES

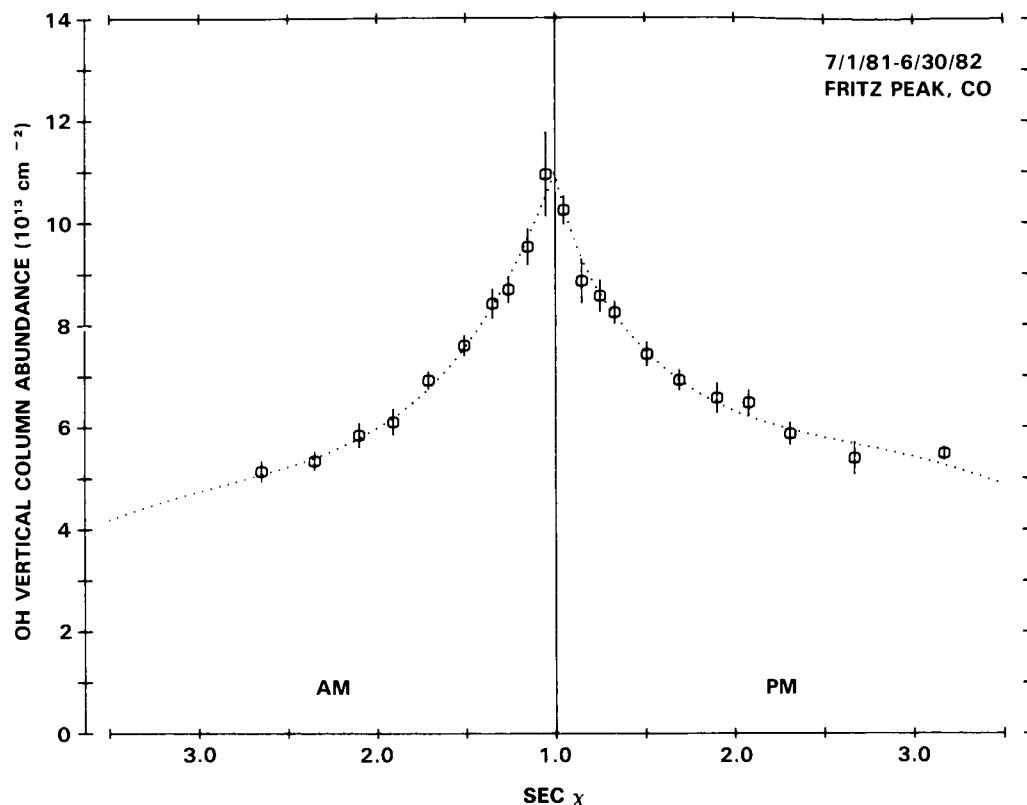


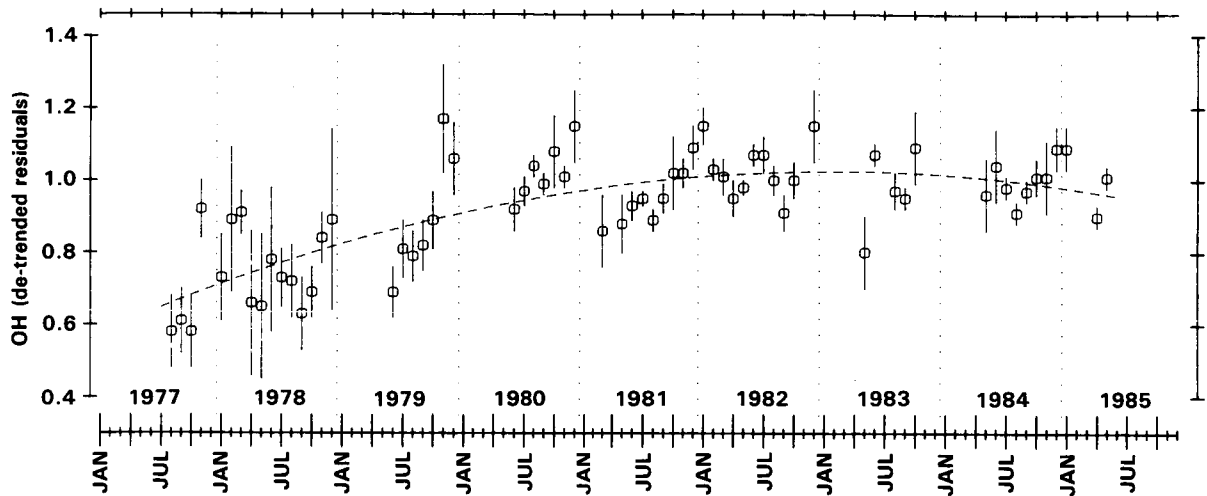
**Figure 9-3.** OH vertical column abundances, July 1, 1981, to June 30, 1982. A full year of OH data taken between July 1981 and June 1982 is shown plotted as a function of  $\sec \chi$ , where  $\chi$  is the solar zenith angle. The averages were determined with each month's average for a given  $\sec \chi$  weighted equally in order to compensate for varying number of data sets per month. (Burnett and Burnett, 1984).

The dependence of the column abundance on solar zenith angle is in accord with photochemical theory. The total measured column abundances are also in general agreement with theory. For example, the column abundances for a solar zenith angle of  $30^\circ$  ranged from  $6.6 \times 10^{13} \text{ cm}^{-2}$  in 1977-79 to  $9.4 \times 10^{13} \text{ cm}^{-2}$  in 1981-1982.

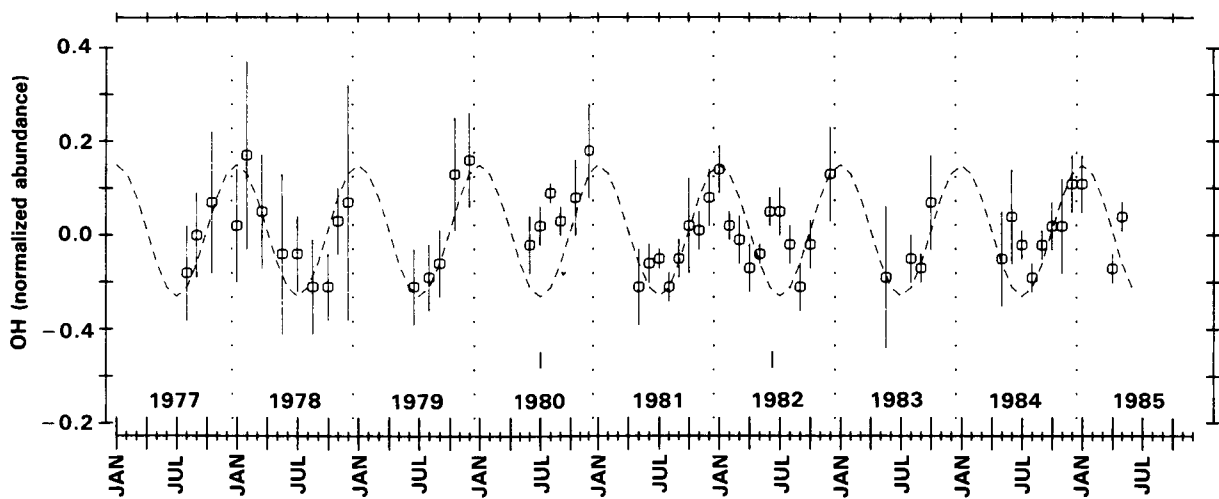
The long-term variability can best be seen from the "normalized abundances" obtained by dividing the observed abundances by the values on the empirical  $\sec \chi$  distribution curve, a procedure which, to a first approximation, eliminates the  $\chi$ -dependence. Figure 9-4a shows the normalized abundances at Fritz Peak during 1977-1984. The levels appear to have increased in the 1977-1980 period, coinciding with the approach to maximum solar activity in the solar cycle [Burnett and Burnett, 1982]. The dashed line in the figure represents one empirical fit to the data, showing a 30% increase. Photochemical models do not predict this trend.

Figure 9-4b shows a seasonal variation of 28%, with winter maxima and summer minima obtained when the long term variation is subtracted from the normalized abundances [Burnett and Burnett, 1984]. The seasonal variation appears to be independent of the long term change. Seasonal temperature changes in the OH rotational population distribution, and seasonal variations in incident solar radiation can account for part of this variation, but a seasonal OH abundance variation of about 21% remains, which must be due to other seasonal changes in atmospheric behavior. Recently observed (LIMS and SAMS data) seasonal cycles in stratospheric  $\text{O}_3$ ,  $\text{H}_2\text{O}$ ,  $\text{NO}_2$  and  $\text{CH}_4$  may lead to substantial variation in OH.

## HYDROGEN SPECIES



**Figure 9-4a.** Normalized monthly OH abundances, 1977-1985 at Fritz Peak Observatory, Colorado (40°N, 105°W). OH abundances have been normalized with respect to the best fit curve representing the 1981-82 AM data. Bars represent the standard error of the mean  $\sigma/\bar{N}$ . The dashed line is one empirical fit to the long term trend.



**Figure 9-4b.** OH residual abundances: seasonal variation, 1977-1985. The empirical long term trend has been removed from the normalized OH abundances from Figure 9-4a. While most departures from the seasonal curve may be attributed to experimental uncertainty, the deviations which appear in summer 1980 and 1982 may be related to the volcanic eruptions of Mount St. Helens and El Chichon, respectively.

## HYDROGEN SPECIES

Column abundances measured at Fritz Peak show a morning (AM) and afternoon (PM) dependence. The AM-PM asymmetry has a large persistent seasonal variation [Burnett and Burnett, 1984]. AM abundances exceed PM abundances in the Spring; PM abundances exceed AM abundances in the fall. Figure 9-5 shows the asymmetry to vary seasonally with an amplitude of 27% around a 7% offset favoring PM abundances. The phase of this behavior is shown in the figure to be identical to that for the seasonal variation in total ozone at this latitude. However, the asymmetry behavior appears to depend on location since the Florida data seems to lack the seasonal behavior. Since such temporal variations can only occur where the lifetimes for the  $\text{HO}_x$  family are longer than 2 hours, these observations indicate a large contribution of mesospheric OH to the measured column abundances.

The column abundances show other geographical differences. The abundances measured during the winter and spring of 1980 at Boca Raton, FL ( $26^\circ\text{N}$ ,  $80^\circ\text{W}$ ) were 40% greater than those measured at

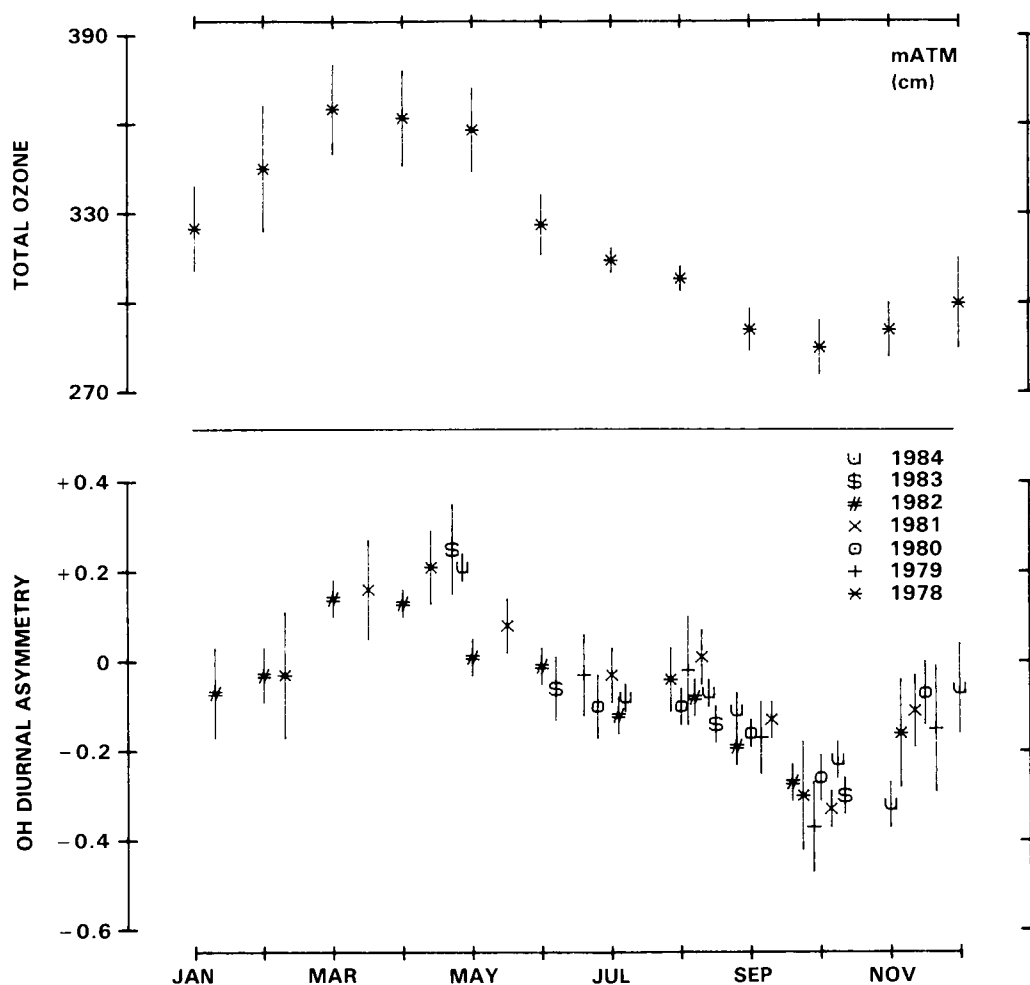


**Figure 9-5.** Average diurnal asymmetry: 1978–1984. The differences between the average morning residual abundances,  $R_{\text{AM}}$  and the PM residual abundance  $R_{\text{PM}}$  are plotted by month. A difference of  $-0.20$  would be interpreted as a month in which afternoon abundances were 20% higher than the corresponding morning values. Data for local noon  $\pm 1$  hour have been omitted. The 1978–1982 Boulder ozone measurements by R. Grass, NOAA, Geophysical Monitoring for Climatic Change (personal communication, 1983), are shown for comparison.

Fritz Peak, CO during the same period although the measurements made during the same period in 1983 were essentially identical at both locations. Measurements made at Poker Flat, AK (65°N, 148°W) during the summer of 1983 were some 30% higher than those observed at Colorado and Florida for the same zenith angles.

Interesting observations were made during the volcanic eruptions in May, 1980 and April, 1982. Burnett and Burnett [1984] observed a positive OH column perturbation of 30% in the edge of the El Chichon cloud in 1982.

The observations made during the partial solar eclipse of May, 1984 were quite unexpected. The measurements made during the eclipse, compared with the average of those made during the preceding 3 days are shown in Figure 9-6. There is an initial decrease in the total column of about 50% followed by recovery and an overshoot of nearly the same magnitude before the end of the eclipse. The continuing transient following the eclipse is increasingly damped, approaching baseline values 2-hour after eclipse [Burnett and Burnett, 1985]. These surprisingly large changes in transient column OH abundances provide a challenging time-dependent test for theoretical models.

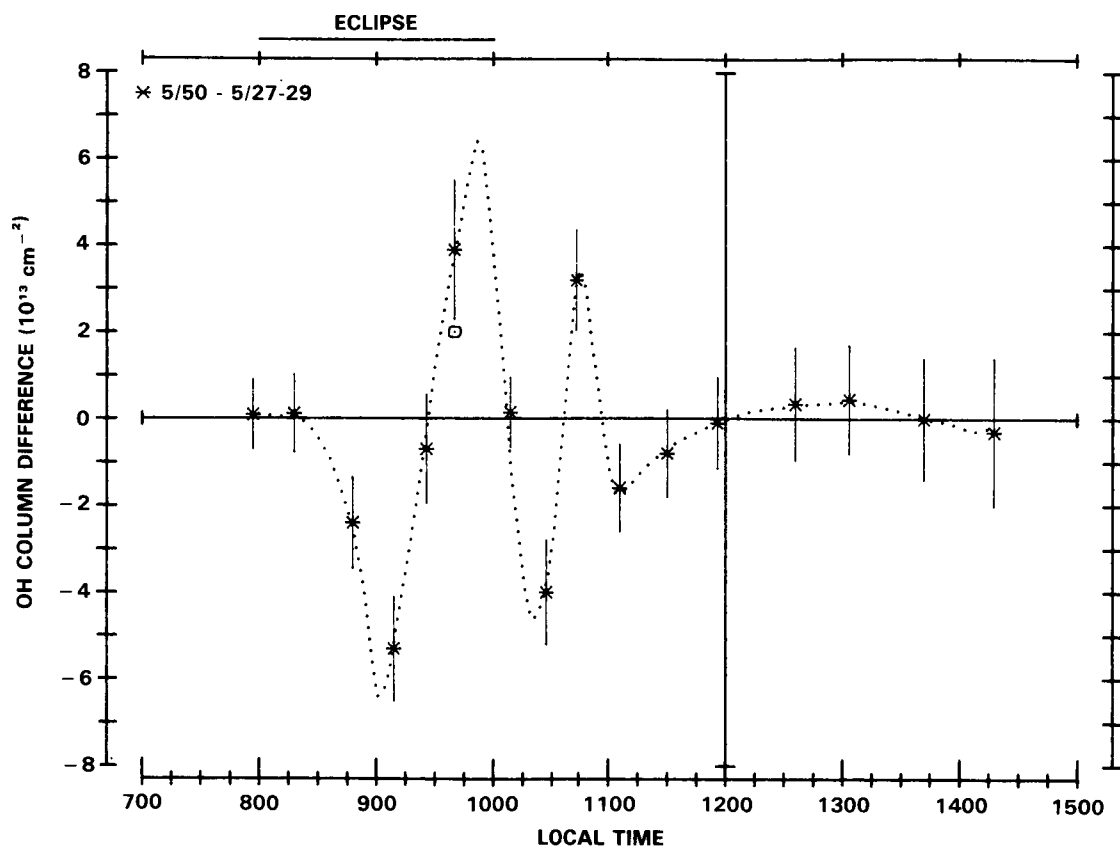


**Figure 9-6.** OH vertical column abundance departures from baseline values for the partial eclipse event of May 30, 1984.  $N_v = N_v(5/30) - N_v(5/27-29)$ , where  $N_v(5/30)$  are the OH abundance data for 5/30 and  $N_v(5/27-29)$  is the corresponding average baseline for the 5/27, 28 and 29 data. An alternative point,  $\square$ , is shown for the possible interpretation of a smoother baseline at 0945 LT. The abundance drop of  $5 \times 10^{13}/\text{cm}^2$  and subsequent overshoot during the eclipse period are evident. These excursions and the transient oscillation after the termination of the eclipse are several times the observational uncertainties. The dashed curve is thought to be a good representation of this oscillatory behavior (Burnett and Burnett, 1985).

## HYDROGEN SPECIES

### 9.2 HYDROPEROXYL (HO<sub>2</sub>) MEASUREMENTS

#### 9.2.1 *In situ* Vertical Profile Measurements of HO<sub>2</sub>

The balloon-borne, *in situ*, cryogenic sampling technique for HO<sub>2</sub> measurements described by Mihelcic, *et al.* [1978] has been improved and used in a series of flights by Helten, *et al.* [1984a; personal communication, 1985] to obtain vertical profile data over the range 16 to 34 km. Observations have been conducted during September and October of 1980 and 1983 over Aire sur l'Adour in southern France (44°N).

The cryogenic sampling technique traps all free radicals on a liquid nitrogen cooled, gold plated, copper finger in a matrix of H<sub>2</sub>O or D<sub>2</sub>O. Up to 10 samples may be collected in sequence during a controlled balloon descent and a vertical resolution of about 3 km is typically obtained. The matrix is isolated and free radical samples are returned to a laboratory for identification and determination of concentration via electron spin resonance spectroscopy.

The signals assigned to HO<sub>2</sub> also include other peroxy radicals, RO<sub>2</sub>. However, the most abundant of these radicals in the stratosphere is CH<sub>3</sub>O<sub>2</sub> and model calculations predict that the concentrations of these radicals are less than 10% as large as the HO<sub>2</sub> concentrations and can therefore be neglected within the uncertainties of the measurements.

Only three data points from the two flights in 1980 have been published to date (Helten *et al.*, 1984a). The overall uncertainty in the measured concentrations is estimated by the authors to be  $\pm 40\%$  for this published data.

Due to technical modifications associated with the other flights, remaining recent data may be subject to small changes in calibration. The results of these flights are reported here, with the caveat that the uncertainties and the accuracy are subject to change once the calibration factors have been finally determined. The authors expect to reduce the overall uncertainty to a value of less than 25% for this data.

The preliminary data from Helten *et al.* (personal communication, 1985) is shown in Figure 9-7. In general the flights reached a maximum altitude of about 34 km and the controlled descent was initiated after dawn at a rate of about 1 m/s. The measurements which were made at high solar zenith angle are shown as open symbols. Since theoretical models predict negligible quantities of HO<sub>2</sub> near 30 km before dawn, rising rapidly over  $\sim 3$  hours to values within  $\sim 25\%$  of the midday maximum, interpretation of the Helten *et al.* data requires input from diurnal modeling to adjust the data to a vertical HO<sub>2</sub> profile at the same time of day. The primary effect will be to shift the data above 25 km to higher values. It should be noted that the 1-D model profile in Figure 9-7 represents the midday maximum mixing ratio, while the 2-D model profiles represent the seasonal range (winter-summer) of the daytime average mixing ratio.

#### 9.2.2 Ground Based HO<sub>2</sub> Measurements

A ground based mm wave rotational emission line measurement reported by de Zafra, *et al.* (1984) provides a measure of HO<sub>2</sub> column amounts above 35 km. A triplet of transitions, spaced about 40 MHz apart near 265.7 GHz, was observed, using a cryogenically cooled mm-wave heterodyne receiver located at Mauna Kea, Hawaii (19.5°N). The measurement was made over several days in late September and early October, 1982.

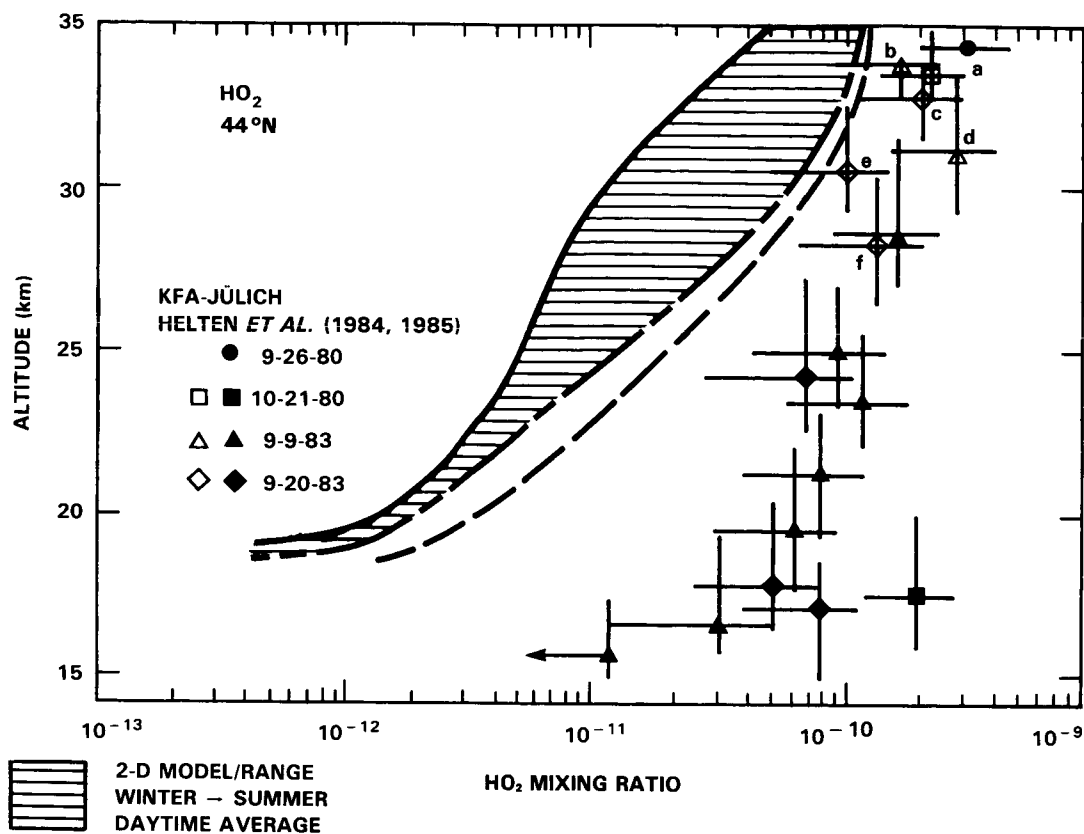


**Figure 9-7.** *In situ* observations of HO<sub>2</sub>, employing the matrix isolation technique of Helten *et al.* (1984a). The samples were collected during several balloon flights at local time between sunrise and approximately noontime. Data for observations made within 3 hours after sunrise are plotted with open symbols, because they should be adjusted (upward in mixing ratio) due to the rather strong diurnal variation of HO<sub>2</sub> within this time period. The zenith angle for these samples are as follows: a: 88.1-78.1; b: 62.3-53.3; c: 95.8-83.9; d: 55.0-46.6; e: 86.8-77.2; f: 80.7-70.5. The dashed line represents a typical altitude profile for HO<sub>2</sub> at midday calculated by Prather using a one-dimensional photochemical model.

In the mm wave emission technique the absolute intensity and the pressure broadened line shape of molecular rotational emission lines are measured. The frequency resolution available allows precise measurements of pressure broadened line shapes. The integrated line intensity is proportional to the molecular column density. Vertical profile information is obtained by best fitting the observed line shape to assumed profiles. In the altitude range below approximately 70 km, where pressure broadening dominates Doppler broadening, each small altitude increment contributes a Lorentzian line shape whose intensity is determined by molecular concentration and whose width is determined by the mean pressure over the altitude increment. The authors estimate that their method is insensitive below 35 km due to the low concentrations of HO<sub>2</sub> in this region of the atmosphere. Below this altitude, the signal attributed to the total lineshape is too weak and broad to be clearly distinguished from baseline curvature of instrumental origin which may be present in the output. This ground based data therefore shares only a small region of overlap with *in situ* balloon-borne measurements [Mihelcic *et al.*, 1978; Anderson, *et al.*, 1981; Helten *et al.*, 1984a; personal communication, 1985].

To minimize the effect of diurnal variation on the measurement value, observing was started about four hours after sunrise each day and continued no later than one hour before sunset. On the basis of

## HYDROGEN SPECIES

full diurnal models by Ko and Sze (1983) and Froidevaux (1983), the authors estimate that a 10-15% correction should be applied to their integrated results when comparing to a theoretical midday peak.

The accuracy of these ground-based results depends on calibration of the mm wave receiver sensitivity and the accuracy with which tropospheric attenuation by water vapor can be determined. The authors estimate the overall, one-sigma, uncertainty for these effects, combined in quadrature, to be 15%. A further uncertainty affecting conversion of the observed line shape and emission intensity to a correctly scaled vertical profile arises from lack of an accurate measure of the pressure broadening coefficient for HO<sub>2</sub> in air. Measured coefficients for other molecules lead to an error estimate of  $\pm 10\%$  from this source. Combination of this uncertainty with that above, again in quadrature, results in an overall estimate of 18% for the total one-sigma error involved in determining column densities above 35 km from the measured data.

The error within which the mixing ratio may be determined at any given altitude depends on that altitude, being worst at the extremes covered here. The strongest of the three measured transitions is compared with the vertical profiles a, b, and c of Figure 9-8 in Figure 9-9. The signal-to-noise ratio of the data seems clearly sufficient to distinguish between vertical profiles a, b, and c in the region above 35 km. It clearly agrees best with profile a. The first of these is typical of profiles obtained using the faster O + HO<sub>2</sub> rates currently used and first recommended in JPL 82-57, while the second is typical of the older values recommended in WMO (1982). Profile c is an arbitrary profile designed to accommodate the much higher

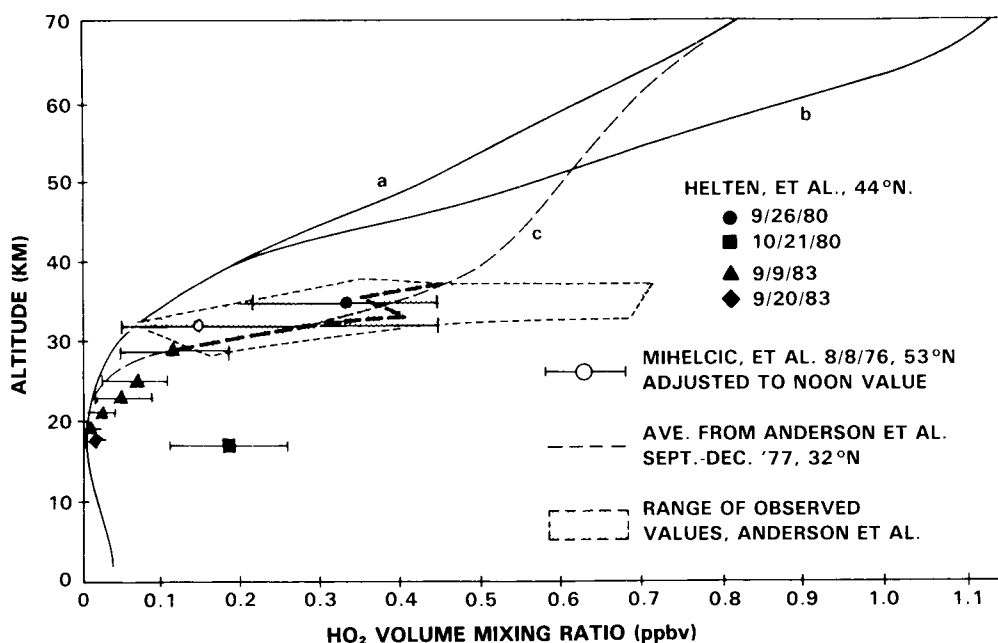


**Figure 9-8.** Theoretical midday mixing ratios for 30°N as a function of altitude, compared with data. Curves a, b, and c define synthesized lineshapes and amplitudes compared against ground based mm data in Figure 9-9. Curve (a) is typical of recent 1 and 2-D models using JPL 82-57 chemistry and curve (b) is typical of the same models using WMO (1982) or similar chemistry embodying a slower reaction rate for O + HO<sub>2</sub>. Curve (c) is an arbitrary profile chosen to blend typical lower altitude data with mesospheric theory predictions. Experimental values of Helten *et al.* (1984a; personal communication, 1985) are limited to those with a mean solar zenith angle of  $\sim 55^\circ$ N and would be subject to relatively small diurnal corrections to midday values. Data of Anderson *et al.* (1981) were taken near local noon. (Adapted from de Zafra, *et al.*, 1984).

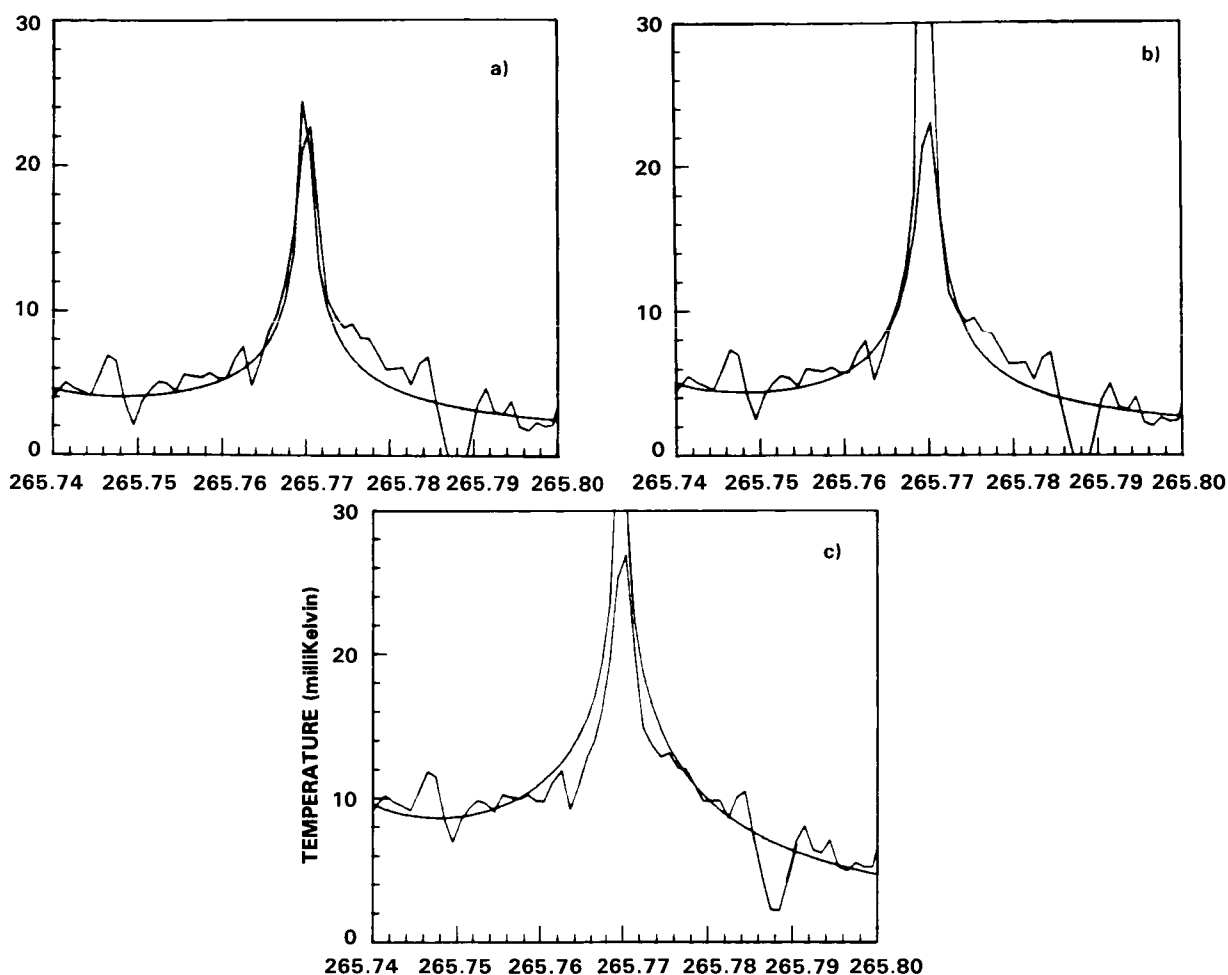


**Figure 9-9.** Observed  $\text{HO}_2$  lineshape of the strongest component from the line triplet at 265 GHz after removal of contributing background from all species except  $\text{HO}_2$ . The smooth line profiles in a, b, and c have been synthesized from the corresponding vertical profiles of Figure 9-8. The ordinates are in milliKelvin equivalent blackbody radiation and the abscissa in GHz. The required diurnal correction of + (10–15)% to midday values (see text) has not been made to the experimental data. This compensates for a positive correction of approximately equal magnitude, also not applied, to convert theoretical mixing ratios for 30°N (from Figure 9-8) to 20°N for comparison with this data. (From de Zafra, *et al.* 1984). Baselines appear to vary from (a) to (c) due to the influence of line wings from the two other members of the triplet lying to the left as the assumed vertical distribution changes.

*in situ* values of  $\text{HO}_2$  mixing ratio reported at lower altitudes by Anderson, *et al.* (1981) and the more recent results from Helten, (personal communication, 1985) merging with the theoretical values at 60–70 km. There is clearly an inconsistency between the ground-based and *in situ* measurements of  $\text{HO}_2$ .

### 9.2.3 Comparisons of Theory and Observations for $\text{HO}_2$

The *in situ* measurements in the 20–35 km range are difficult to reconcile with current theory, being higher than modelled concentrations by factors ranging from more than 2 at 35 km to about 10 below 25 km. Such high concentrations of  $\text{HO}_2$ , along with current reaction rate coefficients, would lead to predictions of  $\text{H}_2\text{O}_2$  and  $\text{HNO}_4$  concentrations well above the observed upper limits.

## HYDROGEN SPECIES

Significant problems are encountered in reconciling the high measurements of HO<sub>2</sub> with the low measurements of OH reported in Section 9.2.1. The ratio of HO<sub>2</sub> to OH is thought to be well understood and to depend mainly on the reactions of HO<sub>2</sub> with NO and O<sub>3</sub> and the reaction of OH with O<sub>3</sub>. If the HO<sub>2</sub>/OH ratio is anywhere near as large as that obtained by combining the HO<sub>2</sub> data of Helten *et al.* and the OH data of Heaps and McGee, substantial changes in currently accepted chemistry will be required. In fact, converting all the OH to HO<sub>2</sub> does not yield sufficient HO<sub>2</sub> to agree with the measurements. Since the main destruction process for the termination of the HO<sub>x</sub> chain above 30 km is the recombination of OH and HO<sub>2</sub>, a reduction in the rate coefficient for this recombination reaction in order to increase the predicted HO<sub>2</sub> concentration would also increase the predicted OH concentration, further increasing the discrepancy with the measurements of Heaps and McGee. If substantial changes are required in our description of HO<sub>x</sub> chemistry then our understanding of the ozone budget would be significantly impacted since HO<sub>x</sub> reactions currently account for as much as half of the ozone loss below 25 km, and OH and HO<sub>2</sub> strongly influence the atmospheric chemistry of nitrogen and chlorine species.

### 9.3 HYDROGEN PEROXIDE (H<sub>2</sub>O<sub>2</sub>) MEASUREMENTS

Hydrogen peroxide is theoretically expected in the stratosphere at concentrations within the detection range of several current techniques. However, attempts by three separate groups have failed to make conclusive detection of this molecule. Current 2D theoretical models predict that, at mid-latitudes, H<sub>2</sub>O<sub>2</sub> should have a mixing ratio peak in the 30 to 35 km range, and should vary seasonally from a summer high of about 0.35 ppbv to a winter low of about 0.15 ppbv. The diurnal variation in this altitude range is predicted to be about 10 percent at most, with a maximum at night.

A tentative detection of H<sub>2</sub>O<sub>2</sub> was reported by Waters *et al.* (1981) using a balloon-borne, microwave limb sounding spectrometer, looking at the thermal emission from a rotational line at 205 GHz (1.5 mm wavelength). The reported value was  $1.1 \pm 0.5$  ppbv in a layer between about 27 and 35 km (in February at 32°N) which is nearly an order of magnitude larger than current theoretical values for this altitude range and season. This tentative detection has not been confirmed in subsequent attempts.

Chance and Traub (1984) reported an altitude-dependent upper limit for H<sub>2</sub>O<sub>2</sub>, using a limb sounding, balloon-borne, far-infrared Fourier transform spectrometer looking at the 112.2 cm<sup>-1</sup> rotational Q branch in thermal emission. The observations were made in January at a latitude of 34°N. The altitudes of the six layers examined ranged from about 22 to 38 km. The most sensitive region of comparison with theoretical models was in the 26 to 34 km range where the measured upper limits of H<sub>2</sub>O<sub>2</sub> ranged from 0.05 to 0.14 ppbv. These limits were set by background noise in the spectra and represent twice its standard deviation; in no instance was a clearly identifiable spectral feature observed which exceeded this noise level. These upper limits are shown in Figure 9-10, along with four theoretical curves for the appropriate season and latitude. Each of these models uses the NASA-JPL (1985) kinetic and photochemical rate coefficients (see Appendix A). With future improvements, this technique should be adequate to detect the higher concentrations expected in summer at the same latitude.

An upper limit for H<sub>2</sub>O<sub>2</sub> was reported by de Zafra *et al.* (1985b) using a ground-based millimeter wave spectrometer looking for a 270 GHz (1.1 mm wavelength) rotational line in thermal emission. The measurements were made in May and June from Mauna Kea, Hawaii (20°N). After 55 hours integration, no signal was detected above the background noise. The authors have interpreted this null result in terms of the signal intensity to be expected from a particular model profile, compared against the noise level reached during data integration. They conclude that no more than twice the H<sub>2</sub>O<sub>2</sub> mixing ratio predicted over the 30-50 km range for a model output for 19°N by Sze and Ko (using JPL 82 chemistry) would

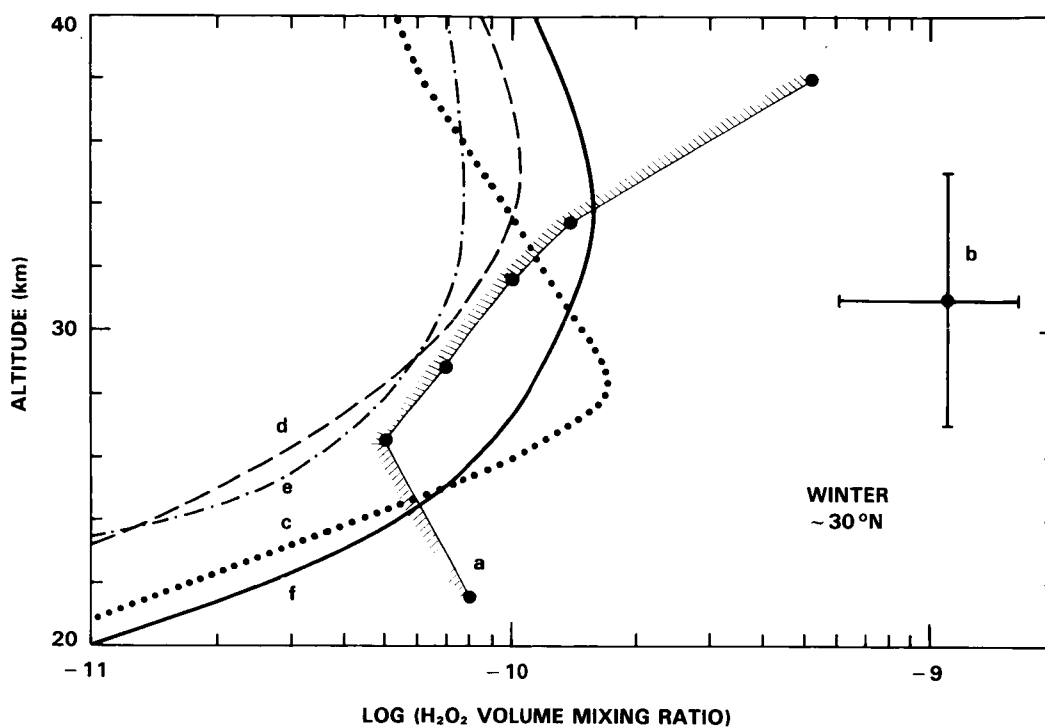


**Figure 9-10.** (a)  $\text{H}_2\text{O}_2$  measured upper limits by Chance and Traub (1984) for January at  $34^\circ\text{N}$  from balloon-borne far IR spectroscopy.

(b)  $\text{H}_2\text{O}_2$  tentative detection by Waters *et al.* (1981), for February at  $32^\circ\text{N}$  from balloon-borne microwave limb sounding spectroscopy.

For comparison, four  $\text{H}_2\text{O}_2$  theoretical profiles are shown, each using 2-D calculations and JPL-1985 reaction rate data, for winter at  $30^\circ\text{N}$ :

- (c) A. Owens, private communication.
- (d) S. Solomon and R. Garcia, private communication.
- (e) P. Guthrie, private communication.
- (f) M. Ko, private communication.

The relatively large dispersion in theoretical values may be largely attributable to relatively small differences in assumed abundances of  $\text{O}_3$ ,  $\text{NO}_2$  and  $\text{H}_2\text{O}$ , as discussed by Connell *et al.* (1985).

have been detectable with a signal-to-noise ratio of one. At 32 km, where the theoretical  $\text{H}_2\text{O}_2$  mixing ratio profile has the peak theoretical value, this implies a one-standard-deviation upper limit of about 0.5 ppbv.

The abundance and vertical distribution of  $\text{H}_2\text{O}_2$  is very sensitive to variations in the long-lived trace species  $\text{O}_3$ ,  $\text{NO}_y$ , and  $\text{H}_2\text{O}$ . The range of theoretical variation in  $\text{H}_2\text{O}_2$  mixing ratios allowed by known or probable variabilities in these species has been addressed by Connell, *et al.* (1985) using a diurnally average 1-D model. Their results, which extend over the range 15-35 km, are shown as the shaded region in Figure 9-11. They conclude that temporal variations as large as a factor of 4 to 5 may be expected within the altitude range considered. Since these calculations assumed NASA-JPL (1981) kinetic parameters they should not be compared too rigorously with the other profiles shown in the figures but should be taken to indicate the range of variability expected. The inclusion of error limits in these quantities would extend the region of variability or uncertainty shown in Figure 9-10.

## HYDROGEN SPECIES

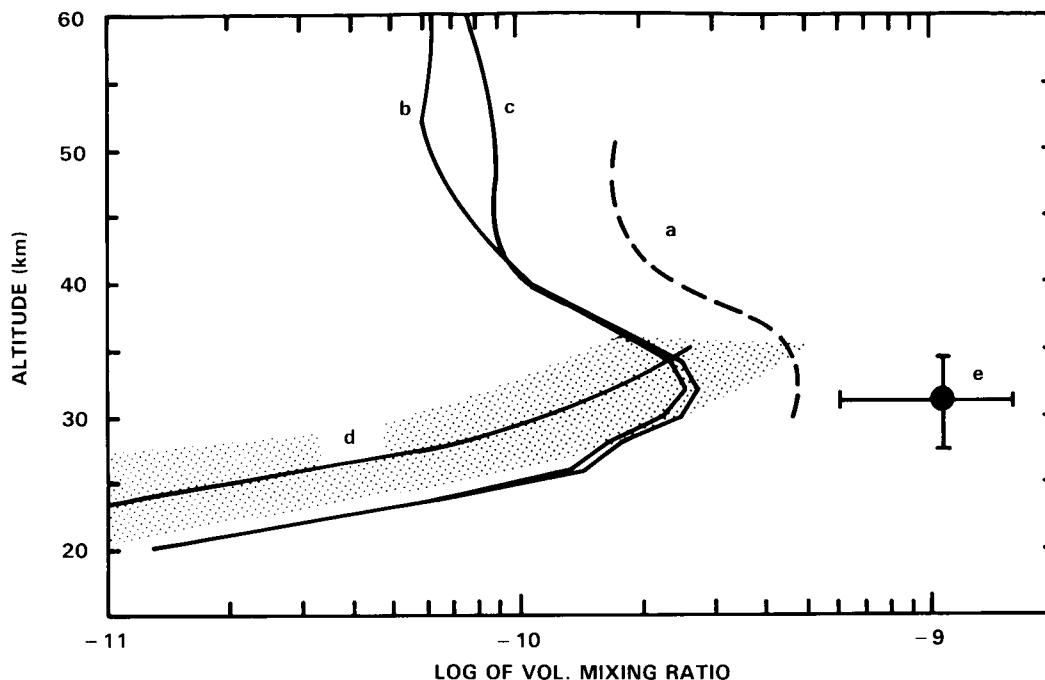


**Figure 9-11.** (a)  $\text{H}_2\text{O}_2$  measured upper limit by de Zafra *et al.* (1985b), for May–June at  $20^\circ\text{N}$  from ground-based mm wave emission spectroscopy. (b) Day and (c) Night  $\text{H}_2\text{O}_2$  theoretical profiles, using 2-D calculations and JPL 82-57 reaction rate data, for the same season and latitude (D. Sze and M. Ko, private communication, (1983). (d) Diurnally-averaged 1-D theoretical  $\text{H}_2\text{O}_2$  profile using JPL 81-3 reaction rate data (Connell *et al.*, 1985); the shaded region shows the possible range of values of  $\text{H}_2\text{O}_2$  from variations in  $\text{O}_3$ ,  $\text{NO}_2$  and  $\text{H}_2\text{O}$ . (e)  $\text{H}_2\text{O}_2$  tentative detection by Waters *et al.* (1981), for February at  $32^\circ\text{N}$  from balloon-borne microwave limb sounding spectroscopy.

In summary, there has not yet been any clear detection of stratospheric  $\text{H}_2\text{O}_2$  despite initial attempts by three groups using different techniques, spectral features and seasons. Judged both by modelling predictions and by the upper limits set by two of these detection efforts, the tentative detection reported by Waters *et al.* appears to be either an anomalous event or an erroneous identification. With improvements in detection techniques measurements of this species are anticipated in the near future.

### 9.4 WATER ( $\text{H}_2\text{O}$ ) MEASUREMENTS

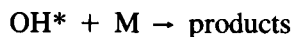
#### 9.4.1 *In Situ* Vertical Profile Measurements of $\text{H}_2\text{O}$

There are two important results that have emerged from *in situ* observations since WMO (1982). The first of these deals with the question of the existence and location of a hygropause or minimum in the mixing ratio of  $\text{H}_2\text{O}$ . The hygropause was first seen in *in situ* data and has now been confirmed by LIMS satellite results which show that the region of minimum  $\text{H}_2\text{O}$  in the lower stratosphere extends from  $\sim 30^\circ\text{N}$  to  $30^\circ\text{S}$  and up to  $\sim 40$  mbar (22 km). The second result concerns the degree of water vapor stratification with altitude in the stratosphere. Both of these points will be discussed in more detail later.

There are two *in situ* measurements techniques which have been used. The first of these, the Ly- $\alpha$  hygrometer (Kley and Stone, 1978) is based on the dissociation of  $\text{H}_2\text{O}$  by Ly ( $\alpha$ ) (121.6 nm) radiation to produce electronically excited  $\text{OH}^*$  radicals.



The intensity of the  $\text{OH}^* \rightarrow \text{OH} + h\nu'$  fluorescence is a measure of the  $\text{H}_2\text{O}$  mixing ratio. The accuracy of the method depends on the accuracy with which the cross section ( $\sigma$ ) of water at 121.6 nm is known. Kley (1984) has measured  $\sigma$  and estimated the accuracy,  $\Delta\sigma/\sigma$  to be 6% at the 95% confidence level. The accuracy is also a function of pressure and, therefore, of altitude. This is because the quenching process:



is pressure dependent. The rate coefficient for quenching is estimated to be known with an accuracy of  $\pm 20\%$ . This error source does not influence the total accuracy of the instrument in the lower stratosphere but becomes the major source of uncertainty at altitudes above 38 km. Other sources of error are considered to be small. These include contamination effects, i.e., possible contributions to the signal from water carried aloft with the instrument or balloon. During the main measurement period the instrument is deployed on a rapidly descending parachute where any balloon wake is absent.

Table 9-1 gives the total estimated accuracy (63% confidence) as a function of height. ( $X$  = mixing ratio,  $\sigma$  = estimated fractional percentage total error, including precision).

**Table 9-1.** Accuracy of the Ly ( $\alpha$ ) Hygrometer for Various Altitudes (%)

$z$ (km)	10	15	20	25	28	30	38	40
$\sigma X/X$	7.0	7.0	7.0	7.0	7.3	7.5	10.0	12.7

The precision of the Ly- $\alpha$  hygrometer is 2% (one sigma standard deviation at typical stratospheric mixing ratios for integration times of 1 second). If small scale variability is observed, it is considered to be real if the amplitude exceeds 0.2 ppmv at a mean value of  $\sim 5$  ppmv.

The second method is the frost-point hygrometer (Mastenbrook, 1968). This technique operates on the principle that an equilibrium exists between the water vapor pressure in the atmosphere and an ice surface at the frost-point temperature. The instrument has been used extensively in past soundings and recently (1977) was redesigned to incorporate solid state circuitry and to develop an instrument for routine measurements by a monitoring network. NOAA has made monthly soundings from Boulder, Colorado, with the new instrument since 1981 (Mastenbrook and Oltmans, 1983). A conservative estimate of the  $\text{H}_2\text{O}$  mixing ratio accuracy is  $\pm 17\%$  ( $\pm 1^\circ\text{C}$  frost point temperature).

Eight profiles of water vapor across the tropical tropopause have been reported by Kley *et al.* (1982, 1983). These were obtained during the NASA sponsored Stratospheric-Tropospheric Exchange-Experiment in 1980. Figure 9-12 shows the mean profiles for water vapor and temperature measured on the eight flights. The mean water vapor mixing ratio of the hygropause was 3.4 ppmv with a standard deviation of 0.24 ppmv. Table 9-2 gives a list of tropical soundings of the mixing ratio of water vapor at the hygropause by *in situ* instruments.

## HYDROGEN SPECIES

Table 9-2. Mixing Ratio of Water Vapor at the Hygropause

Hygropause Mixing Ratio	Location	Time of Measurement	Reference
3.4	Trinidad W.I.	monthly, 1964 and 1965	Mastenbrook, (1968)
2.7	Brazil	27 Sept 1978	Kley <i>et al.</i> (1979)
3.4	Panama	8 values Aug/Sept 1980	Kley <i>et al.</i> (1982, 1983)
3.1	Wyoming*	Feb. 1 1979	Danielsen and Kley (1985)

\*As discussed by Danielsen and Kley (1985), the air traveled to Wyoming from the tropics in about 5 days.

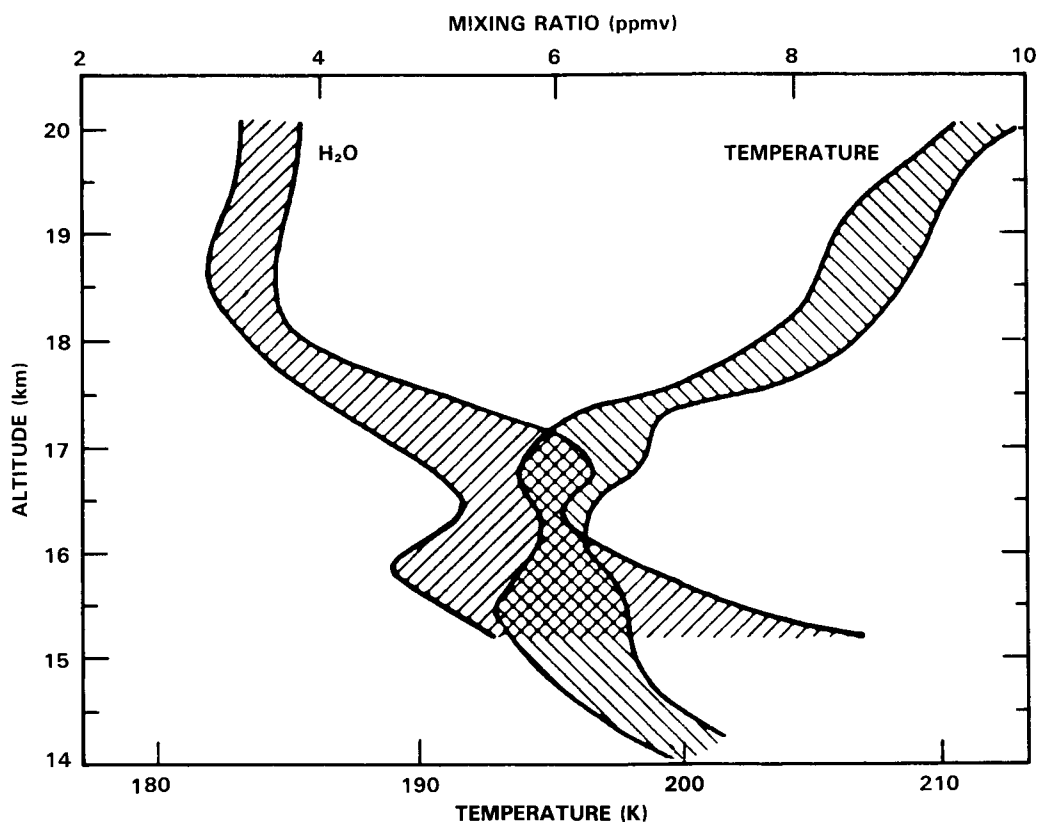
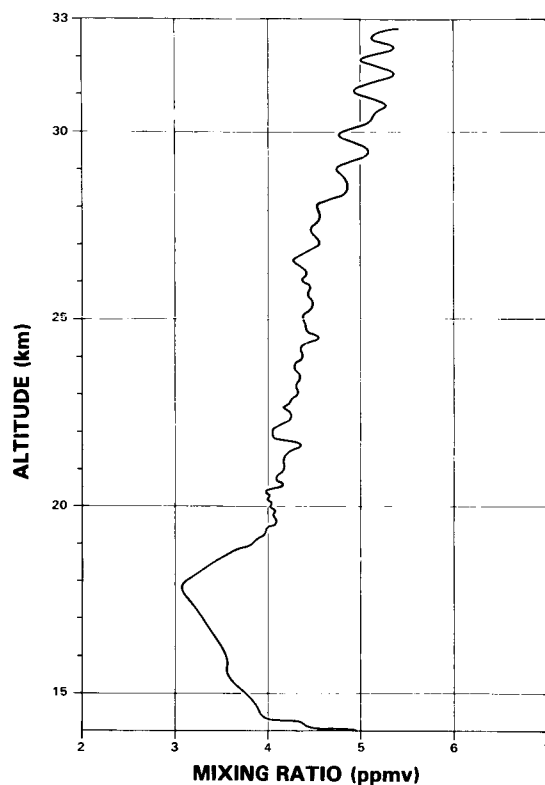


Figure 9-12. Standard deviations from the mean ( $\pm 1\sigma$ ) of eight profiles of H<sub>2</sub>O and temperature measured by instruments on the NASA U-2 aircraft over Panama, 1980. Areas between the lines defining  $-1\sigma$  and  $+1\sigma$  are hatched. The H<sub>2</sub>O data has been multiplied by a factor of 0.88 due to changes in the calibration factor.



**Figure 9-13.** Microstructure of water vapor observed over Palestine, Texas, May 7, 1981 (Kley *et al.*, 1985, unpublished).

These *in situ* data provide evidence for a mixing ratio of slightly less than 3.4 ppmv at the tropical hygropause. Compared to this, the LIMS data discussed later are slightly lower ( $\approx 2.7$  ppmv). However, a secular trend has been observed in water vapor mixing ratio in the lower stratosphere at extratropical latitudes (cf Foot, 1984, and references therein) which may or may not be present in the tropics. Furthermore, Mastenbrook and Oltmans (1983) find a weak quasi-biennial oscillation (QBO) in the water mixing ratio over Washington, D.C. and Boulder, Colorado. A similar QBO discussed by Hyson (1978) is present over Australia. Because of a lack of data nothing can be said about a QBO in the tropical stratosphere. A direct comparison of hygropause mixing ratios from LIMS and balloon *in situ* measurements is therefore not possible. The Wyoming flight (Danielsen and Kley, 1985) was made during the time that LIMS operated and the observed minimum of the mixing ratio of 3.1 ppmv was traced back to the lower tropical stratosphere. Although the travel time was short ( $\approx 5$  days) some "filling up" of the minimum could have occurred during the transit, so that 3.1 ppmv would represent an upper limit of the hygropause mixing ratio consistent with the LIMS value. Further studies are required to resolve the discrepancy between the satellite and the *in situ* results.

Kley *et al.* (1980) reported a very strong vertical stratification of stratospheric water vapor. Since the time of the early measurement, similar features have been found on subsequent flights. Figure 9-13 gives a more recent example. Kley *et al.* suggest that this oscillatory behavior of middle and upper stratospheric water vapor is most probably of photochemical origin via  $\text{CH}_4$  oxidation. This conclusion is derived from the argument that the amplitude of the oscillation tends to grow larger with increasing

## HYDROGEN SPECIES

altitude which indicates that any variability which might be generated by the dynamics of the troposphere/stratosphere exchange process cannot be responsible. Changes in water vapor mixing ratio, due to photochemistry, happen on a long time scale ( $> 1$  year) in the stratosphere. The observed local variability must, it seems, be caused by quasi-horizontal, highly stratified and stable advection from regions of the stratosphere where, due to the slow photochemistry, large scale anticorrelative regions of  $H_2O$  and  $CH_4$  exist. The most plausible explanation of the oscillation over a fixed location is long-range transport from those regions. Wind speeds must be highly oscillatory in altitude but stable over several days in order to achieve the observed variability.

A number of other water vapor profiles have been measured since WMO (1982), using mass spectrometric, cryogenic sampling and remote sensing techniques. Descriptions of these techniques are not included here. Many of them have been used in the *in situ*  $H_2O$  vapor and BIC intercomparison campaigns and are discussed in Appendix C. Rippel (1984a) recently conducted occultation measurements of  $H_2O$  at Aire Sur L'Adour ( $44^\circ N$ ) from a balloon over the altitude range 26 to 38 km and obtained an essentially constant mixing ratio of  $\sim 3.5$  to  $4.0$  ppmv. In general all the data since WMO (1982) (i.e. satellite, BIC, and *in situ*) are consistent with the picture of increasing mixing ratio with altitude in the tropics and low values of  $\sim 3$  ppmv at the hygropause location. The *in situ* measurements shown in Figures 9-14 and 9-15 and the remote sensing measurements shown in Figures 9-16 and 9-17 made during the *in situ* and BIC campaigns, respectively, are typical.

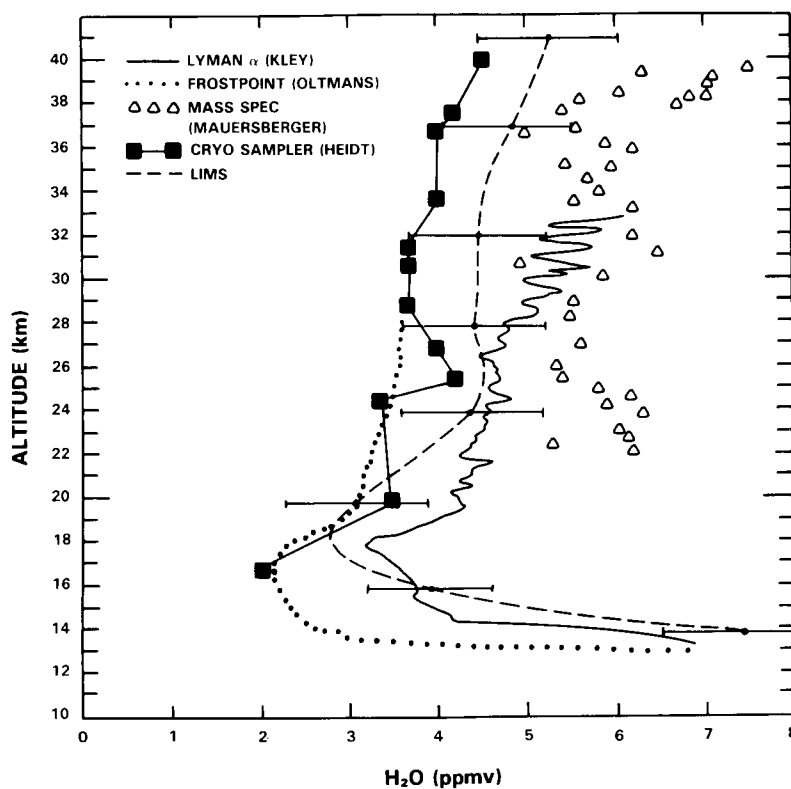


**Figure 9-14.** Final results from the *in situ* samplers of stratospheric water vapor of the first International Water Vapor Intercomparison, held over Palestine, Texas, May 7, 1981. (see Appendix C). LIMS zonal mean profile for  $32^\circ N$  and May 6–10, 1979 is given by dashed line.

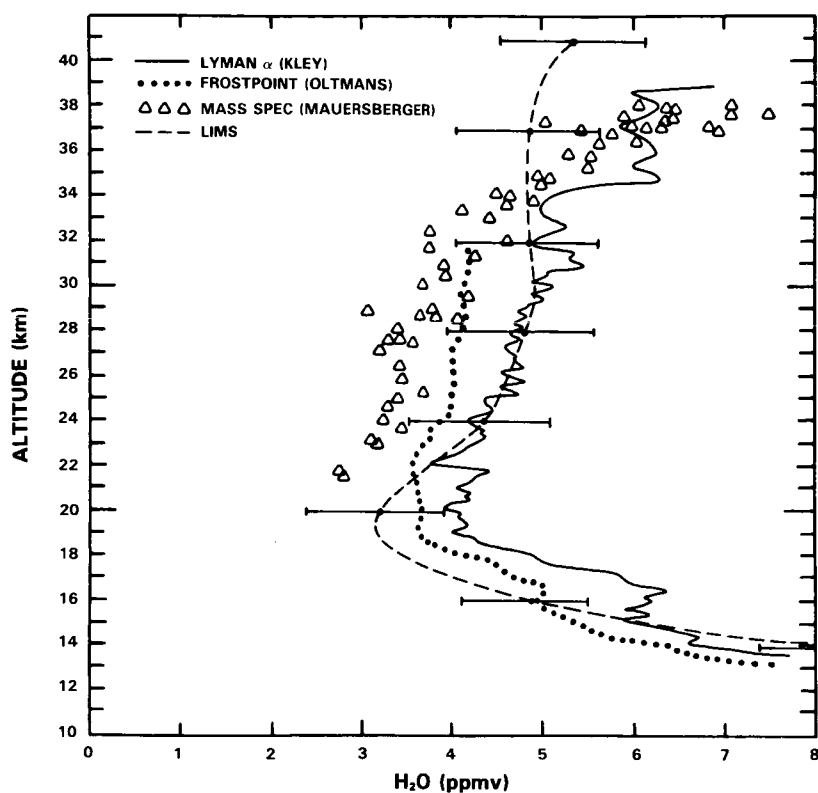


**Figure 9-15.** Preliminary results from the in situ samplers of stratospheric water vapor of the second International Water Vapor Intercomparison, held over Palestine, Texas, October 11, 1983. (see Appendix C). LIMS Zonal Mean Profile for 32°N and October 27-31, 1978 is given by dashed line.

#### 9.4.2 LIMS Water Vapor Measurements

The LIMS instrument is a limb scanning radiometer with six channels centered at wavelengths between 6.2  $\mu\text{m}$  and 15  $\mu\text{m}$ . It flew aboard the Nimbus 7 spacecraft operating from the time of launch on October 24, 1978, until the end of the planned lifetime of the solid cryogen cooler on May 28, 1979. The standard IR limb sounding approach was used; vertical profiles of radiance emitted by the 15  $\mu\text{m}$   $\text{CO}_2$  band were inverted to obtain temperature profiles and this information was then used with the 6.3  $\mu\text{m}$  band water vapor radiances (covering the 1370  $\text{cm}^{-1}$  to 1560  $\text{cm}^{-1}$  range) to obtain vertical water vapor mixing ratio profiles. The vertical resolution of the measurements was 4 km. These data have been reduced and archived in the National Space Sciences Data Center (NSSDC). The archived results cover the altitude range from about 100 mb (16 km) to 1 mb (50 km) and extend from 64°S to 84°N in 4° latitude increments. The measurements were made night and day almost continuously during the mission (11 days on, 1 day off duty cycle).

An extensive discussion of efforts to validate the LIMS water vapor results has been presented by Russell *et al.* (1984c). The validation approach included detailed ground simulations taking various experimental error sources into account in order to assess accuracy and precision, verification of calculated precision values by studying consecutive orbital data, and comparisons with data collected in 13 balloon underflights to obtain further confidence in orbital results. Five LIMS profiles, covering  $\pm 2^\circ$  of latitude were averaged and compared to balloon data. The mean difference with balloon results was  $\sim 7$  to  $\sim 20\%$  ( $\sim 0.1$  to  $0.3$  ppmv) over the 5 to 100 mb ( $\sim 40$  km to  $\sim 16$  km) range. The primary systematic error sources in order of importance are temperature profile errors, molecular oxygen absorption coefficient

## HYDROGEN SPECIES

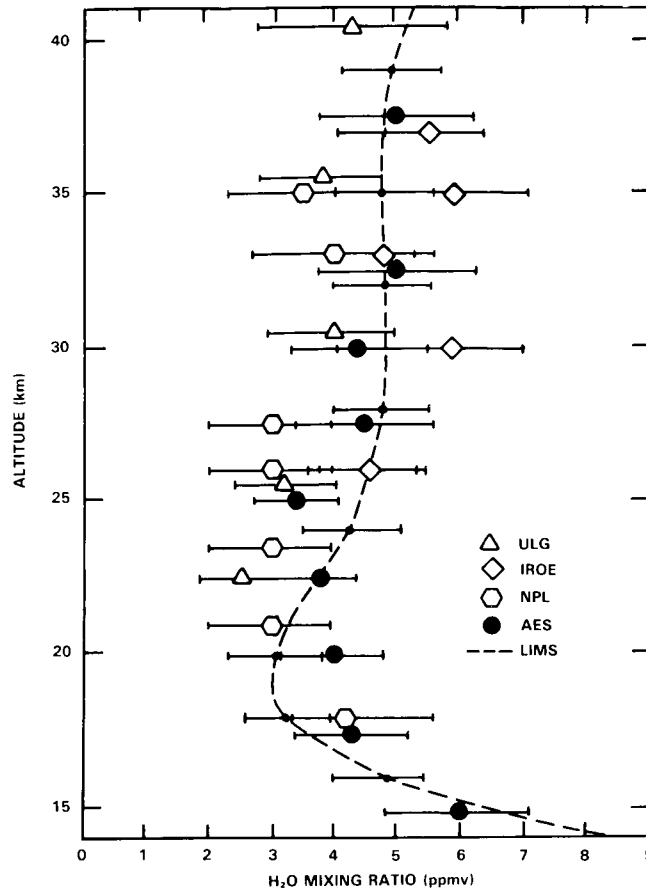


**Figure 9-16.** H<sub>2</sub>O profiles obtained during BIC I using remote sensing techniques. The AES data were obtained on September 22, NPL and IROE data on October 5, 1982. The error bars of each measurement are one standard deviation and include both random and estimated systematic errors. The LIMS 5 day zonal mean profile for October 27–31, 1978, is also shown in the figure. Such a comparison presumes that interannual variability is small and that the BIC air mass is representative of the zonal mean.

errors (for altitudes < 20 km), spectral parameter errors, instrument vertical field of view errors, and other instrumental effects. Temperature error effects are dominant at all levels above about 18 km. The estimated single profile accuracy is 20% from 20 km to 45 km and 30 to 35% at 50 km. The LIMS data showed apparent profile-to-profile variations in mixing ratios which approach 40% near 50 km. Such variations are only of the order of 10% below 30 km. These variations occurred somewhat randomly along an orbit track and are believed to be due to a combination of spacecraft motion effects and possibly small variations in radiance bias error. For these and other reasons, the LIMS team has placed more confidence in zonal mean profiles rather than single profiles. The comparisons with balloon data showing overlap of the LIMS and balloon data error bars, and the high precision estimated from orbital data give high confidence in the LIMS results.

Of special interest are the error estimates for zonal mean profiles at tropical latitudes in the 50 mb (20 km) to 70 mb (18 km) range where the hygropause (Kley *et al.*, 1982) is located. The major error sources in this pressure range are temperature and molecular oxygen effects. Spatial sampling biases due to loss of data from cloud contamination in the tropics is also a consideration at 70 mb (18 km) and below. As discussed in Remsberg *et al.* (1984b), simulations were done using realistic LIMS temperature bias errors of +1K at 50 mb (20 km) and +4K at 70 mb (18 km) (Gille *et al.*, 1984b) combined with a

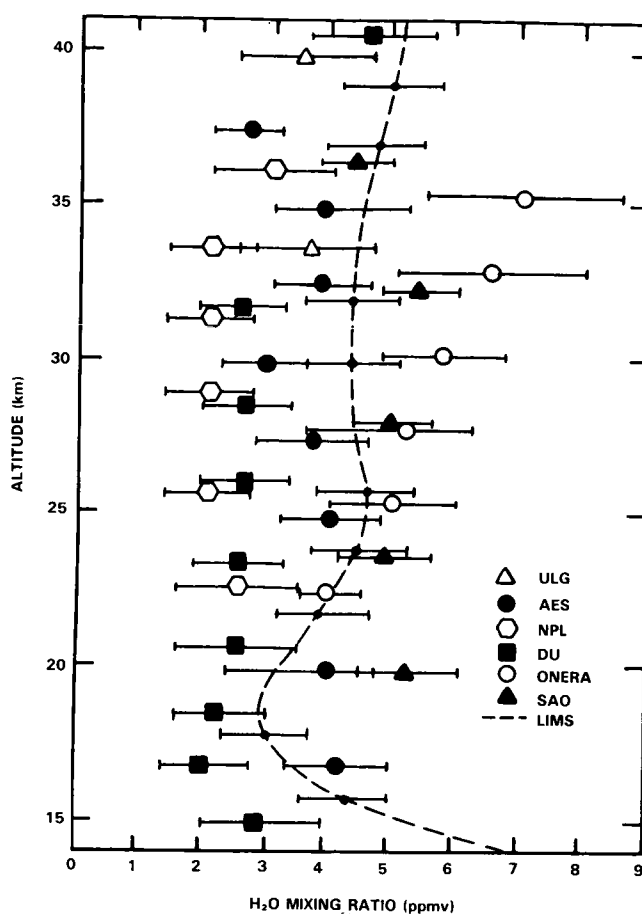


**Figure 9-17.** H<sub>2</sub>O profiles obtained during BIC II using remote sensing techniques. The AES, SAO, NPL, and ONERA data were obtained on June 20. The DU and ULG data were obtained on June 17, 1983. The error bars of each measurement are one standard deviation and include both random and estimated systematic errors. The LIMS 5-day zonal mean profile for May 23–27, 1979, is also shown in the figure.

20% uncertainty in O<sub>2</sub> emission. Temperature bias error effects near the tropopause are not too severe due to compensating differences in vertical resolution of the temperature and H<sub>2</sub>O channels (Russell *et al.*, 1984c). Based on these calculations, it was estimated that between  $\pm 15^\circ$  latitude the archived results are too low by 0.3 ppmv at 50 mb and 0.6 ppmv at 70 mb with much smaller biases at  $\pm 25^\circ$  latitude. Even after allowing for such biases a distinct hygropause is still evident. Remsberg *et al.* (1984c) also point out that the altitude position of the minimum water vapor mixing ratio in the lower stratosphere for tropical latitudes is likely to be 1 to 2 km too high.

Russell *et al.* (1984c) have noted that there is an apparent diurnal variation in water vapor (day values higher than night values) of about 1 ppmv to 2 ppmv at 1 mb (50 km) decreasing to negligible values at about 10 mb (30 km). This is most likely due to day/night temperature effects from LIMS temperature profiles used for retrieval or non-local thermodynamic equilibrium effects (not included in LIMS H<sub>2</sub>O retrievals). An unaccounted-for physical phenomenon giving a radiance change equal only to the radiance noise can cause this effect. As a result, the nighttime results are probably more reliable, especially for quantitative studies of vertical mixing ratio changes.

## HYDROGEN SPECIES

**Table 9-3.** LIMS Estimated Accuracy and Precision for H<sub>2</sub>O Measurements

Parameter	Altitude			
	16 km	18 - 20 km	20 - 40 km	50 km
<i>Accuracy (ppmv)</i>				
tropics (1)	±0.7	±0.3 to ±0.6	±0.8	±1.5
mid and high latitudes	±0.4	±0.4	±0.8	±1.5
<i>Precision ppmv (2)</i>				
	±0.1	±0.3	±0.3	±0.5

(1) These apply to single profiles. Some systematic effects will be reduced when zonal mean profiles are calculated. Thus the estimates are somewhat conservative.

(2) These values apply to single profiles as determined by calculating standard deviations of a series of 6 sequential scans about the 6 scan mean as a function of latitude.

Ground simulation and orbital results were both in accord, giving single profile precision values which varied from 0.1 ppmv to 0.3 ppmv in the altitude range from 16 km to 40 km. Again, the precision of the zonal mean product is improved over the single profile results (e.g. by a factor of 2 for daily zonal means). The largest variation occurs near the stratopause where the standard deviation of the daily zonal mean about the monthly zonal mean is typically 0.4 ppmv to 0.8 ppmv. At least part of this variation is due to true atmospheric changes, but some portion is due to the spacecraft motion or radiance bias effects discussed above. A summary of estimated LIMS water vapor accuracy and precision is included in Table 9-3.

Typical water vapor zonal mean nighttime profiles for November 1978 from LIMS are shown in Figure 9-18. The profiles show a clear, well developed minimum in mixing ratio (hygropause) that occurs above the tropopause. This feature is evident at low to mid latitudes between 100 mb (16km) to 30 mb (24km). There is a slight trace of the hygropause present even at 56°S. Other features that should be noted are an increase in mixing ratio with height in tropical latitudes that appears to be consistent with the methane oxidation theory (see section 2.4.8) and a constant mixing ratio profile or even a slight decrease with altitude at mid to high latitudes. There are some variations in the profile during the seven months of LIMS data, but this general description suffices to describe the distribution.

The zonal mean pressure versus latitude cross sections of monthly averaged nighttime water vapor are shown in Figures 9-19 and 9-20. A number of important characteristics emerge upon examination of these plots. The results show a broad minimum in mixing ratio that persists during all 7 months and occurs mainly in the tropics in the pressure range from 100 mb (16 km) to 30 mb (24km). Based on LIMS latitude versus longitude plots and time series analyses, we can conclude that variability in the latitude-altitude hygropause area is small over the life of LIMS and is quite uniform with longitude.

# HYDROGEN SPECIES

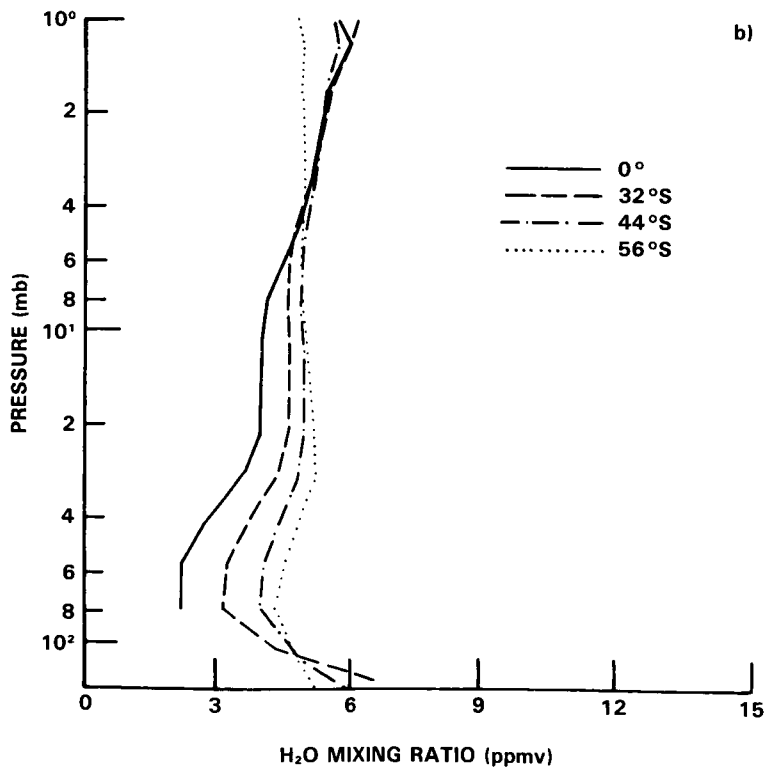
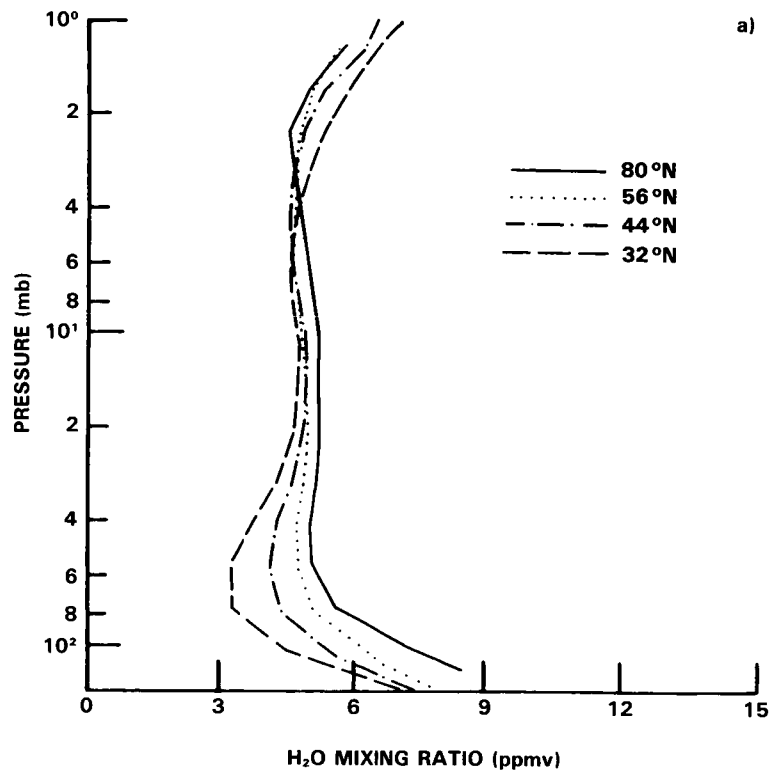


**Figure 9-18.** (a) LIMS Monthly Mean H<sub>2</sub>O Mixing Ratio for November 1978 in the Northern Hemisphere. (b) LIMS Monthly Mean H<sub>2</sub>O Mixing Ratio for November, 1978 in the Southern Hemisphere.

# HYDROGEN SPECIES

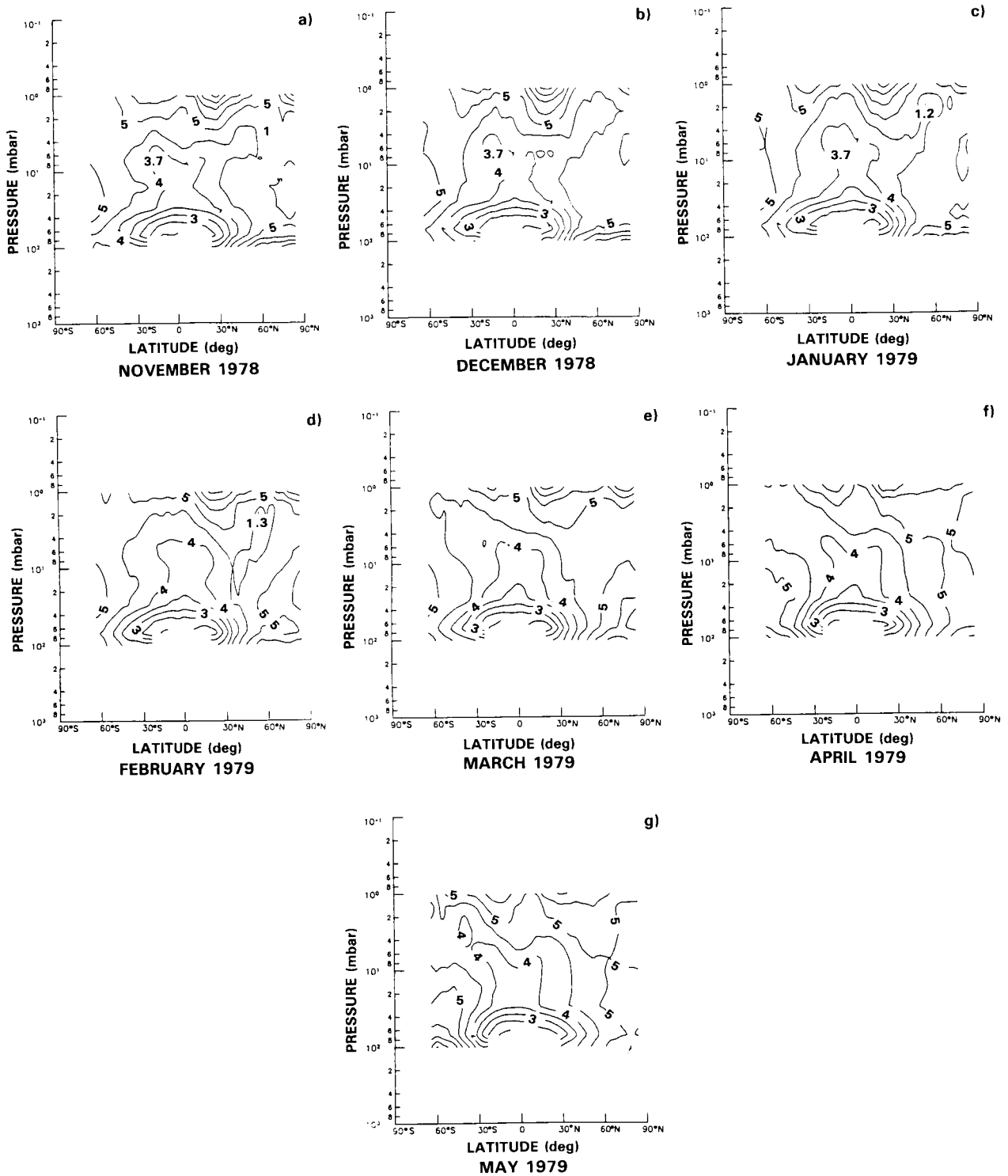


**Figure 9-19.** LIMS monthly zonal mean water vapor pressure versus latitude cross sections for (a) November, and (b) December, 1978, and (c) January, (d) February, (e) March, (f) April, and (g) May, 1979 (0.5 ppmv contour intervals)

ORIGINAL PAGE  
COLOR PHOTOGRAPH

HYDROGEN SPECIES

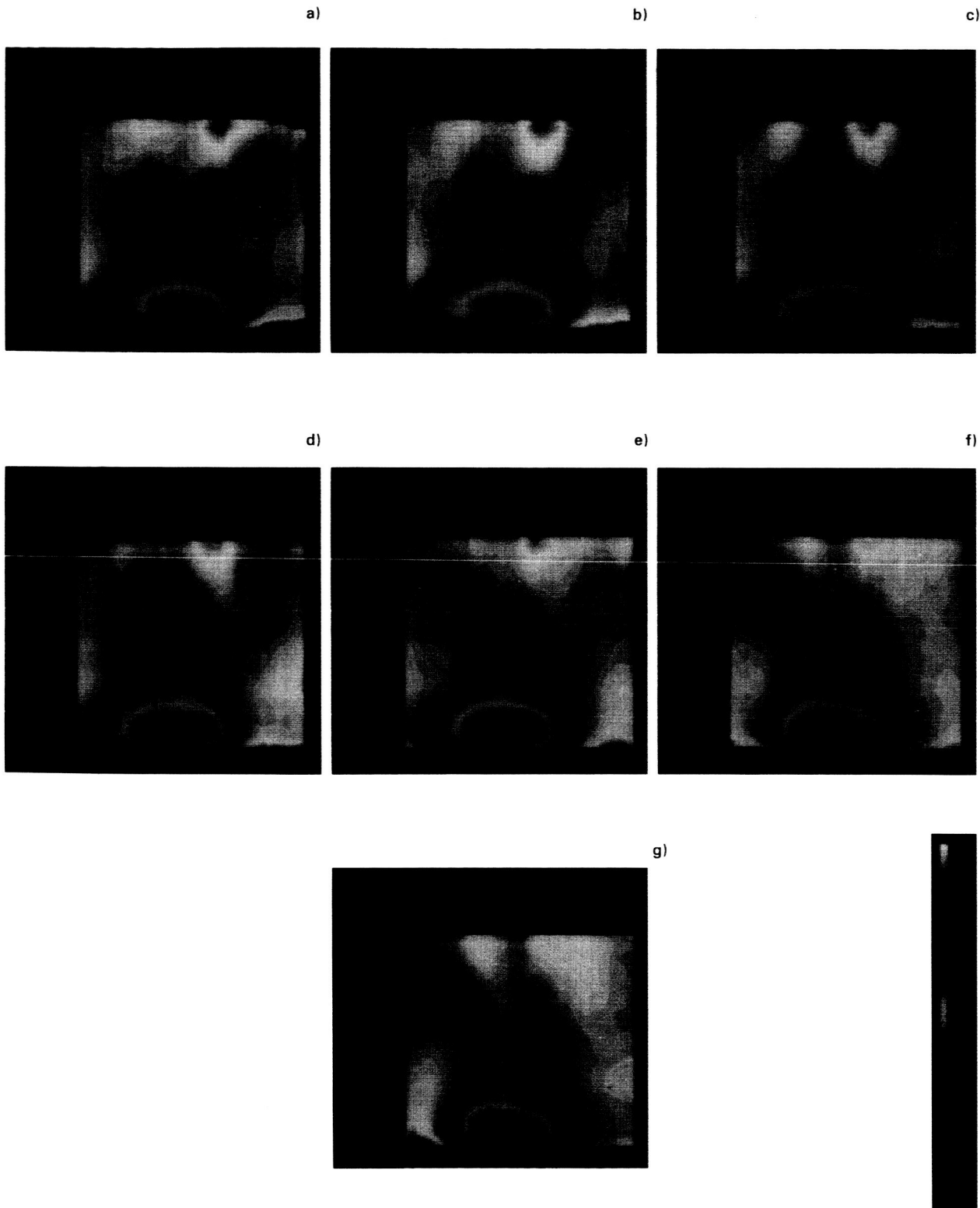


**Figure 9-20.** LIMS monthly zonal mean water pressure versus latitude vapor cross section for (a) November, and (b) December, 1978, and (c) January, (d) February, (e) March, (f) April, and (g) May, 1979.

## HYDROGEN SPECIES

In the tropics near the 10 mb ( $\sim 30$  km) level, the presence of a double minimum in mixing ratio exists which correlates closely with a double maximum in SAMS  $\text{CH}_4$  and  $\text{N}_2\text{O}$  measurements. This suggests an upward motion carrying water vapor from the dry region below and then branching northward and southward. In November, the "dry" contours (e.g. 4 to 4.5 ppmv) extend toward the 1 mb ( $\approx 50$  km) level at high northern latitudes. At the same time, in high altitudes and latitudes of the Southern Hemisphere, a broad region of higher mixing ratio (5 ppmv) exists. This picture gradually changes until in March the "dry" contours have reversed to extend southward and upward. In May, the Southern Hemisphere low water vapor air extends further toward high altitudes and southern latitudes. This is further emphasized in Figure 9-21, which compares LIMS  $\text{H}_2\text{O}$  and SAMS  $\text{CH}_4$  monthly zonal mean results. Note that where LIMS  $\text{H}_2\text{O}$  is low, SAMS  $\text{CH}_4$  is high. The tropical methane source region is obvious in this figure. There are regions of maximum  $\text{H}_2\text{O}$  mixing ratio near the 1 mb ( $\approx 50$  km) level in the tropics that occur on each side of the equator and tend to persist in all 7 months. The maximum values are consistent with the oxidation of methane as a water vapor source.

There is an increasing gradient of mixing ratio poleward both north and south at all levels from 100 mb to about 4 mb. Here, the direction of the gradient gradually reverses with increasing altitude. In the lower

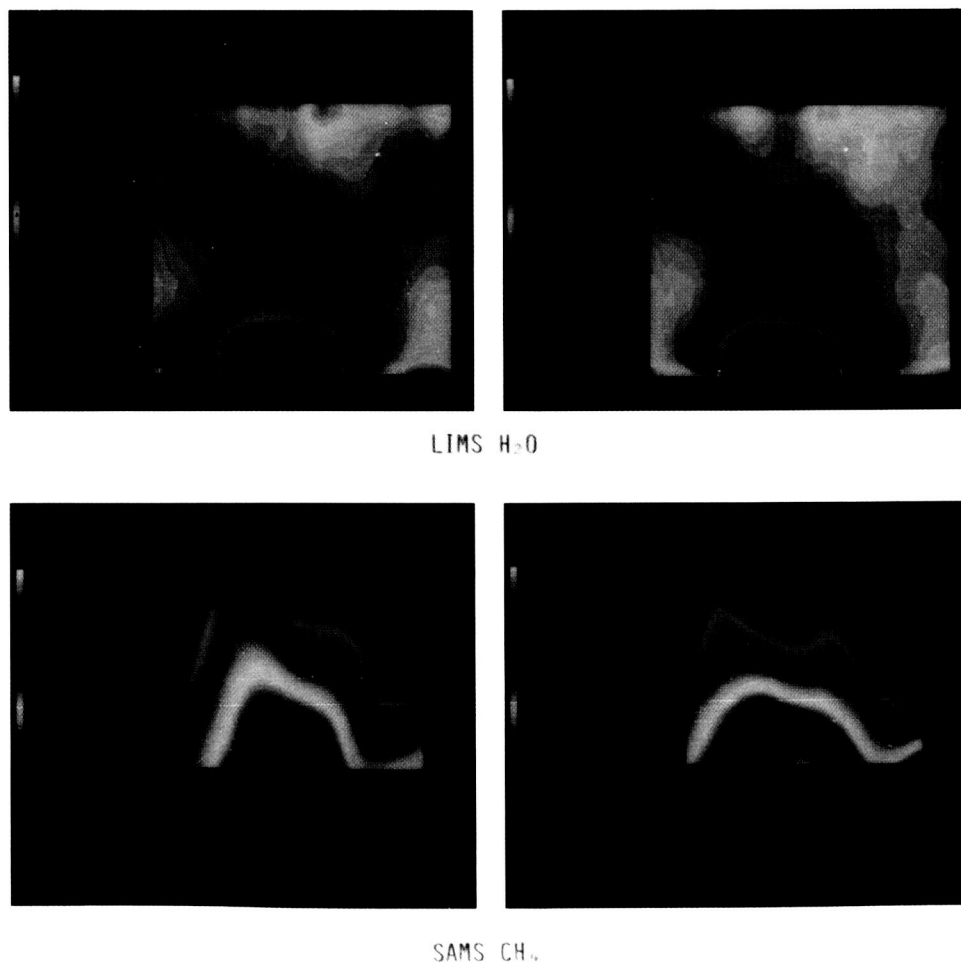


**Figure 9-21.** LIMS  $\text{H}_2\text{O}$  and SAMS  $\text{CH}_4$  monthly zonal mean pressure versus latitude cross sections for March and April 1979.

stratosphere, the data imply the presence of a low altitude net circulation with the strongest circulation toward the summer pole. Such an implied mechanistic circulation is counter to the calculated circulations reported in Chapter 6 which show stronger net transport by waves towards the winter pole in the lower stratosphere. Note the elongated contours of minimum mixing ratio extending horizontally from the hygropause region in the 100 mb (16 km) to 30 mb (24 km) range to about 60° S during November through March but then going through a rather quick reversal so that in May, the low mixing ratio contours extend to 60° N. This behavior is accompanied by a significant change in mixing ratio in the low stratosphere at high latitudes. In the Northern Hemisphere, at 60° N and 100 mb (16 km) in November, the mixing ratio is 6.5 ppmv. During the mission, it gradually decays to 6 ppmv in March and 5 ppmv in May. At the same time, at 60° S the opposite trend occurs, i.e. in November the mixing ratio is 4.5 ppmv, 5 ppmv in March, and 6.5 ppmv in May. Examination of the changes in each hemisphere near 60° latitude and at levels up to about 40 mb (22km) show a general increase in water vapor during winter. The data seem to suggest a mechanistic model where water vapor is being mixed into the stratosphere from the troposphere during these times, possibly because of northern advection of water vapor through the tropopause break region near 30°N.

It is apparent that the LIMS water vapor cross sections contain much information not only on the water vapor budget in the stratosphere but also on the net circulation patterns as suggested in this brief description. Since CH<sub>4</sub> oxidation, the primary source of H<sub>2</sub>O, is generally much slower than transport effects over most of the stratosphere, the water data should be useful in transport studies. Nevertheless, both processes must be considered in attempting to understand the observed distribution. A combination of SAMS and LIMS data should prove to be most helpful in any such studies.

The variability in zonal mean water vapor observed by LIMS in the 16 km to 50 km range is generally small with the greatest changes occurring in the high latitudes of the winter hemisphere. Figures 9-22a,b show pressure versus latitude cross sections of the standard deviation of daily zonal mean profiles about the monthly zonal mean for November and May. Throughout most of the stratosphere, this variation is very small (< 0.2 ppmv). Evidence of increased changes at high winter or fall latitudes in the middle stratosphere is indicated by the closed contour at ≈ 60°N in November and 45°S in May. The changes at the extreme upper altitude near 1 mb are in part real, but it is difficult to say how much of this variation is driven by the spacecraft motion and the variable bias problem discussed previously.

One of the important questions that prevailed prior to LIMS dealt with the issue of spatial and temporal variability of H<sub>2</sub>O. Much of this question has been answered by LIMS results. Figure 9-23a,b shows 5-day zonal mean latitude versus time cross sections at 50 mb (≈ 20 km) and 10 mb (≈ 30 km). These pressure levels were chosen to show changes in the hygropause region and in the mid stratosphere. The lowest water values at 50 mb occur in the ≈ ±15° latitude range and have a value of ≈ 2.7 ppmv (2.4 + 0.3 ppmv for the temperature bias effect). The variation in these minimum values (cf Figure 9-23) is only ~0.3 ppmv over the life of LIMS. Note the rather sharp latitudinal gradients. The region of greatest "short term" variability lies above ≈ 50°N in winter and is on the order of 0.5 ppmv. The greatest long term changes occur in the high latitudes of both hemispheres as already discussed. The same kind of plot at 10 mb (30 km) shows a rather different picture. The latitudinal gradients are greatly reduced at 10 mb and the variation is < 0.25 ppmv at all latitudes up to about 50N and on the order of 0.3 ppmv at higher latitudes. Variations at all altitudes for the equator and 60°S are shown in Figures 9-24a,b. The vertical mixing ratio gradient at 60°S is much smaller than at the equator throughout the mission. The mixing ratio is nearly constant with altitude until fall and early winter approaches. At that time, there is a mixing ratio rise in the lower stratosphere and a slight decline near 50 km. There appears to be more variability at the equator than at 60°S most of the time although absolute variation differences are still small.

# HYDROGEN SPECIES

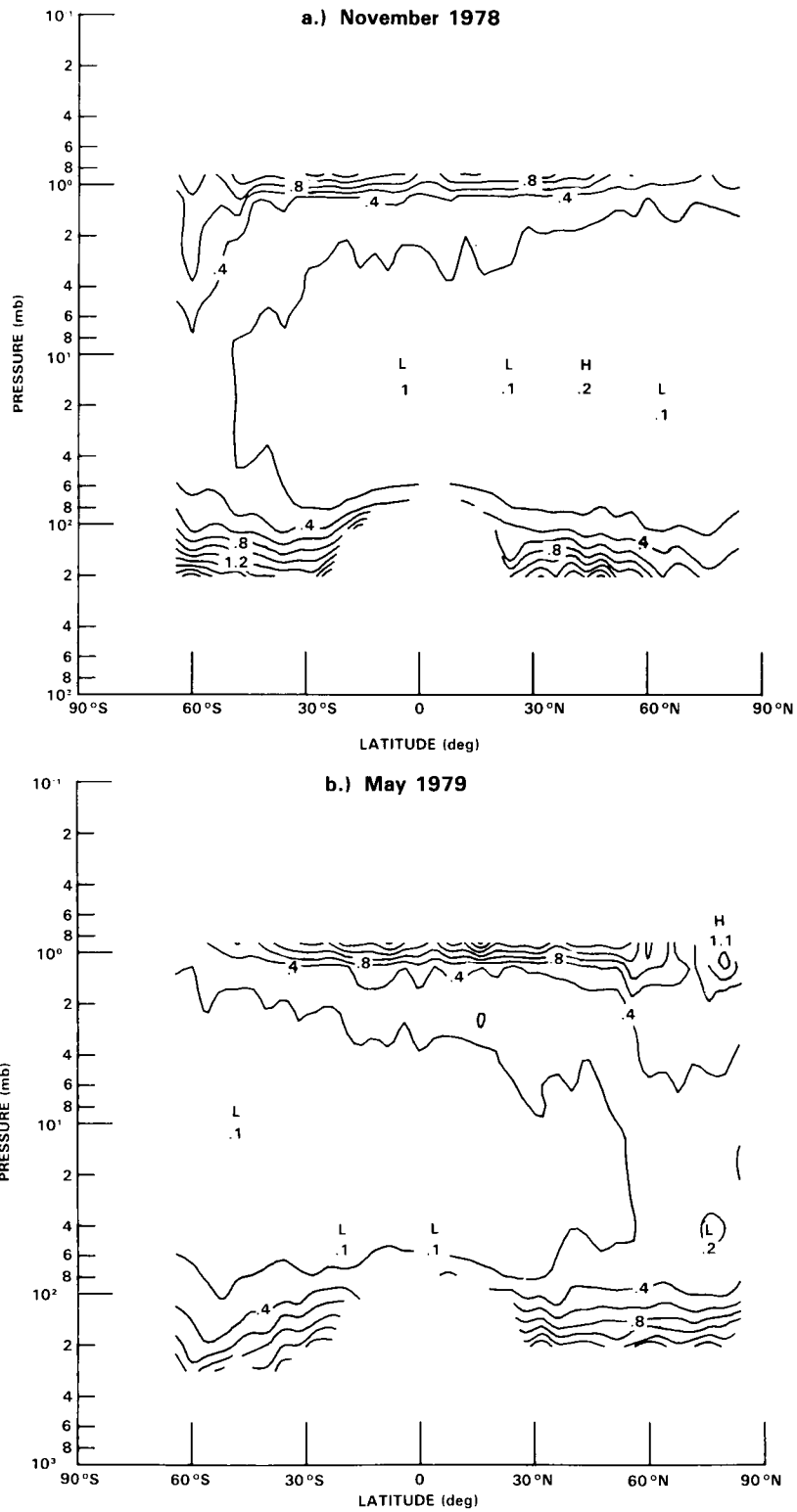


**Figure 9-22.** LIMS H<sub>2</sub>O standard deviation of daily zonal mean profiles about zonal mean for (a) November, 1978 and (b) May 1979

HYDROGEN SPECIES

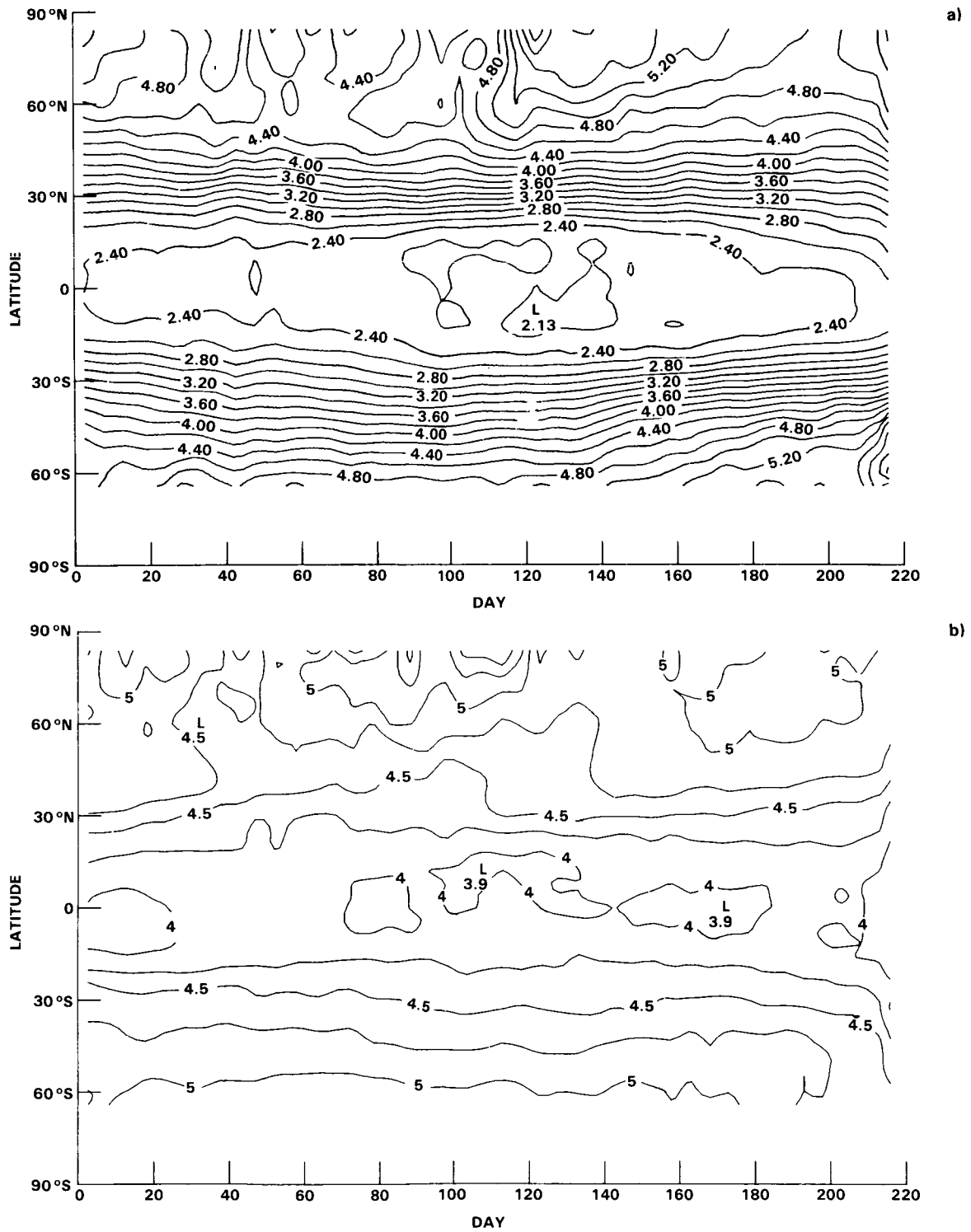


Figure 9-23. LIMS H<sub>2</sub>O latitude versus time cross section at (a) 50 mb and (b) 10 mb (0.25 ppmv intervals, 5 day means).

HYDROGEN SPECIES

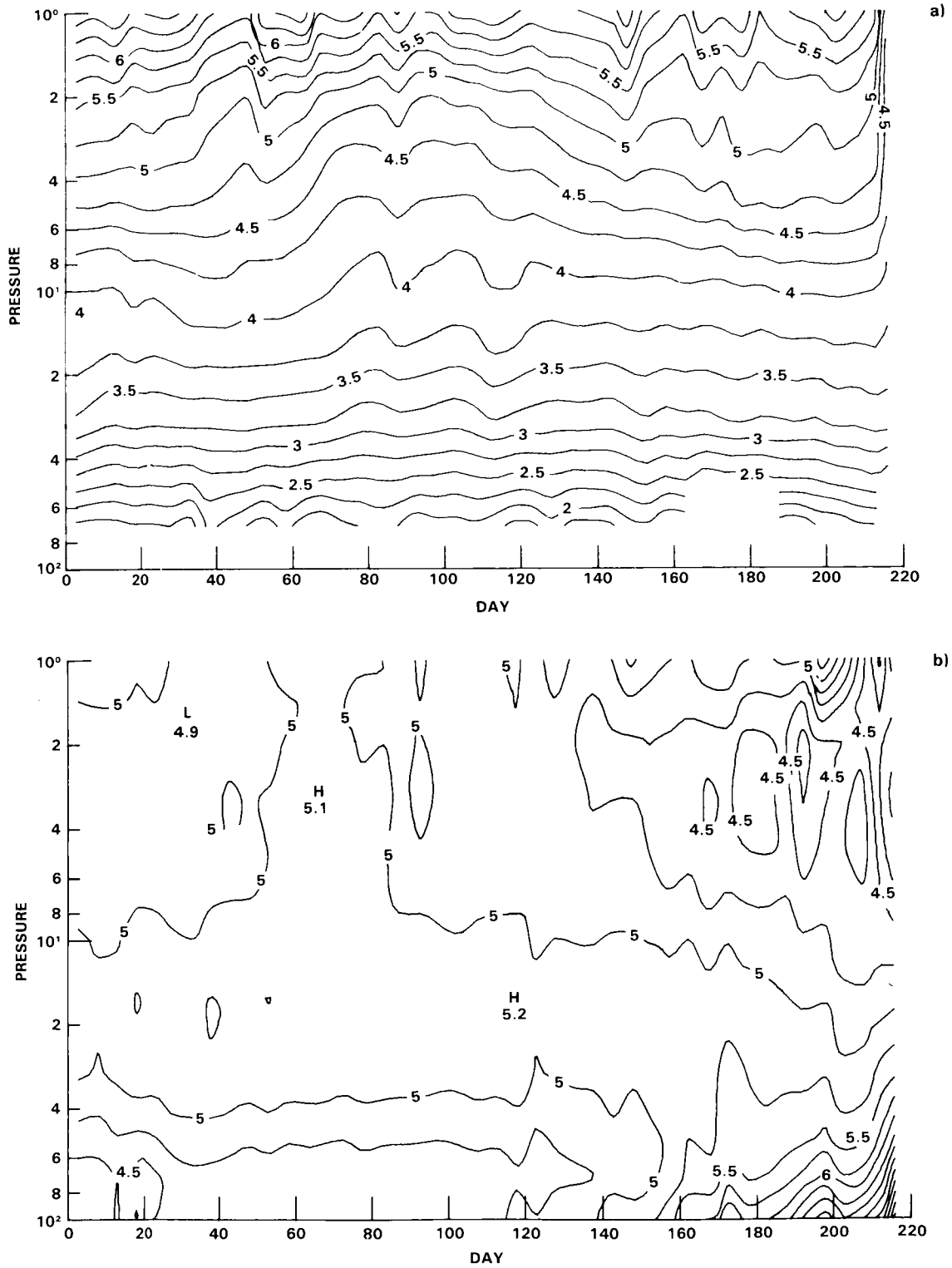


Figure 9-24. LIMS H<sub>2</sub>O pressure versus time cross section at (a) the Equator and 60°S (0.25 ppmv intervals, 5 day means).

Figure 9-25 is a polar stereographic plot of water vapor at 50 mb ( $\approx 20$  km) for February 2, 1979, Northern Hemisphere. This plot was made from the LIMS mapped results. Mapping was done using the sequential estimator Kalman filter method of Rodgers (1976b). Up to 13 Fourier coefficients were obtained defining a zonal mean and six longitudinal wave numbers at each of 38 LIMS latitude points  $\sim 4^\circ$  increments. Because fewer profiles are available (due to cloud contamination) for the low altitude 50 mb analysis, (Figure 9-25) only the largest wave numbers, up to wave number 4 have been calculated. The strong meridional gradient showing the extension of the hygropause to mid latitudes is evident, with some interesting variations at high latitude that seem to reflect the advection of low water vapor to higher latitudes. The high latitude variations are typical of dynamically disturbed periods. Longitudinal variations are also present at low latitudes, but the amplitude is only of the order of 0.2 ppmv.

In summary, the LIMS H<sub>2</sub>O data show a zonal mean vertical profile which increases with increasing altitude in the tropics to a maximum value of  $\approx 5.5$  to 6 ppmv at the [1mb] 50 km level. The profile in mid to high latitudes shows either a constant value or a slight decrease with altitude. The zonal mean altitude versus latitude cross section shows a broad region of low mixing ratio ( $\approx 2$ -3 ppmv) [the hygropause] from 35°N/S to 45°N/S and extending to  $\sim 40$  mb. The data show evidence of dry air being carried upward and branching north and south in accord with the Brewer-Dobson theory. The strongest implied net circulation is toward the winter pole at high altitudes. The high latitude ( $> 50^\circ$ ), winter, lower stratosphere ( $p > \approx 60$  mb) appears to be a region where water enters the stratosphere from below. It is not clear, however, how important this is in terms of the total water vapor budget or what the exact mechanism could be. A latitudinal gradient in mixing ratio exists at all times during the LIMS mission with a poleward increase at low to middle stratosphere altitudes and a poleward decrease higher up. Variability in the zonal mean mixing ratio is small most of the time and is greatest in winter high latitudes. Longitudinal variability in the tropics is  $< 0.5$  ppmv and on the order of 1 to 1.5 ppmv at mid and high latitudes.

Comparisons were made between LIMS and balloon H<sub>2</sub>O measurements as part of the *in situ* and BIC intercomparison campaigns. It should be noted though that LIMS data were taken about 4 years earlier. Therefore, care must be exercised in making such comparisons. The comparison is valid to the extent that interannual variability is small. Examples of these comparisons are shown in Figures 9-14 to 9-17 and are discussed in Appendix C. In general, the vertical profile structures are similar and the uncertainties in the measurements overlap. A major discrepancy exists between satellite results and the mean of three February profiles measured by Evans (1983) during 1977, 1978 and 1979 at 58°N. Evans (1983) shows low mixing ratio ( $\approx 2.5$  ppmv) in the lower stratosphere as contrasted with values of 4.5 to 5 ppmv from LIMS. The reason for these differences are not known at present.

#### 9.4.3 Measurements of H<sub>2</sub>O in the Upper Stratosphere and Mesosphere

The water vapor content in the upper stratosphere and in the mesosphere and its temporal variation have been the subject of a recent series of studies using ground-based microwave spectroscopy to measure the  $6_{1,6} - 5_{2,3}$  rotational emission line of water vapor at 22.2 GHz (Thacker *et al.*, 1981, Bevilacqua, *et al.*, 1983, Schwartz *et al.*, 1983, Bevilacqua *et al.*, 1985). The weak transition yields an unsaturated line even when looking through tropospheric water vapor from a sea-level location, and with a moderately high resolution, filter-bank spectrometer ( $<$  a few tens of KHz per channel) the narrow collision-broadened mesospheric component of the water vapor emission may be singled out for study. The techniques used for recovering a vertical profile from the observed pressured-broadened line shape, as well as the capabilities of the equipment being used, have been steadily improved during the course of these measurements. With the exception of the last cited reference, all of this work was carried out at the Haystack Observatory in Massachusetts (72°W, 42°N) at various times of year. Recently, a second instrument has been built and operated by Jet Propulsion Laboratory at Pasadena, CA (117°W, 34°N).

HYDROGEN SPECIES

Earlier conclusions regarding vertical profiles and mixing ratios (Thacker *et al.*, 1981, Gibbins *et al.*, 1982) have been somewhat modified by improved data reduction and deconvolution procedures [Bevilacqua *et al.*, 1983] but four general conclusions remain.

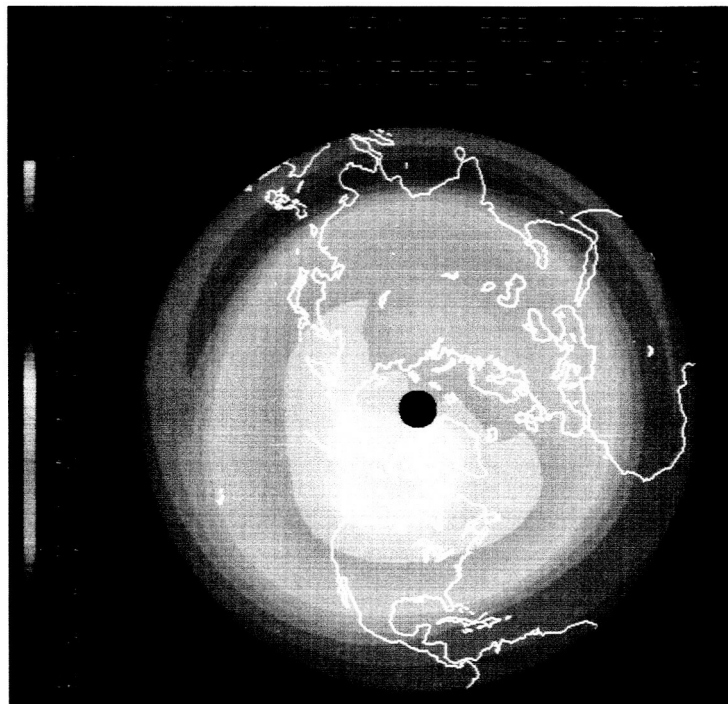
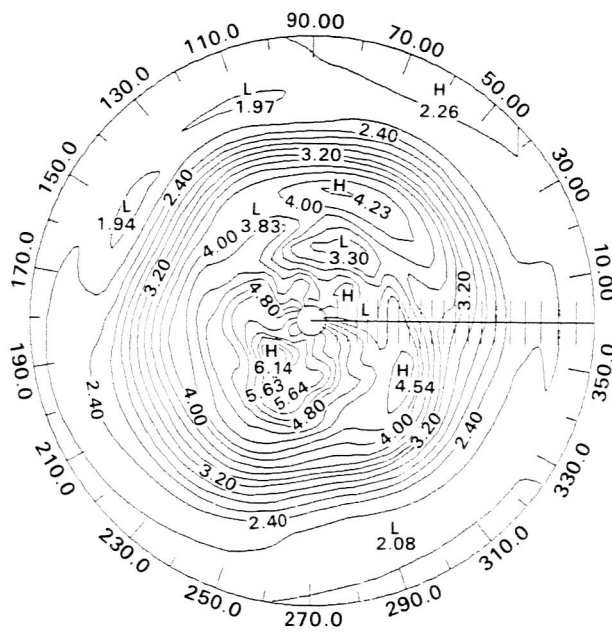


Figure 9-25a and b. Polar stereographic map of LIMS H<sub>2</sub>O at 50 mb for Northern Hemisphere for February 2, 1979 (0.20 ppmv intervals).

(1) A significant variability is observed in the mesospheric water vapor profile and column density on a time scale of  $< 1$  day.

(2) Above approximately 65 km, the mixing ratio decreases more rapidly than predicted on the basis of "standard" values for the vertical component of the upper mesospheric eddy diffusion coefficient (see Figures 9-26 and 9-27). Evidence of this decrease is also seen in unpublished LIMS data and the Spacelab I Grille Spectrometer results and (Lippens *et al.*, 1984).

(3) Water vapor increases throughout the stratosphere and lower mesosphere to a peak in mixing ratio in the range of 55 to 65 km altitude.

(4) There is some evidence for seasonal variation in mesospheric water vapor (see Figures 9-26, 9-27).

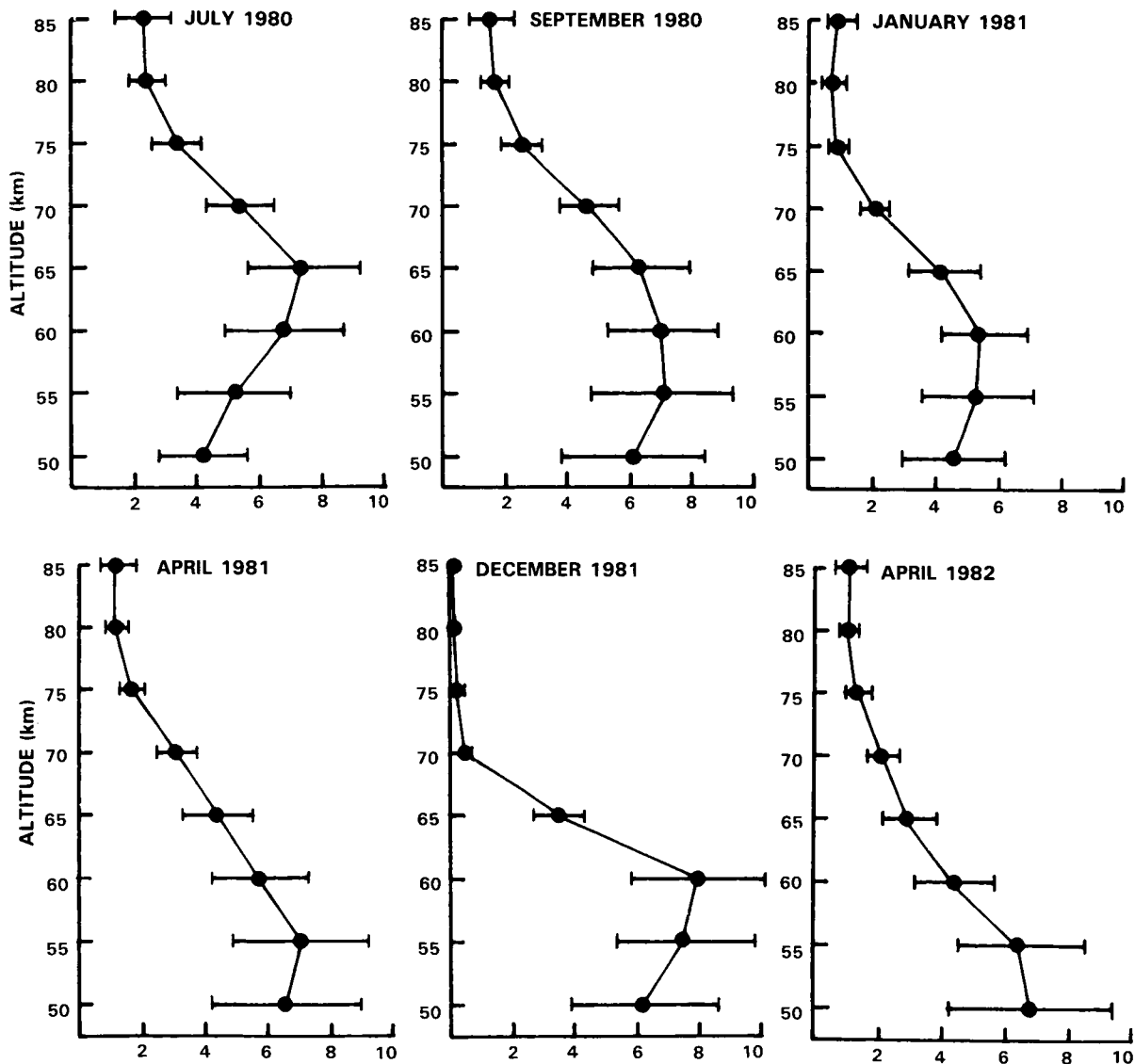


**Figure 9-26.** Averaged water vapor mixing ratio profiles retrieved by deconvolution of pressure-broadened line shapes. The horizontal bars represent  $1\sigma$  error levels in the profile retrievals. Data from Haystack Observatory, Massachusetts ( $42^\circ\text{N}$ ). From Bevilacqua, *et al.* 1983.

## HYDROGEN SPECIES

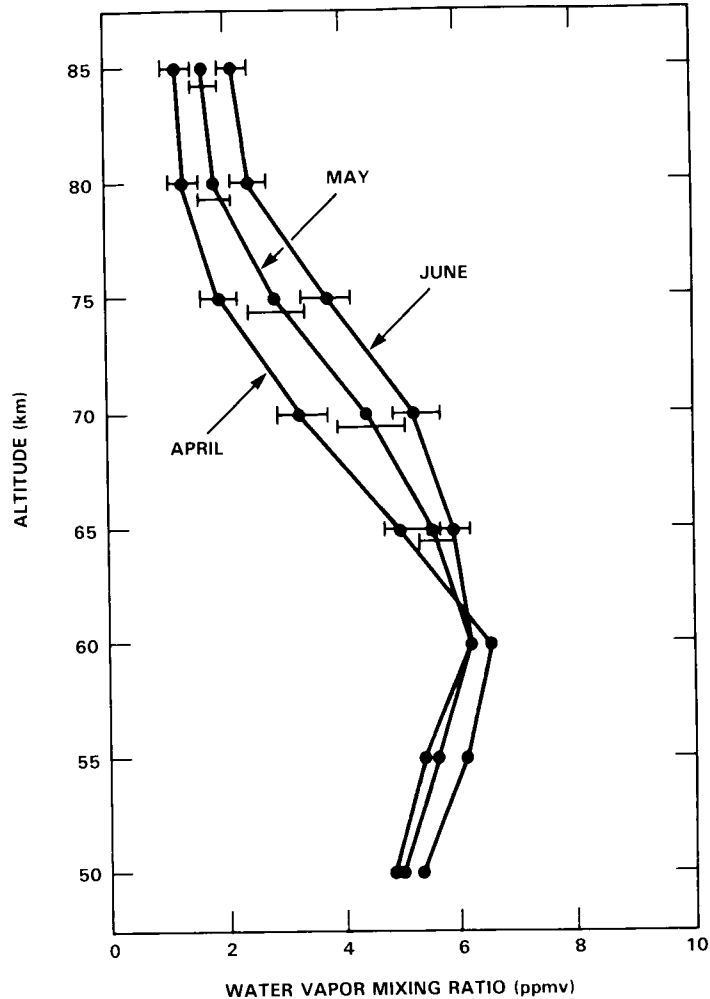


**Figure 9-27.** Monthly-mean water vapor profiles measured at Pasadena, California (34°N) over the period March 27, 1984 to April 11, 1984 and May 4, 1984 to July 1, 1984 showing evidence for a seasonal trend towards larger mixing ratios above 65 km.

## 9.5 METHANE (CH<sub>4</sub>) MEASUREMENTS

### 9.5.1 Vertical Profiles of CH<sub>4</sub> by *In Situ* Measurements

Most of the measurements of low and mid stratospheric CH<sub>4</sub> have been made using the cryogenic sampling technique. Two groups are responsible for the bulk of these measurements, one at the Kernforschungsanlage, Jülich (KFA), and the other at the Max-Planck Institut für Aeronomie, Lindau (MPI).

Improvements have been made in the technique by both groups. The new balloon-borne cryosamplers allow collection of up to 15 distinct samples per flight, each having a volume of at least 20 l STP. The samples are collected beneath the balloon during slow descent to avoid contamination of the samples by the balloon or the gondola structure. During the 20 to 30 minutes required to collect a sample, the balloon descends over a range of about 1-2 km in the middle stratosphere and a range of less than 0.5 km in the lower stratosphere. This determines the vertical resolution of the observations.

Analyses of the samples are made in the laboratory using gas chromatographic techniques, which give high sensitivity and precision. The precision of the analyses is about 3%. In instances where two samples were collected simultaneously the measured CH<sub>4</sub> mixing ratios were found to differ by less than 4%, indicating that the error in the sampling process is comparable with the precision of the analysis. The accuracy of the calibration is of the order of 5%.

The vertical profile data was extended into the upper stratosphere and mesosphere by a set of new measurements made by a group at the University of Pittsburgh (Zipf *et al.* unpublished 1985). A rocket borne cryogenic whole air sampler is used that condenses large air samples (~4 l STP) on gold plated cold fingers cooled to 15 K. Typical height intervals for distinct samples that are collected during a rocket flight are about 3 km at altitudes below 50 km and increase to about 5 km above 70 km altitude. After recovery the samples are transferred into stainless steel containers and their CH<sub>4</sub> content measured by gas chromatography. The samples are calibrated against commercial calibration gases to an accuracy of better than 5%. The precision of the analyses is estimated by the authors to be about 1%.

The vertical profiles obtained from these *in situ* measurements are shown in Figures 9-28a and 9-28b. The composite data display the same principal features as those discussed in the last assessment document (WMO, 1982) for mid-latitudes. However, more structure is revealed as a result of the improved vertical resolution.

The variance of CH<sub>4</sub> mixing ratios increases with altitude. Up to altitudes of about 24 km it is less than 10% (compared with an experimental accuracy of ~3-5%), but at higher altitudes relatively large deviations from the "average" vertical distribution are observed. The spread of observed mixing ratios is as large as 0.3 ppmv around 30 km. For the data presented in Figure 9-28a, this is most clearly apparent in the two observations made in October 1982 and late September 1980. Both flights show mixing ratios above 26 km that are considerably lower than the other data observed in this altitude range (Schmidt *et al.*, 1984). All the other profiles display mixing ratio values in excess of 0.7 ppmv around 30 km altitude, and rather weak gradients in the middle stratosphere compared to the sharp decreases observed lower down (< 24 km).

Some individual profiles display a stepwise structure (Fabian *et al.*, 1981b, Schmidt *et al.*, 1984) reminiscent of the structure seen in the H<sub>2</sub>O profiles (Figure 9-28b). Since the large number of samples collected per sampling flight allows better height resolution, the existence of layers with rather weak mixing ratio gradients is clearly visible. In the case of the profile observed on 9/10/83 the nearly uniform layer extends over almost 10 km. Because of the long (years) photochemical time constants for CH<sub>4</sub> destruction at these altitudes, structure of this kind is thought to be due to the effects of horizontal transport processes (Ehhalt and Tonnissen, 1980). In support of this explanation, recent *in situ* observations at 44°N have shown similar structure in the profiles of other long-lived trace gases, such as N<sub>2</sub>O, CF<sub>2</sub>Cl<sub>2</sub>, and CFC<sub>13</sub> (Schmidt *et al.* 1984). The relative variance of the mixing ratio of long-lived gases that is caused by such structures is quite different for different species. Ehhalt *et al.* (1983a) have shown that these differences are reduced when the local mean standard deviation of a given species is normalized to its vertical gradient. They defined the ratio:

$$\Delta = \delta(z) / \frac{dH}{dz}$$

as the 'equivalent displacement height'. This quantity shows very similar vertical profiles for various long-lived species, and even for ozone in the lower stratosphere which shows that the scatter in the observation is due to common causes other than experimental uncertainties.

## HYDROGEN SPECIES

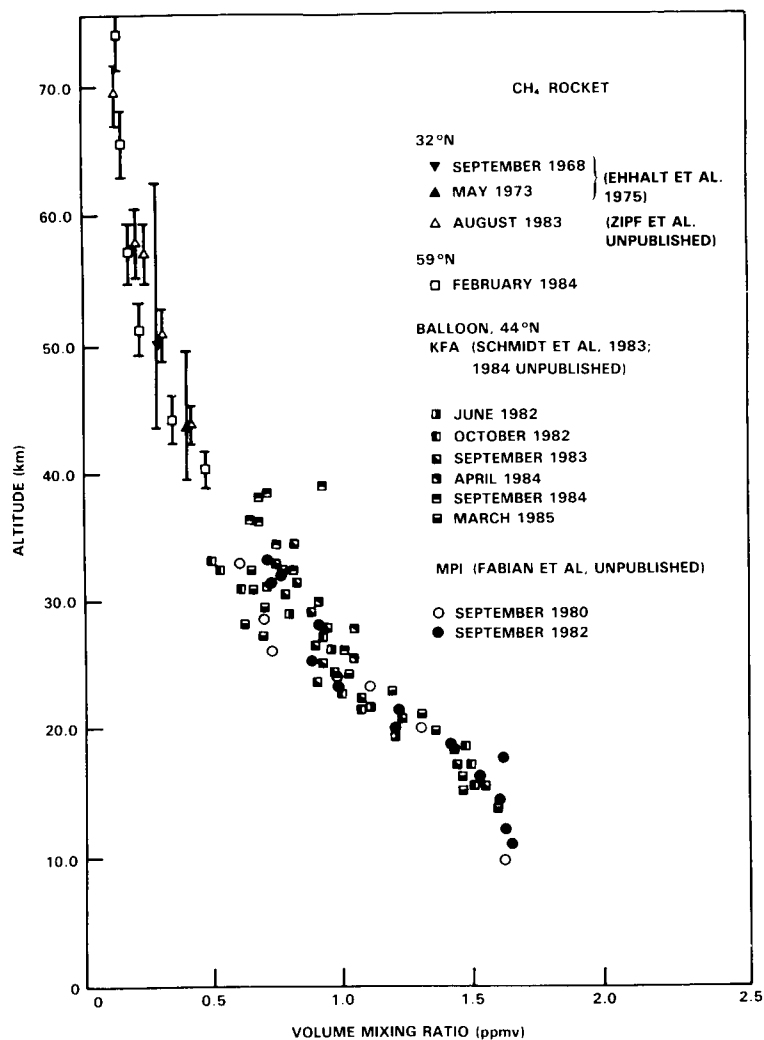


**Figure 9-28a.** *In situ* measurements of the CH<sub>4</sub> mixing ratio by balloon-borne and rocket-borne cryogenic sampling techniques in the stratosphere and lower mesosphere.

This behavior is in general agreement with the features seen in the SAMS data for northern mid-latitudes in autumn (see Figure 9-29). At levels above 10 mb (31 km) the SAMS data show enhanced latitudinal gradients for this time period. For active dynamical conditions one might therefore expect air masses for higher latitudes with low CH<sub>4</sub> mixing ratios to be transported towards the equator. During the summer months the SAMS data show a more uniform distribution of the CH<sub>4</sub> mixing ratio (Figure 9-29). Again this is confirmed by the moderate variance in the *in situ* data obtained during the other flights.

The upper stratosphere and mesosphere data obtained with the rocket borne cryosampler (Zipf *et al.*, unpublished, 1985) are also shown in Figure 9-28a. They constitute an important addition and extension of the earlier *in situ* observations made by Ehhalt *et al.* (1975). The new data show CH<sub>4</sub> mixing ratios decreasing from 0.48 ppmv at about 40 km to values of 0.14 ppmv at about 75 km. They agree well with the average CH<sub>4</sub> distribution as derived from the SAMS observations at these latitudes. The lower mesosphere observations are still too limited to allow for any assessment of the range of variation of the CH<sub>4</sub> mixing ratio in that region.

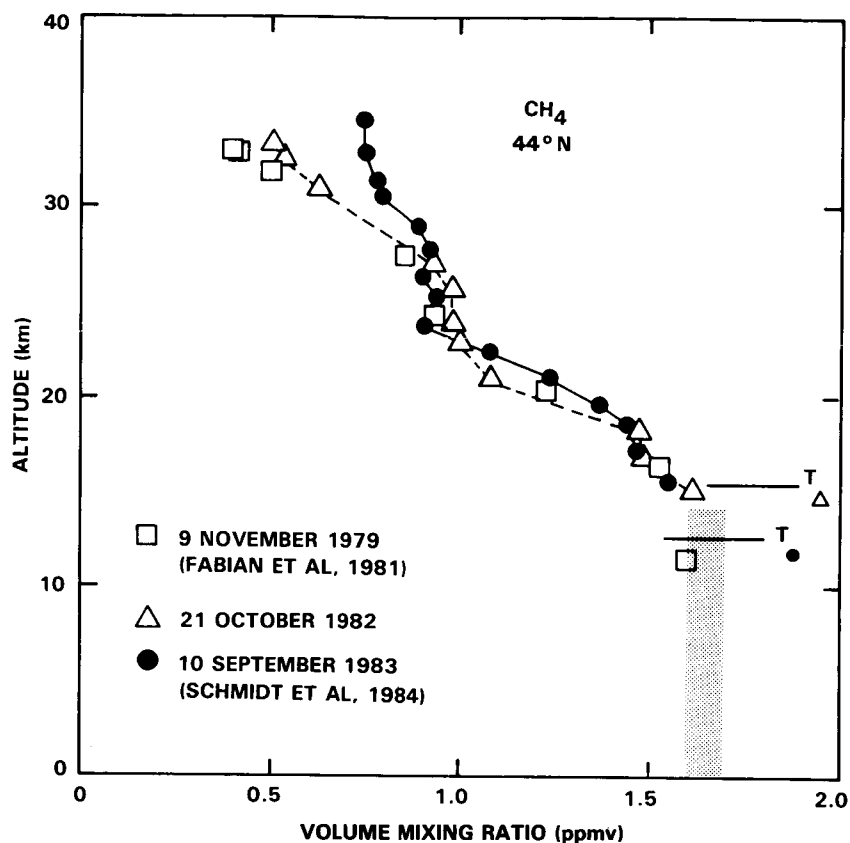


Figure 9-28b. In situ measurements of the CH<sub>4</sub> mixing ratio in the stratosphere (from Fabian *et al.*, 1981 and Schmidt *et al.*, 1984). These data form a subset of the data in Figure 9-28a.

### 9.5.2 Vertical Profiles of CH<sub>4</sub> by Remote Sensing

A number of CH<sub>4</sub> profile measurements were made during the two balloon intercomparison campaigns (BIC) in Sept/Oct 1982 and May 1983 (Figure 9-30). Details of results of these campaigns as well as a discussion of the accuracies and precisions of the various instruments may be found in Appendix C.

A grille spectrometer was flown on the Spacelab One mission (December 3, 1983 launch) to measure the abundances of a number of minor atmospheric constituents. The instrument (Laurent *et al.*, 1983) uses solar absorption spectroscopy to observe spectral features of CH<sub>4</sub> at around 3000 cm<sup>-1</sup>. Scans of spectral features taken at different tangent heights were used to derive mixing ratio profiles in the upper stratosphere and mesosphere at two locations at 27°N, 161°E and 176°W. The experimenters (Muller *et al.*, 1985) report high accuracy and precision, with 1σ errors of ~15% at all levels. A breakdown of this figure into individual error sources and with altitude is given by Ackerman *et al.* (1985).

Two profiles obtained by the grille spectrometer, taken 1.5 hours apart, are shown in Figure 9-31. Different spectral features around 3000 cm<sup>-1</sup> were used for the two retrievals. The data extend from ~27 km to above 70 km and show high mixing ratios (1 - 1.5 ppmv) in the low stratosphere, falling to ~0.5 ppmv at 50 km. Above 50 km the profiles show different characteristics, that taken at 161°E showing a continued gradual fall-off and that at 176°W showing a more uniformly mixed region centered at 65 km with some indication of an increase above. The data therefore show that little or no longitudinal

HYDROGEN SPECIES

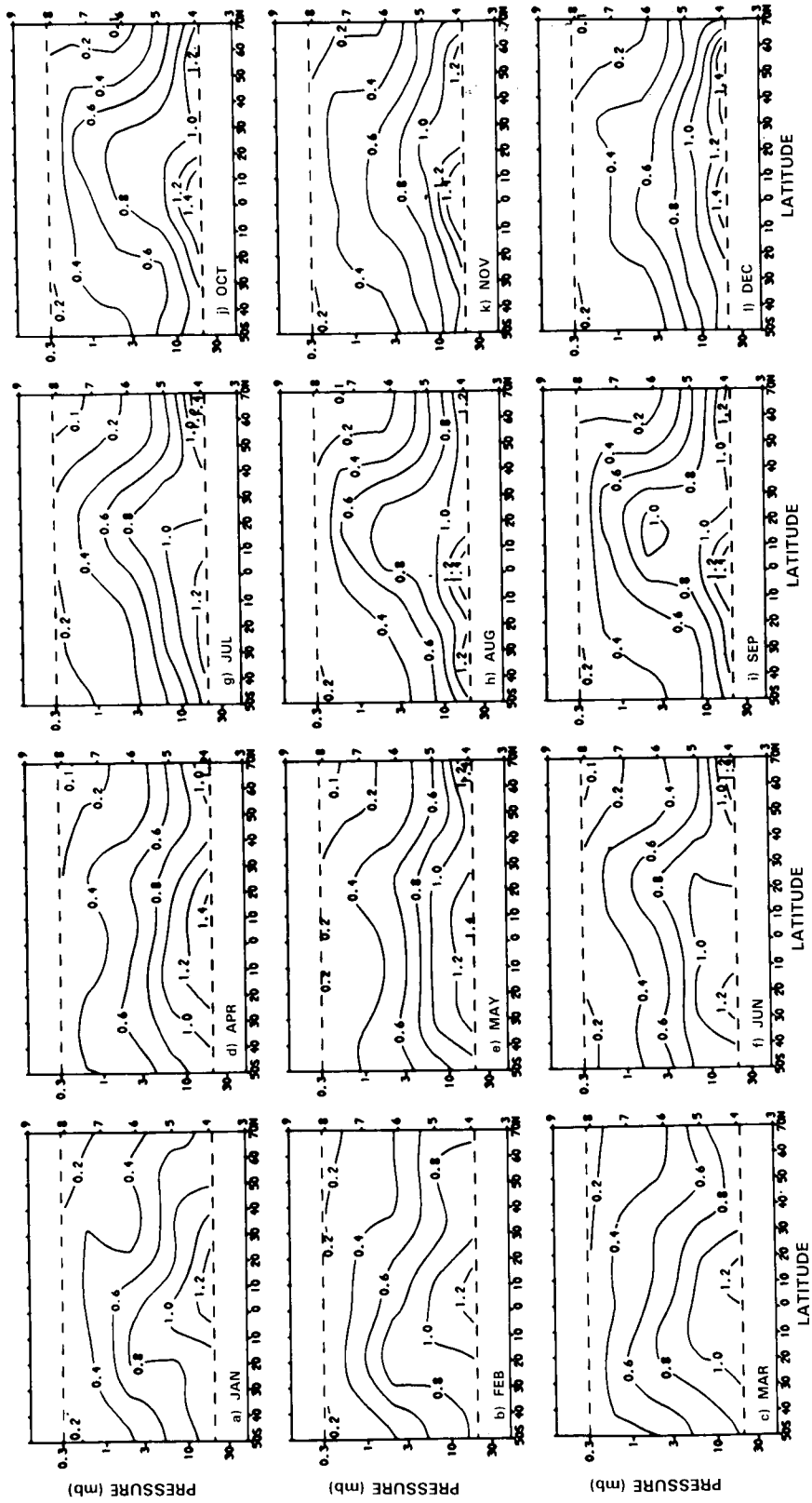
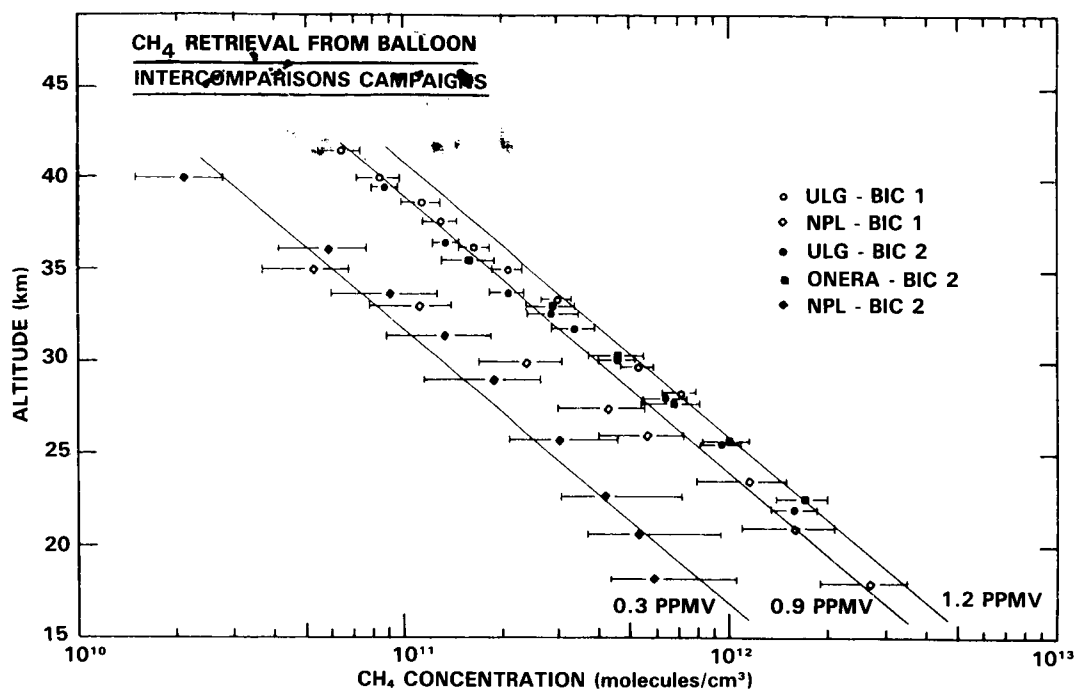


Figure 9-29. Monthly mean zonal mean cross-sections of methane (ppmv) for 1979 measured by the Stratospheric and Mesospheric Sounder (SAMS) instrument on Nimbus 7 (taken from Jones and Pyle, 1984. Note that the coverage is asymmetric about the equator, extending from 50°S - 70°N.

0.2



**Figure 9-30.** Methane concentration profiles retrieved during BIC I (open signs) and BIC II (filled signs). The error bars associated to the retrieved points do not include uncertainties on spectroscopic parameters used in the retrievals.

structure existed in the stratosphere at that time and location, with apparently more variability in the mesosphere (Ackerman *et al.* 1985).

### 9.5.3 Satellite Measurements of CH<sub>4</sub>

The SAMS instrument launched on the Nimbus 7 satellite in October 1978 was a multichannel, limb scanning, infrared radiometer measuring atmospheric temperature, line-of-sight pressure and the abundances of a number of minor atmospheric constituents. Measurements of thermal emission from the  $\nu_4$  band of CH<sub>4</sub> between 1200 and 1340 cm<sup>-1</sup> were used to derive CH<sub>4</sub> mixing ratios between 20 mb (~28 km) and 0.3 mb (~58 km) with a vertical resolution of ~8 km. The orbit configuration and viewing geometry of SAMS provided coverage from 50°S to 70°N each day.

Details of the instrument design may be found in Drummond *et al.* (1980). The use of a common optical chain and detector for both the CH<sub>4</sub> and the N<sub>2</sub>O channels meant that these gases could not be observed simultaneously and were measured on alternate 24 hour periods. With the SAMS duty cycle of three operational days in four, CH<sub>4</sub> measurements were thus made on about 12 days per month.

The details of the CH<sub>4</sub> channel on SAMS were, in many respects, similar to those of the N<sub>2</sub>O channel, which has been described in the NO<sub>x</sub> chapter. A statistical inversion method was used to retrieve mixing ratios from the radiance data. Details of this and the instrument calibration procedures may be found in Rodgers *et al.* (1984) and Wale and Peskett (1984) respectively.

A detailed investigation of the sources of errors in the SAMS CH<sub>4</sub> observations has been described by Jones and Pyle (1984). They found that systematic errors in the retrieved CH<sub>4</sub> fields fell into four main

## HYDROGEN SPECIES

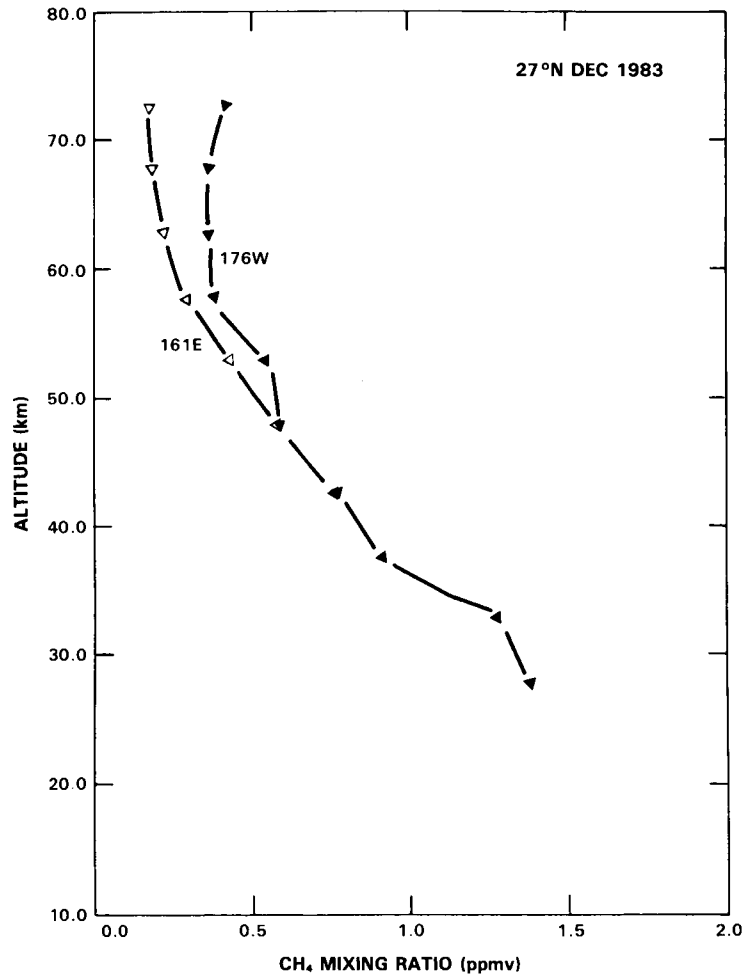


**Figure 9-31.** Profiles of CH<sub>4</sub> (ppmv) measured by the grille spectrometer on Spacelab One (Ackerman *et al.*, 1985). Errors on the data are estimated to be  $\pm 15\%$ . The two profiles were obtained 1.5 hours apart.

categories: (1) uncertainties in the spectroscopy of CH<sub>4</sub> and of any other overlapping gases (mainly N<sub>2</sub>O); (2) instrumental and calibration uncertainties; (3) limitations and simplifications in the retrieval method and algorithm, and (4) inaccurate knowledge of the atmospheric state (mainly the temperature structure).

To estimate the impacts of these various systematic error sources, a synthetic radiance profile was computed using typical mixing ratio and temperature profiles with all the uncertain parameters set to their nominal values. The simulated data set was then retrieved with the uncertain parameters offset, in turn, to their uncertainty limits, and the profiles thus obtained compared each time with the original.

There was a significant random component to the error budget even when zonal means were considered. The effects of this on the retrieved profiles was quantified during the retrieval process by means of an error covariance matrix. In practice, only the diagonal elements of this matrix were used. This simplification, which ignores correlations between measurement errors at different levels of the atmosphere, tends to overestimate the random error at all levels.

A summary of the error budget of the SAMS CH<sub>4</sub> observations is shown for various pressure levels in Table 9-4.

Table 9-4. SAMS Estimated Accuracy and Precision for CH<sub>4</sub> Measurements

Pressure Level (mbar)	20	7	2	0.6	0.2
1. Spectroscopy	± 7%	± 7%	± 5%	± 5%	± 5%
2. Field of View	± 2%	± 1%	± 3%	± 6%	± 3%
3. Mean PMC Pressure	± 3%	± 2%	± 6%	± 6%	± 3%
4. Uncompensated Doppler shifts	± 1.5%	± 1%	± 1.5%	± 6%	± 7%
5. Zonal Averaging	± 8%	± 8%	± 8%	± 8%	± 8%
6. Interference of N <sub>2</sub> O	± 5%	± 2%	± 0.5%	—	
7. Temperature (2K)	± 50%	± 15%	± 10%	± 10%	± 10%
8. Line-of-sight attitude (+ 0.006)	± 4%	± 2%	± 6%	± 10%	± 6%
9. RMS of latitude and time dependent errors	± 51%	± 15%	± 12%	± 17%	± 14%
10. RMS of bias errors	± 9%	± 6%	± 8%	± 10%	± 7%
11. Net RMS accuracy	±52%	± 18%	±17%	± 21%	± 17%
12. Precision of monthly mean cross section	±5-15%	±3-10%	±3-13%	±4-13%	±20-40%

Overall, the most important error sources are thought to be uncertainties in spectroscopy, the direct evaluation from zonal mean radiance and temperature profiles of a zonal mean mixing ratio profile, and uncertainties in the line of sight attitude and atmospheric temperature. The effects of uncompensated Doppler shifts contribute somewhat at upper levels (above 0.6 mb). The net RMS accuracy is ~20% above 7 mb, increasing, due to uncertainties in atmospheric temperature below, to ~50% at 20 mb. By comparison, random errors on a monthly mean zonal mean cross section vary between 3 and 15% below 0.6 mb, depending on the temperature and mixing ratio fields, increasing somewhat above this level.

The data from the three year period, 1978-81 have been studied in detail. Figures 9-29 (a)-(l) and 9-32 show monthly mean cross sections of CH<sub>4</sub> measured by SAMS for January to December 1979. The data are not symmetric about the equator, extending from 50°S to 70°N. Useful coverage is obtained between ~20 and 0.2 mb, covering the middle and upper stratosphere and the low mesosphere. Each monthly mean comprises approximately 12 days data per month.

The gross structure shown by these data is of a low stratosphere, low latitude mixing ratio maximum of ~1.2 ppmv at 20 mb (27 km), falling to 0.3 - 0.1 ppmv at the stratopause. Closer inspection reveals pronounced seasonal differences.

In January 1979 (Figures 9-29a and 9-32a) there was a marked asymmetry in the CH<sub>4</sub> field, with a region of elevated mixing ratio extending from the equator at 20 mb, tilting into the Southern (summer) Hemisphere, reaching ~20°S by the stratopause level. This feature persisted through February (Figures 9-29b and 32b), giving rise to sharp latitudinal gradients at high southern latitudes, with somewhat weaker gradients in the Northern Hemisphere. By March (Figures 9-29c and 32c) a second maximum began to emerge in the Northern Hemisphere as the first began to subside giving, by March and April (Figures 9-29c and d and 32c and d), an almost symmetrical appearance with, on a fixed pressure surface, two low latitude mixing ratio maxima separated by an equatorial minimum. This changeover continued

ORIGINAL PAGE  
COLOR PHOTOGRAPH

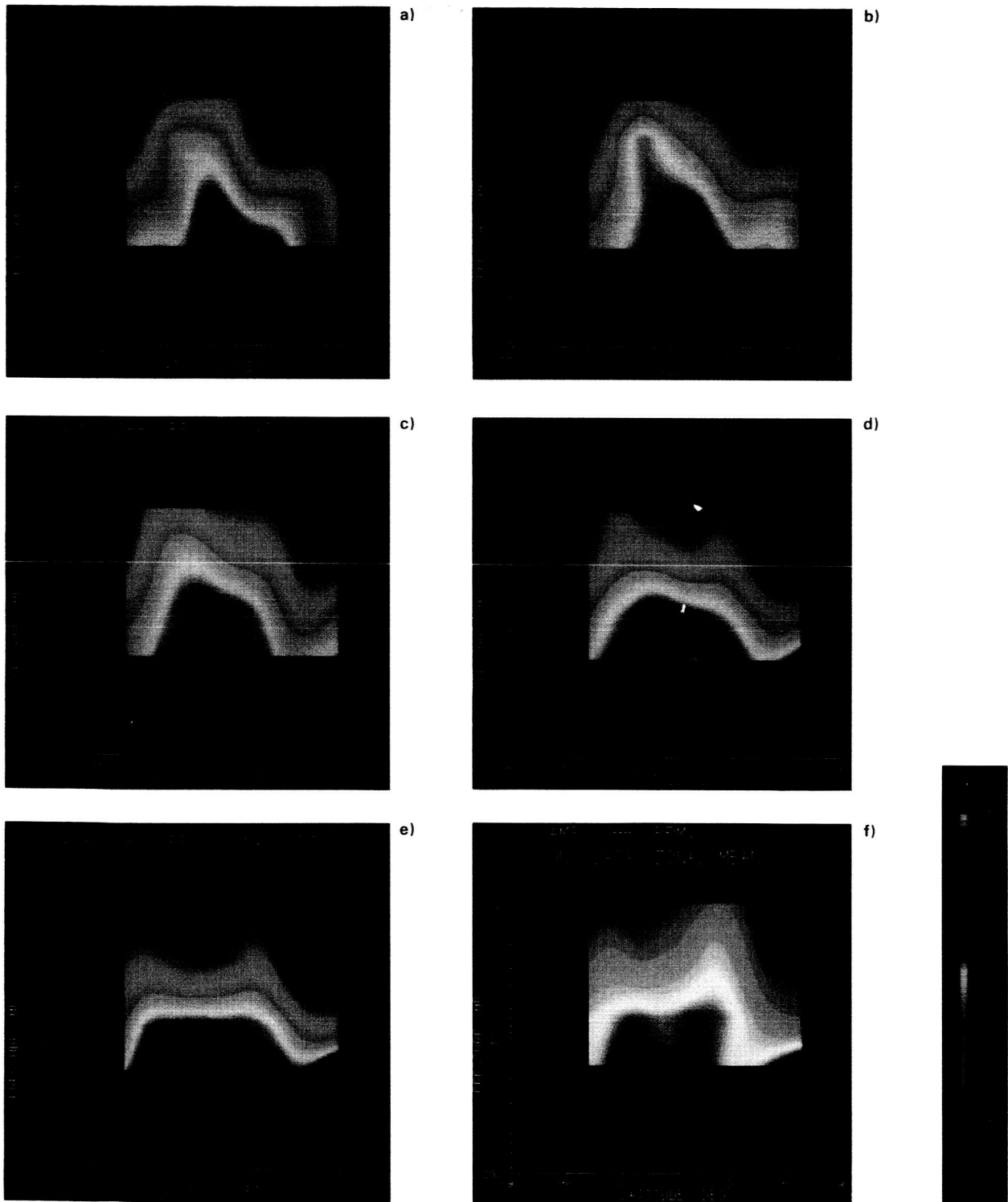


**Figure 9-32.** Monthly mean zonal cross-sections of methane (ppmv) measured by the Stratospheric and Mesospheric Sounder (SAMS) instrument on Nimbus 7 for (a) January 1979, (b) February 1979, (c) March 1979, (d) April 1979, (e) May 1979 and (f) June 1979. These data form a subset of the data shown in Figure 9-29.

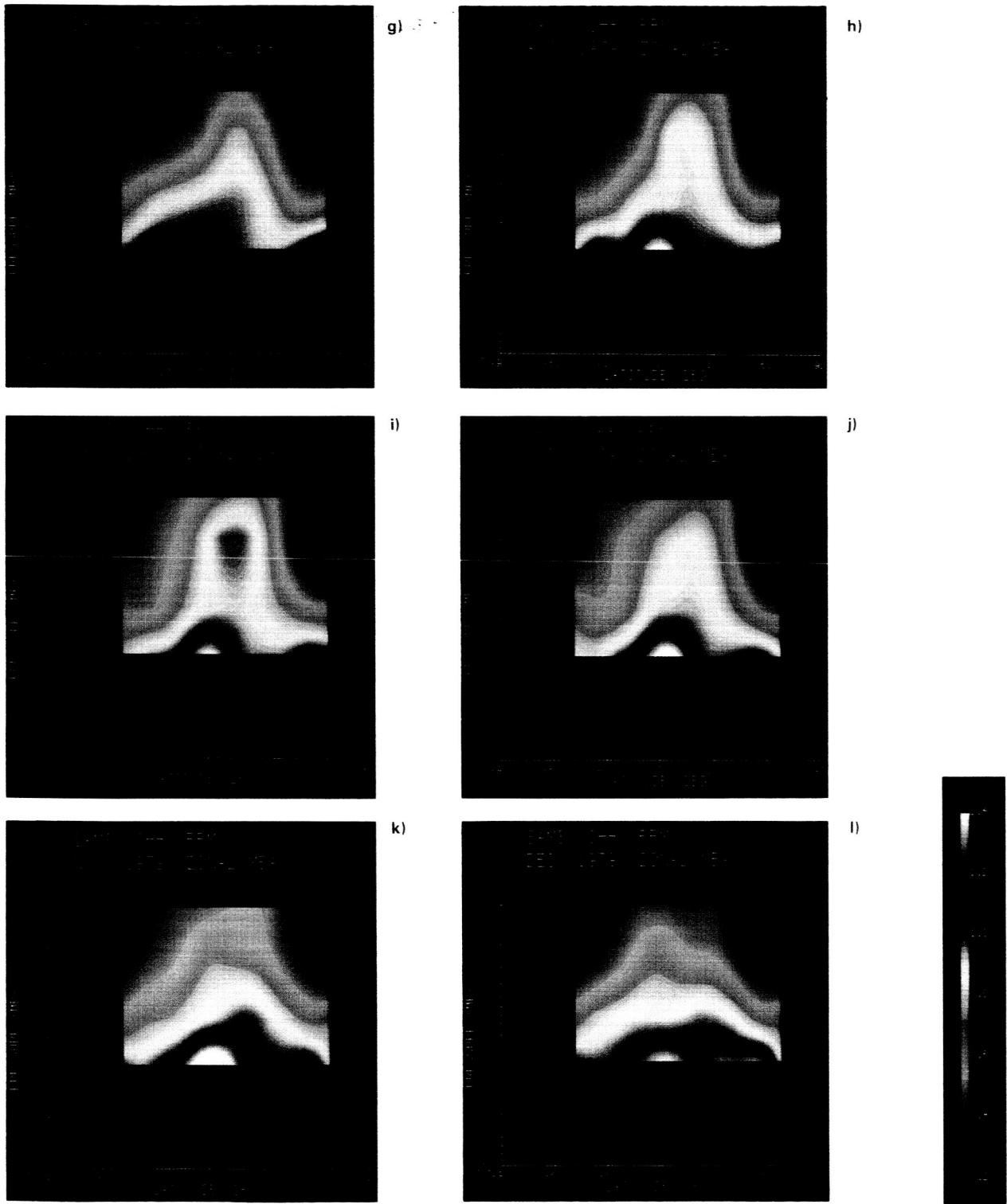


**Figure 9-32.** Monthly mean zonal cross-sections of methane (ppmv) measured by the Stratospheric and Mesospheric Sounder (SAMS) instrument on Nimbus 7 for each month in 1979 beginning with (g) July through (l) December 1979. These data form a subset of the data shown in Figure 9-29.

## HYDROGEN SPECIES

through June (Figures 9-29f and 32f) giving, by July (Figures 9-29g and 32g), a single maximum extending into the Northern Hemisphere. The distribution observed during July was essentially a reversal of that seen during January, with sharp latitudinal gradients at high northern latitudes and weaker gradients everywhere in the Southern Hemisphere.

The behavior during the second half of 1979 differed in many respects from that of the first. During August and September (Figures 9-29h and i, and 32h and i), the Northern Hemisphere maximum intensified considerably, giving rise to an almost uniformly mixed region at high northern latitudes in the upper stratosphere until October (Figures 9-29j and 32j). Interestingly, the pronounced "double peak" structure evident during May that year was not repeated. In the final three months of 1979 the maximum subsided to give an almost symmetrical distribution by December (Figures 9-29l and 32l).

Three years of CH<sub>4</sub> data have now been examined. It appears (Jones, 1984) that, while minor differences do occur from year to year, the seasonal behavior remained essentially unchanged from that of 1979. For example, Figure 9-33 shows monthly mean cross-sections for January, April, July and October for the years 1979, 1980 and 1981. These months are chosen to emphasize the contrast between the methane distributions observed at different times of the year. All three years show regions of elevated mixing ratio extending into the summer hemisphere in January and July, with the "double peak" apparent in all three years, although less markedly in April 1981, being most pronounced during May of that year.

While the similarities between the structure seen during the three years are obvious, some differences warrant comment. Figure 9-34 shows time marches of CH<sub>4</sub> mixing ratios at 3 levels (10, 3, and 1 mb) at 65°N for the three years of data. While the three summers (April to September) are remarkably consistent from year to year, the winter periods differ markedly. For example, while the vertical gradient was maintained throughout the winter of 1979/80, there were periods in both 1978/79 and 1980/81 when there was no decrease of CH<sub>4</sub> with height at this latitude. The arrows on the upper margin of the figure identify the active periods during each winter. For the purposes of the study these were identified with maxima in the 10 mb temperature at the north pole as indicated by Labitzke (1979) and Labitzke *et al.* (1980, 1981). The large arrows denote major (~20 K) increases, the smaller arrows more minor ones. The major events in the CH<sub>4</sub> time marches are correlated with the active periods during the warmings which differ from year to year.

The CH<sub>4</sub> data from SAMS have shown many new and hitherto unseen features. Foremost among these is the branching of air into the summer hemisphere giving, at certain times of the year, a "double peak" in mixing ratio with a local minimum at the equator. Similar features have been observed for N<sub>2</sub>O (Jones and Pyle, 1984) and H<sub>2</sub>O (Russell *et al.*, 1984c), both measured from the Nimbus 7 satellite.

There are substantial semiannual variations in the data. For example, no "double peak" is seen in the latter half of the years studied to date. Seasonal changes show a high degree of consistency from year to year, with some differences in the winter hemispheres. It would appear that the three years of SAMS CH<sub>4</sub> data represent a useful climatology of that gas.

The global data sets on CH<sub>4</sub> (and N<sub>2</sub>O) from SAMS and on H<sub>2</sub>O from LIMS offer an important opportunity for understanding the transport of tracers in the stratosphere. One of the most interesting features of the observed fields is the presence, at certain times of the year, of 'double peaks' in equatorial latitudes. This structure was not anticipated by theory.

Recent modelling work appears to have explained the 'double peaks' and helped in the general understanding of transport processes. In a two dimensional model study, Gray and Pyle (1985) were able to

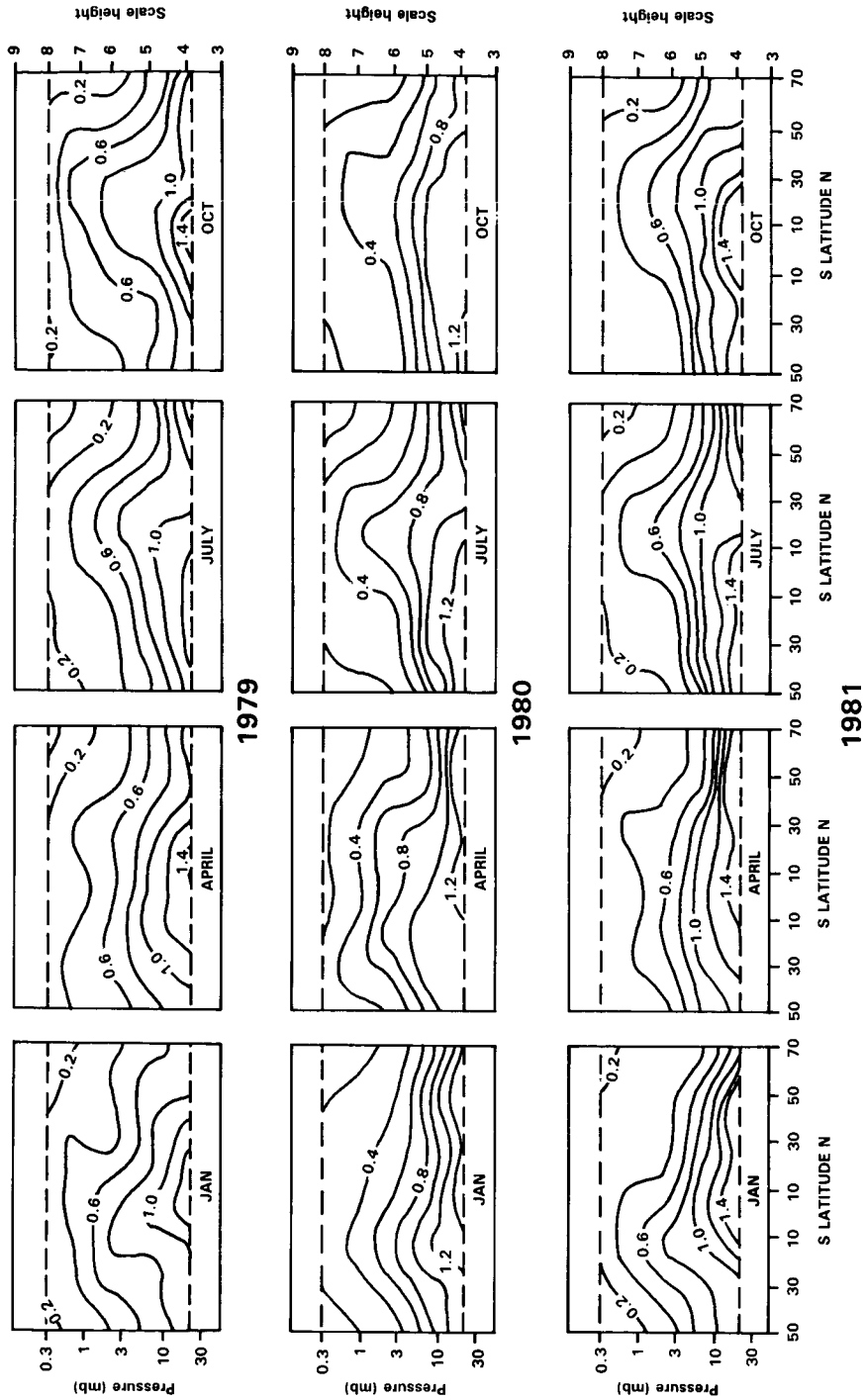


**Figure 9-33.** Monthly mean zonal mean cross-sections of methane (ppmv) for January, April, July and October for the years 1979, 1980 and 1981. Note the asymmetric coverage about the equator. The cross sections illustrate the small interannual variability compared with the marked seasonal changes. Note that the "double peak" is seen in all three years of data (from Jones, 1984).

## HYDROGEN SPECIES

reproduce the main features of the equatorial behavior only when they included the forcing of the semi-annual oscillation. They successfully modelled the double peak improving the seasonal behavior in low latitudes compared with model studies excluding the semiannual oscillation (see Chapter 12.6). This particular model interpretation of the satellite data has pointed to an important role for equatorial dynamics in determining the observed distributions of tracers. Solomon *et al.* (1986) have also reproduced the double peak in CH<sub>4</sub> in a model study in which the transport is effected by the diabatic circulation, diagnosed from LIMS ozone and temperature data. They find excellent agreement with the observed CH<sub>4</sub> fields in low latitudes (see Chapter 12.6 for a more complete discussion).

Another interesting feature of CH<sub>4</sub> data from SAMS is the presence of regions of weak and strong horizontal gradients. These can throw some light on the importance of eddy transport. Weak gradients generally lie along observed isotropic surfaces indicating strong mixing. The relationship of the mixing to the 'surf zone' ideas of McIntyre and Palmer (1984) is still to be explained in detail.

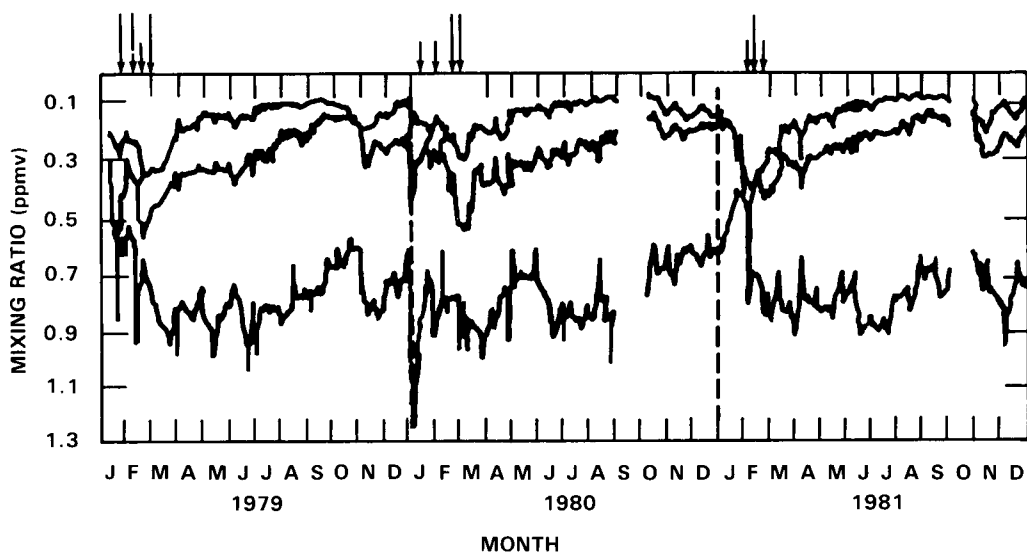


**Figure 9-34.** Mixing ratios of CH<sub>4</sub> at 10, 3 and 1 mb for the latitude band centered at 65°N for the period 1979–81 measured by SAMS. While relatively little variability is seen, particularly at upper levels during the summer, marked fluctuations correlating with warming events (arrows) are seen during winter months (from Jones, 1984).

### 9.5.4 Intercomparison of CH<sub>4</sub> Data

The different measurement times, locations, and techniques prevent a direct intercomparison of all the CH<sub>4</sub> data presented above. For example, no upper stratospheric *in situ* measurements were made during the lifetime of the SAMS instrument. While comparisons such as those during BIC and MAP-GLOBUS are described elsewhere, this section aims at giving an overall picture of the consistency of the CH<sub>4</sub> data now available. Since the only new data in the Southern Hemisphere has come from the SAMS instrument, such a comparison is only meaningful for the Northern Hemisphere.

Only the SAMS instrument provided high quality zonal mean data. Comparison of this data with *in situ* and other local measurements is limited by the substantial variability exhibited by the *in situ* data and the absence of any clearly defined seasonal behavior (see e.g. Figure 9-34). The approach taken here follows

that adopted by Jones and Pyle (1984). Annual mean profiles from SAMS have been plotted with all the available *in situ* data within specific latitude bands. Figures 9-35 to 9-38 show such comparisons at equatorial latitudes, 20–40°N, 40–60°N and 60–70°N respectively.

At equatorial latitudes (Figure 9-35) there has been no new, *in situ* data since WMO 1982. The SAMS data extends to much higher level at this latitude (55 km compared with 35 km), and is in good agreement at low levels (~30 km).

A variety of new observations have been made between 20°N–40°N (Figure 9-36) since WMO 1982. Despite the different techniques used, there is a broad consistency in the CH<sub>4</sub> profiles in this latitude range, with CH<sub>4</sub> mixing ratios falling almost linearly from 1.6 ppmv at the tropopause to around 0.5 ppmv at 50 km. Above this level both the rocket borne, *in situ* and the grille spectrometer profiles show the gradient lessening. The profiles obtained during the balloon intercomparison campaigns deviate somewhat from this picture, as described in Appendix C.

There is also good consistency in the range 40–60° N (Figure 9-37) between the SAMS data and the *in situ* measurements (both balloon and rocket) above ~30 km, with some suggestion that the SAMS data has a positive bias at lower altitudes as discussed by Jones and Pyle (1984). The 1975 AES profile

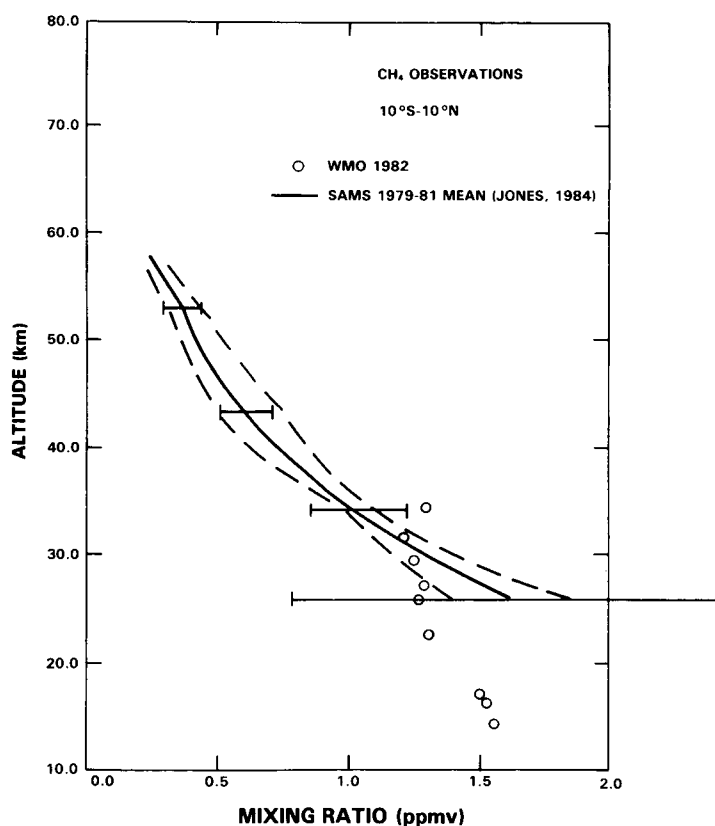


**Figure 9-35.** Comparison of the SAMS 1979–81 mean vertical profile for CH<sub>4</sub> between 10°S and 10°N (Jones, 1984) with *in situ* data taken within the same latitude band. The dashed lines represent the standard deviation of the monthly mean SAMS profiles over this period and the horizontal bars the estimated measurement accuracy.

## HYDROGEN SPECIES

appears to be rather low below 25 km. Evans (1985) suggests that this is an indication of a trend in atmospheric  $\text{CH}_4$ . The data at this latitude show a clear picture of mixing ratios falling almost linearly up to  $\sim 40$  km from around 1.5 ppmv to  $\sim 0.4$  ppmv, with much weaker gradients above.

There are no new *in situ* observations at latitudes higher than  $60^\circ\text{N}$ . Between  $60 - 70^\circ\text{N}$  the SAMS annual mean profile shows good agreement with the earlier *in situ* data (Figure 9-38). The data show a sharp fall off in mixing ratio to around 0.25 ppmv at 40 km with a more uniformly mixed region above, similar to the behavior observed between  $40-60^\circ\text{N}$ .

### 9.5.5 Total Hydrogen Content of the Stratosphere

Current understanding of stratospheric chemistry predicts that  $\text{CH}_4$  is oxidized into  $\text{CO}_2$  and  $\text{H}_2\text{O}$ . If there is no heterogeneous removal of water from the stratosphere, hydrogen should be conserved in

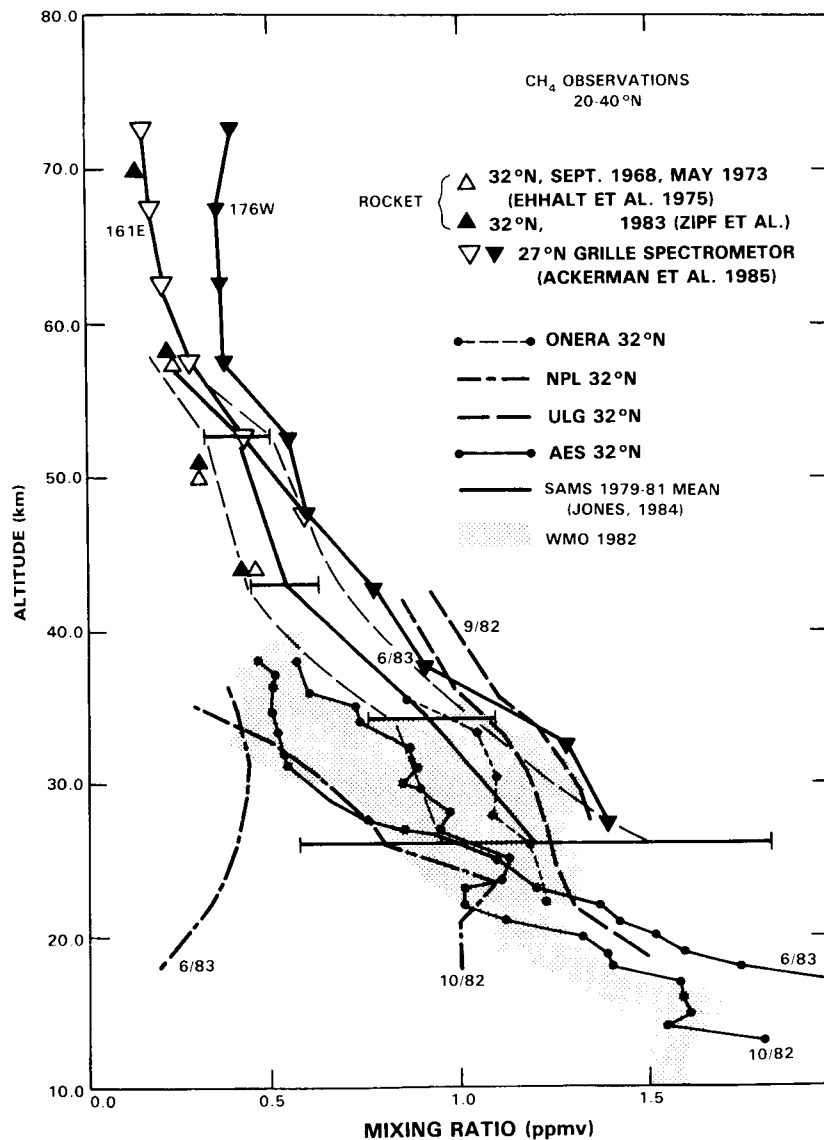


Figure 9-36. As for Figure 9-35 except for latitudes  $20-40^\circ\text{N}$ .

this process. The total hydrogen should be closely approximated by the sum  $2 \times \text{CH}_4 + \text{H}_2\text{O}$ . Strictly speaking, molecular hydrogen ( $\text{H}_2$ ) should also be included, but since its contribution is less than either of the other species and it is essentially uniformly distributed with height (see for example Ehhalt *et al.* (1975a); Volz *et al.* (1981)) its omission does not have serious consequences and may in most cases be treated as an offset of approximately 0.5 ppmv ( $\text{H}_2$ ).

The total hydrogen content of stratospheric air using local measurements has been investigated by Pollock *et al.* (1980) and Rinsland *et al.* (1984b). The former study was based on 6 flights of a balloon-borne cryogenic sampler between 1975 and 1978 and included molecular hydrogen in the sum. The study of Rinsland (1984) used  $\text{CH}_4$  and  $\text{H}_2\text{O}$  profiles derived from solar occultation spectra taken during a single flight of a balloon-borne Fourier transform interferometer. The two studies show a good degree of consistency, giving approximately 6 ppmv of total hydrogen.

Jones *et al.* (1985) have combined simultaneous satellite data for  $\text{CH}_4$  and  $\text{H}_2\text{O}$ . They showed that, for the 30 to 40 km region from  $60^\circ\text{S}$  to  $80^\circ\text{N}$ , the sum of  $\text{H}_2\text{O} + 2 \times \text{CH}_4$  is, on average, about 6 ppmv,

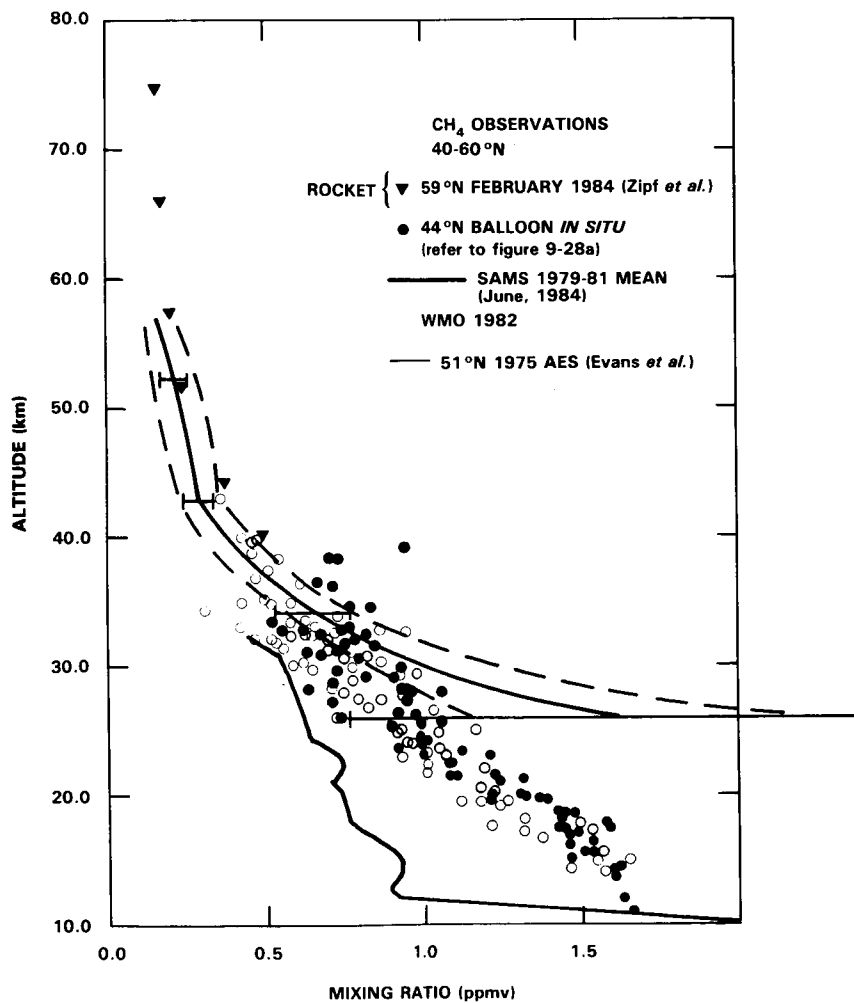
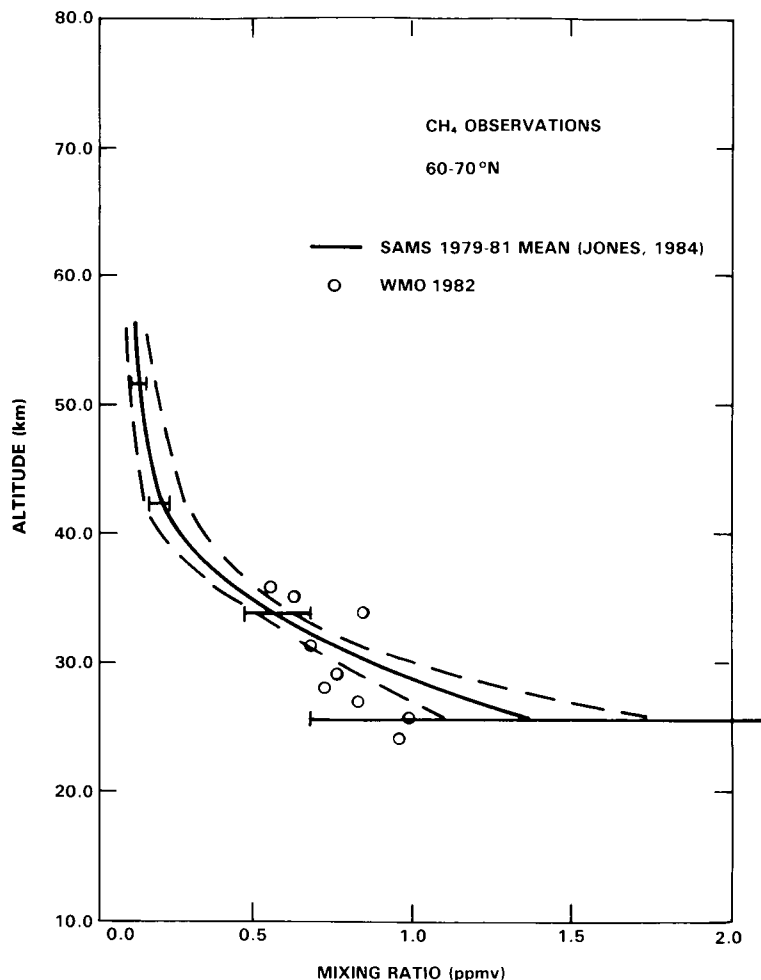


Figure 9-37. As for Figure 9-35 except for latitudes  $40\text{-}60^\circ\text{N}$ .

## HYDROGEN SPECIES



**Figure 9-38.** As for Figure 9-35 except for latitudes between 60–70°N.

to an accuracy of  $\pm 0.5$  ppmv. Figure 9-39 and 9-40 show cross-sections of this sum based on monthly mean observations from January and May 1979 respectively, from the LIMS and SAMS instruments. Structure in this sum above 3 mb is not significant when compared with the estimated error in the sum ( $\sim 0.5$  ppmv). Other months examined reveal the same featureless fields. The fact that the sum is so invariant in time and space points to CH<sub>4</sub> and H<sub>2</sub>O forming a chemical family in which CH<sub>4</sub> is the dominant stratospheric source of water vapor, i.e., the CH<sub>4</sub> oxidation hypothesis is correct. The decrease in CH<sub>4</sub> with increasing altitudes and latitudes must therefore be accompanied by a corresponding increase in H<sub>2</sub>O. The variations of the sum at the 10% accuracy level may reflect the precision of the satellite data rather than a true atmospheric variation.

The demonstration of the CH<sub>4</sub> oxidation process in the stratosphere raises the interesting question of whether this uniformity in total hydrogen conservation holds to the 10% level on a local, *in situ* basis throughout the middle stratosphere. If this were the case, the circulation of water in the stratosphere would be highly constrained so that all air entering the stratosphere must have been processed through the same, hygroscopic cold trap. Variations in total hydrogen in the order of 10% in individual air parcels might

HYDROGEN SPECIES

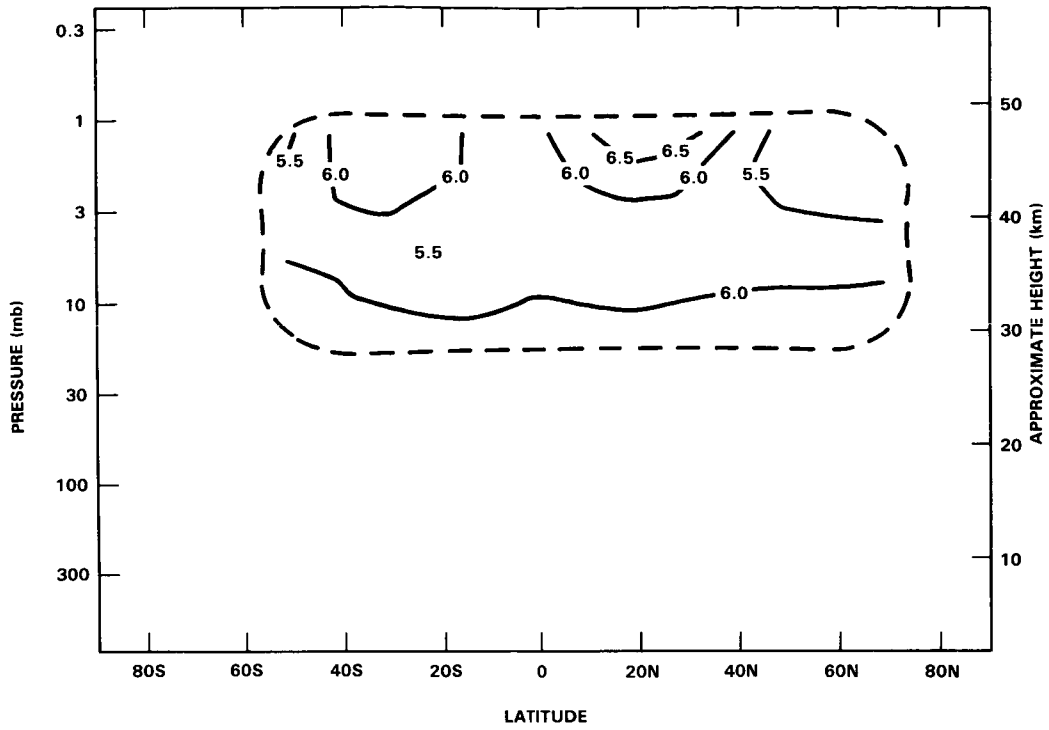


Figure 9-39. Cross section of  $2 \times \text{CH}_4 + \text{H}_2\text{O}$  from SAMS and LIMS data. The data were derived from January, 1979 monthly mean data. (Jones *et al.*, 1985).

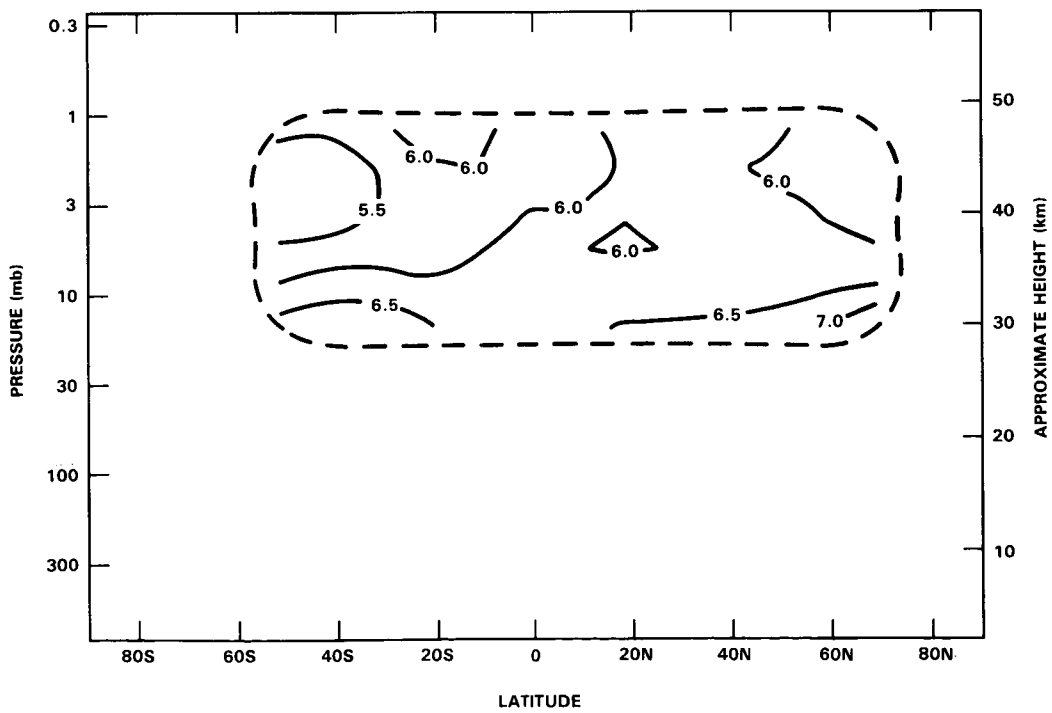


Figure 9-40. Cross section of  $2 \times \text{CH}_4 + \text{H}_2\text{O}$  for May, 1979 from SAMS and LIMS data.

## HYDROGEN SPECIES

be expected if air entering the stratosphere passed through a cold trap at the tropical tropopause with seasonally or spatially varying temperatures or if more than one mechanism is responsible for drying the stratosphere.

The recent measurements by Kley *et al.* show structure in water vapor concentrations, with vertical features as small as 100 m in the lower stratosphere. This variability may be associated either with differing photochemical evolution among air parcels (i.e., conversion of CH<sub>4</sub> into H<sub>2</sub>O) or with inherent variations in the hygroscopic mechanisms which dry out stratospheric air. In either case the existence of thin, distinct layers with differing composition must be evaluated in terms of their role in large-scale transport of trace species in the stratosphere, especially since no current models are capable of resolving these features.

### 9.6 CONCLUSIONS

The data base for OH, HO<sub>2</sub> and H<sub>2</sub>O<sub>2</sub> vertical profiles has not expanded in a major way since the last assessment.

Only one new OH profile measurement has been obtained. It extended over an altitude range of 28–38 km. The new profile is lower than most of the earlier profiles and current model predictions. However, given the precision of the data and the wide range of values predicted by the models the discrepancy cannot be considered to be serious. It is clear that the data is insufficient to provide a critical test of the HO<sub>x</sub> partitioning and budget. The profile data for OH has been complemented by 7 years of quasi-continuous, ground-based, solar absorption column measurements which show a long term trend, seasonal, diurnal and geographical variability and response to volcanic eruptions and solar eclipse. This column data for OH is a valuable record awaiting theoretical interpretation.

For HO<sub>2</sub>, two independent data sets, obtained from balloon-borne *in situ* cryogenic sampling and ground-based mm-wave techniques cover the range 16–34 km and 35–60 km, respectively. The HO<sub>2</sub> concentrations measured in the 16–34 km range are substantially higher than those predicted from theoretical models, and are not consistent with the ground-based mm wave observations. This discrepancy suggests a problem either in the *in situ* measurements or in our current understanding of HO<sub>x</sub> chemistry. The HO<sub>2</sub> measurements in the 35–60 km range are consistent with current theoretical predictions.

Although there have been only a limited number of observations of OH and HO<sub>2</sub> profiles over the past four years there have been major advances in observing systems for these species. Four new, balloon-borne instruments have demonstrated their capabilities for observing the diurnal variability of OH, and the potential for HO<sub>2</sub> measurements looks promising. A substantial expansion of the data bases for both these species is anticipated.

Major improvements have occurred in our knowledge of the spatial and temporal distributions of stratospheric and mesospheric H<sub>2</sub>O and CH<sub>4</sub>. While most of these improvements have come from satellite observations, significant new information has also been obtained from balloon *in situ* and ground-based measurements, particularly for H<sub>2</sub>O. Clear evidence has been obtained for the existence of a hygropause, a region of minimum H<sub>2</sub>O mixing ratios, just above the tropopause. Structure in the vertical profiles for both species, but especially for H<sub>2</sub>O has been observed as a result of the improved vertical resolution (~0.5 km) of the *in situ* measurements. Also measurements both by *in situ*-sampler and remote methods have extended the data for H<sub>2</sub>O and CH<sub>4</sub> throughout the mesosphere.

Observations by the LIMS instrument on Nimbus 7 over the period October, 1978 to May 1979 have revealed the global distributions (64°S to 84°N) of H<sub>2</sub>O from 100 to 1 mb (16 to 50 km) for the first

time. The key observations are: (a) the zonal means show a region of low mixing ratio ( $\sim 3$  ppmv) at  $\sim 60$  mb ( $\sim 22$  km) extending over low latitudes (the hygropause region); (b) the mixing ratio generally increased poleward and upwards in tropical regions reaching a maximum value of  $\sim 6$  ppmv; (c) the variability in mean zonal mixing ratios is small except in high latitude winter; (d) the longitudinal variability in mixing ratio is 0.5 ppmv in the tropics, and ranges from 1 to 1.5 ppmv at mid-to-high latitudes.

The SAMS instrument on Nimbus 7 has provided near global observations ( $50^\circ\text{S}$  to  $70^\circ\text{N}$ ) of  $\text{CH}_4$  from October, 1978 to June, 1983 from 20 to 0.3 mb (27 to 55 km). The data show: (a) a low latitude, low stratospheric maximum, with mixing ratios generally decreasing polewards and upwards; (b) gradients in the vertical distributions exhibit a wide range depending on latitude and season; (c) significant seasonal changes with a marked asymmetry between the equinoxes each year; (d) little interannual variability.

The satellite data set of  $\text{H}_2\text{O}$  and  $\text{CH}_4$  have clearly demonstrated that air is transported upward and poleward from the tropics. The transport of dry air in this fashion is consistent with the Brewer-Dobson hypothesis. The combination of these data sets has demonstrated that the total hydrogen budget of the stratosphere, viz  $\text{H}_2\text{O} + 2 \text{CH}_4$ , is relatively constant at values ranging from 6 to 7 ppmv. The satellite data also shows enhanced  $\text{H}_2\text{O}$  levels in the lower stratosphere at high latitudes ( $> 50$ ) in the winter indicating that not all the  $\text{H}_2\text{O}$  in the stratosphere can be explained by exchange in the tropics and  $\text{CH}_4$  oxidation. Simulation of the observed variability in the spatial and temporal distribution of  $\text{CH}_4$  and  $\text{H}_2\text{O}$  utilizing multidimensional models present a major challenge to the modelling community.

## 9.7 FUTURE RESEARCH NEEDS

Despite the fundamental role of the  $\text{HO}_x$  family ( $\text{HO}$ ,  $\text{HO}_2$ ,  $\text{H}_2\text{O}_2$ ) in stratospheric chemistry, the data base for that group remains one of the poorest of all species in the atmosphere. Very few definitive measurements are available for the needed quantities, which are the concentrations of the species, the partitioning between the family members, and the latitudinal, diurnal, and seasonal variations.

Ultimately, measurements must be made simultaneously of as many family members as possible, and it will also be especially important to make concurrent measurements of those species such as  $\text{O}$ ,  $\text{O}_3$ ,  $\text{NO}$ , etc., which control the partitioning between family members.

A substantial complement of instrumentation exists for the *in situ* and remote sensing of the  $\text{HO}_x$  species. The principal need at the present time is for the verification and application of these capabilities. The achievement of this goal has been greatly hindered by unreliability and failure of the balloon platforms, which are required for virtually all of these instruments. There is thus an urgent need for the resolution of the balloon reliability problem, and it is doubtful that a substantial data base on  $\text{HO}_x$  can be acquired until this has been accomplished (this is obviously also true for measurements of  $\text{NO}_x$  and  $\text{ClO}_x$  species).

Ground-based instruments, which are free of the limitations of balloon platforms, may have a useful role in future programs, provided that adequate accuracy, sensitivity, and altitude resolution can be achieved. The existing data base of Burnett for column  $\text{OH}$  should be fully exploited. However, total column measurements of  $\text{OH}$  suffer from the disadvantage of domination by the mesospheric component, and in any case total  $\text{OH}$  measurements alone do not provide an adequate test of model validity.

The mesospheric region requires further observational and theoretical investigation, because ozone concentrations in that part of the atmosphere are photochemically controlled and the photochemistry is dominated by the  $\text{HO}_x$  family. The mesosphere thus provides a good test of  $\text{HO}_x$  chemistry.

## HYDROGEN SPECIES

Beyond the capabilities of the existing instrumentation, and without regard for the choice of platform, there is a general need for development of new sensors with increased accuracy, reliability, and sensitivity. However, such development must not in any way impede the expeditious implementation of existing instruments.

One of the principal requirements for understanding the chemistry of  $\text{HO}_x$  is the development of a method for global monitoring of  $\text{H}_2\text{O}$ , with good signal-to-noise ratio, which can be accurately calibrated and supported by ground truth (*in situ* or actual ground-based) measurements. In this connection ATMOS data may be useful for correlative measurements of  $\text{H}_2\text{O}$  vapor. Further development of microwave ground-based measurements is also warranted. All of these measurements must be made on a long term basis, both to verify the methods and to observe trends.

The mechanism of  $\text{H}_2\text{O}$  exchange with the troposphere, which is the subject of another chapter, must be fully understood in order to predict future effects of possible atmospheric changes on the rate of  $\text{H}_2\text{O}$  influx into the stratosphere. Observations such as enhanced  $\text{H}_2\text{O}$  vapor concentrations in the high latitude, lower stratosphere regions must be understood.

A clearer picture is needed of the overall hydrogen balance, particularly the contribution of  $\text{CH}_4$  oxidation to  $\text{H}_2\text{O}$  and the relative importance of  $\text{H}_2$ . These objectives will require continuous global measurements of the  $\text{CH}_4$  concentrations and altitude profiles, along with those of  $\text{H}_2\text{O}$ .

Further laboratory research is needed in support of instrument development, calibration, and sensitivity improvement. Accurate measurements of pressure broadening coefficients are especially important. As discussed in the chapter on chemistry, some laboratory simulations of  $\text{HO}_x/\text{O}_3$  photochemistry may prove to be useful for testing the accuracy and completeness of the photochemical models.